R. & M. No. 3262

MINISTRY OF AVIATION

AERONAUTICAL RESEARCH COUNCIL
REPORTS AND MEMORANDA

Interactions between Normal Shock Waves and Turbulent Boundary Layers

By G. E. GADD, Ph.D.
OF THE AERODYNAMICS DIVISION, N.P.L.

LONDON: HER MAJESTY'S STATIONERY OFFICE
1962
PRICE £1 7s. 6d. NET

Interactions between Normal Shock Waves and Turbulent Boundary Layers

By G. E. GADD, Ph.D.*

OF THE AERODYNAMICS DIVISION, N.P.L.

Reports and Memoranda No. 3262†

February, 1961

Summary. A theory, involving a simple new method for turbulent boundary layers, is presented for interactions between normal shocks and turbulent boundary layers on flat surfaces. Experiments in a pipe confirm the theory's general validity. Effects on separation of convex surface curvature and sweepback of the shock are then considered.

1. *Introduction.* When a nearly-normal shock wave occurs on an aerofoil in transonic flow, as in Fig. 1, the pressure p_b at the surface just behind the shock is of course greater than the pressure p_1 just in front. The pressure ratio p_b/p_1 depends in part on the Mach number M_1, which is defined according to the isentropic flow relations by the ratio p_1/H_0, where H_0 is the stagnation pressure. However, even in the absence of separation, p_b/p_1 is almost never as great as the value predicted by inviscid-flow theory for a normal shock with an upstream Mach number M_1.

To see why this is so, consider first the simpler case of a normal shock in a uniform stream past a flat plate, as in Fig. 2. In inviscid flow the pressure at the surface would rise discontinuously under the shock, but the boundary layer cannot support a discontinuous rise of pressure. Hence the external flow pattern becomes modified so that near the wall the shock is replaced by a band of compression waves. At the surface the initial rise of pressure is very steep if the boundary layer is turbulent, but downstream the gradients become much less steep. For weak shocks this falling off of the pressure gradients begins to occur somewhere near the point where the pressure p is equal to the sonic value, $0{\cdot}528H_0$. For stronger shocks, where separation occurs at a point whose pressure is below sonic, the falling off in gradient occurs just downstream of separation, and the flow pattern then becomes as shown in Fig. 3. In either case on a flat plate the overall rise of pressure would be the same as in inviscid flow, but we may say that locally under the shock the pressure only rises sharply to a value p_b, less than the full normal-shock downstream pressure, and defined, say, as the point of maximum curvature on the pressure distribution. It is this sort of pressure that is picked out as the pressure p_b just behind the shock on an aerofoil. The sharp rise of pressure from p_1 to p_b typically occurs within about 3 to 5 boundary-layer thicknesses. The much more gradual pressure gradients downstream merge with the general shape of the pressure distribution, which depends on the shape of the aerofoil. Thus there is not in general any well-defined point on the pressure distribution corresponding to the full normal-shock pressure rise.

* Now of Ship Division, N.P.L. Previously issued as A.R.C. 22,559.

† Published with the permission of the Director, National Physical Laboratory.

When, as is often the case, the aerofoil surface has an appreciable curvature, convex to the flow, we might expect an additional effect to be superimposed on the above. In inviscid flow it can be shown[1, 2] that the pressure at the surface under the shock would rise abruptly to the full normal-shock value, but would fall rapidly again just downstream. Thus there is a sharp pressure peak, and it would not seem surprising that the boundary layer should smooth this off, giving a downstream pressure p_b less than the full normal-shock value. In closer detail, however, the flow pattern must still be modified by the boundary layer in much the same way as it is on a flat plate (Fig. 2). Where the external flow is supersonic there will be a compression-wave region, and since the compressions are abrupt the surface slope is not likely to change much under this region, except for sharply-curved aerofoils. Thus on this closer view we should expect that the compression-wave region would be much as on a flat plate, and that only the downstream part of the pressure distribution would be significantly affected by the curvature. Hence p_b itself might not be very greatly different from its value on a flat plate.

The above discussion assumes the thickness of the boundary layer to be, say, of the order of 1 per cent of the chord, as typically encountered on an aerofoil not too close to the leading edge. If the boundary layer is exceptionally thin, the pressure rise under the shock, though spread out over many boundary-layer thicknesses, will still not be greatly spread out relative to the chord, and p_b may therefore be judged to be much closer to the inviscid value.

Usually, however, the interaction between the shock wave and the boundary layer directly affects the pressure distribution over a region of the order of 30 per cent of the chord. It may have a still more important indirect effect if it causes the boundary layer near the trailing edge to thicken markedly, as this will affect the circulation round the aerofoil and hence the shock position. Such effects on the circulation are usually only important if the shock is strong enough to cause separation, though even then there may not be any serious effects if reattachment occurs a short way behind the shock. Clearly, however, general studies of the interaction between turbulent boundary layers and normal shocks, with special reference to the occurrence of separation, will be helpful in increasing our understanding of the behaviour of aerofoils and wings in transonic flow, and this Paper is intended as a contribution to that end. It is also of course relevant to other practical situations, such as intake flows, which may involve interactions between normal shocks and turbulent boundary layers.

The Paper is divided into several parts. The first following this introductory section is a theoretical study of the interaction between the turbulent boundary layer on a flat plate and a normal shock in a uniform stream, the configuration of Fig. 2. Next an experiment on normal shocks in a pipe of circular cross section is described, and its findings compared with those of the above-mentioned theory. The effects of surface curvature on the minimum local upstream Mach number M_1 for which separation occurs are then discussed, with reference to experiments carried out on aerofoils of different shapes. The final section considers how far the findings concerning separation in two-dimensional flows are applicable to sweptback shocks on three-dimensional swept wings.

2. *The Interaction between the Turbulent Boundary Layer on a Flat Plate and a Normal Shock in a Uniform Mainstream.* This problem was considered earlier by the present author in Ref. 3, but that theory has now been improved, especially with regard to the treatment of the boundary layer.

The overall flow pattern is as shown in Figs. 2 and 3. The boundary layer thickens under the action of the adverse pressure gradients, and this displaces the external flow away from the wall.

The pressure distribution in the external flow is in turn governed by this displacement, and hence the theoretical problem, as with all cases of interactions between shock waves and boundary layers, is to determine the conditions under which the pressure distribution can be matched to the boundary-layer thickening. Most previous interaction analyses have, however, been concerned with laminar boundary layers and with mainstream flows that are everywhere supersonic. The present problem is more difficult both because turbulent boundary layers are less tractable theoretically than laminar ones, and also because the flow outside the boundary layer is partially subsonic. Where the flow is supersonic and of the simple-wave type the pressure is simply related to the flow direction, but in subsonic flow the pressure at any point depends on the configuration of the flow as a whole. Moreover behind the shock, local Mach numbers up to 1 are encountered, so that the relevant equations are non-linear, and not of the relatively simple Laplace type. All this means that any theoretical solution of the problem can only be roughly approximate.

When the shock is fairly weak, so that separation, if it occurs, is not extensive, the flow pattern resembles Fig. 2 rather than Fig. 3. The present Paper will be concerned in the main with such relatively weak shocks. It is assumed that the compression-wave region shown in Fig. 2 is of the simple-wave type, with the Mach waves emanating from the edge of the boundary layer intersecting the shock wave and being terminated by it. This terminating shock wave is vanishingly weak at the edge of the boundary layer, so that the layer is not called upon to support any discontinuous jump of pressure. Away from the wall the shock becomes stronger. At the point where the most upstream Mach wave of the compression-wave region intersects the shock, the latter is somewhat inclined, and the pressure just behind it is less than the full normal-shock downstream pressure. However, with increasing distance from the wall the shock becomes more nearly normal. It is assumed that the distance of the shock from the line $x = 0$ perpendicular to the wall and passing through the end of the shock at the edge of the boundary layer is everywhere fairly small, say less than 5 times the thickness of the boundary layer just upstream of the interaction region. The experiments of Section 3 appear to justify this assumption. Then to a rough approximation the boundary conditions imposed by the shock on the flow downstream may be taken as applying along the line $x = 0$. These boundary conditions are, in the outer part of the flow, the relations between the downstream pressure and the flow angle appropriate to a shock with a Mach number M_1 just upstream of it. Nearer the edge of the boundary layer the relations are in theory more complicated, since the flow deflection is then made up of a part achieved continuously in the simple-wave flow, and of a part occurring abruptly through the shock. However, it is shown in Section 2.1 that it is reasonably accurate to take a single form of relation between pressure and flow angle as applying everywhere behind the shock.

Section 2.1 also gives the relation between pressure and flow angle in the simple-wave region, as it applies along the edge of the boundary layer upstream of the shock, and Section 2.2 sets out the equations for the external flow downstream of the shock. Section 2.3 presents the boundary-layer analysis, showing how the thickness of the layer may be related to the pressure, which is assumed to be constant across the boundary layer. This assumption is probably fairly accurate except near the upstream end of the interaction region at the higher upstream Mach numbers. It is also shown how the skin friction may be roughly predicted. Section 2.4 combines the results of Sections 2.1 and 2.3 to predict the pressure distribution at the wall upstream of the shock. Section 2.5 gives a very crude analysis for the pressures at the wall and in the stream downstream of the shock, and finally Section 2.6 discusses the complete solution, including the conditions for boundary-layer separation.

2.1. *The Relations between Pressure and Flow Angle in the Compression-Wave Region and just behind the Shock.* Consider first the simple-wave compression region.

Let a parameter k, related to the pressure p, be defined by

$$\frac{p}{p_1} = 1 + \frac{2\gamma}{\gamma+1}(M_1^2-1)(1-k) \tag{1}$$

where suffix 1 denotes conditions in the external flow upstream of the shock, γ is the specific-heat ratio, and M is the Mach number. Thus $k = 1$ upstream, and $k \to 0$ downstream, where the pressure must approach the full normal-shock value. In other words $1-k = (p-p_1)/(p_2-p_1)$, where p_2 is the pressure far downstream. In the external flow the relationship between the Mach number M and k may be derived in the following way:

$$I\left(1+\frac{\gamma-1}{2}M^2\right) = I_1\left(1+\frac{\gamma-1}{2}M_1^2\right)$$

where I is the enthalpy, so that

$$M^2-1 = \frac{(\gamma+1)}{\gamma-1}\left(\frac{I_1}{I}-1\right)+\frac{I_1}{I}(M_1^2-1).$$

The external flow is everywhere approximately isentropic if M_1 is not too large (say $\leqslant 1{\cdot}3$), and hence

$$\frac{I_1}{I} = \left(\frac{p}{p_1}\right)^{-(\gamma-1)/\gamma} \simeq 1 - \frac{2(\gamma-1)}{\gamma+1}(1-k)(M_1^2-1)$$

from (1). Hence approximately

$$M^2-1 = (2k-1)(M_1^2-1). \tag{2}$$

For M_1 as large as $1{\cdot}3$, this relation is fairly accurate upstream of the shock, where $1 \leqslant k \leqslant \frac{1}{2}$, but it is inaccurate downstream where, however, it is not required.

Consider Fig. 4, showing a short length ac of a streamline in the simple-wave region. The line ab is a Mach line so that k is constant along ab, and bc is normal to ac. The angle abc is $\tan^{-1}(M^2-1)^{1/2} \simeq \tan^{-1}[(2k-1)^{1/2}(M_1^2-1)^{1/2}]$ by Equation (2). Hence if n represents distance along the normal and s distance along the streamline,

$$\frac{\partial k}{\partial n} = \frac{k_b-k_c}{bc} = \frac{k_a-k_c}{bc} = \frac{(k_a-k_c)}{ac}(2k-1)^{1/2}(M_1^2-1)^{1/2}$$

$$= -(2k-1)^{1/2}(M_1^2-1)^{1/2}\frac{\partial k}{\partial s}.$$

The pressure gradient normal to the streamline balances the centrifugal force associated with the streamline curvature. Thus if the angle of the streamline to the wall is α,

$$\frac{\partial p}{\partial n} = -\rho q^2\frac{\partial \alpha}{\partial s} = -\gamma p M^2\frac{\partial \alpha}{\partial s},$$

where ρ is the density and q the speed along the streamline. The product pM^2 does not vary enormously throughout the interaction region, as can be seen from the following Table:

M	1	1·1	1·2	1·3
pM^2/H_0	0·528	0·567	0·594	0·610

Hence approximately

$$\frac{\partial p}{\partial n} = -\gamma p_1 M_1^2 \frac{\partial \alpha}{\partial s}.$$

But

$$\frac{\partial p}{\partial n} = -\frac{2\gamma p_1}{\gamma+1}(M_1^2-1)\frac{\partial k}{\partial n}, \text{ by (1)}$$

Hence

$$\frac{\partial \alpha}{\partial s} = \frac{2(M_1^2-1)}{(\gamma+1)M_1^2}\frac{\partial k}{\partial n} = -\frac{2(M_1^2-1)^{3/2}}{(\gamma+1)M_1^2}(2k-1)^{1/2}\frac{\partial k}{\partial s},$$

and

$$\alpha = \frac{2(M_1^2-1)^{3/2}}{3(\gamma+1)M_1^2}[1-(2k-1)^{3/2}], \tag{3}$$

since $\alpha = 0$ when $k = 1$, in the undisturbed free stream. Equation (3) is of course only valid for $1 \geqslant k \geqslant \frac{1}{2}$, the range of k for which the flow is supersonic. When k is very close to 1, Equation (3) approximates to the well-known form

$$\alpha = \frac{(M_1^2-1)^{1/2}}{\gamma M_1^2}\left(\frac{p}{p_1}-1\right),$$

but this is not valid for local Mach numbers close to 1, when k approaches $\frac{1}{2}$.

Consider now the shock wave. In general this is inclined as shown in Fig. 5. Let quantities just upstream of the shock be distinguished by suffix u. Far away from the wall these upstream quantities will take their undisturbed free-stream values, denoted by suffix 1, but near the wall the shock will occur as the termination of a compression-wave region, as shown in Fig. 2, and hence here the flow conditions just upstream of the shock will differ from those in the free stream. If quantities just downstream of the shock are distinguished by suffix d, then ϵ, the deflection which streamlines undergo on passing through the shock, and p_d, ρ_d, and q_d, will depend on p_u, ρ_u, and q_u and on the angle ζ which the shock makes with the streamlines upstream of the shock. Four equations may be written down in the usual way, namely those of energy, momentum parallel to the shock, momentum perpendicular to the shock, and continuity, so that any four of the quantities ϵ, p_d, ρ_d, q_d, and ζ may be eliminated. The oblique-shock relations usually presented in the literature leave ζ in as a variable, but it can of course be eliminated and ϵ can be expressed merely as a function of p_d and the upstream conditions. The resulting relation[3] is

$$\sin^2\epsilon\left\{\frac{\gamma p_u}{(\gamma-1)(p_d-p_u)}+\frac{\gamma+1}{2(\gamma-1)}-\frac{\gamma(p_d-p_u)}{(\gamma-1)\rho_u q_u^2}-\frac{2\gamma p_u}{(\gamma-1)\rho_u q_u^2}\right\}$$
$$=\frac{(p_d-p_u)}{(\gamma-1)\rho_u q_u^2}\left\{1-\frac{\gamma p_u}{\rho_u q_u^2}-\frac{(\gamma+1)(p_d-p_u)}{2\rho_u q_u^2}\right\}. \tag{4}$$

From Equation (1)

$$\frac{p_d-p_u}{p_u} \simeq \frac{2\gamma}{\gamma+1}(M_1^2-1)(k_u-k_d) \tag{5}$$

and from (2)

$$M_u^2 - 1 = (2k_u-1)(M_1^2-1).$$

Hence (4) becomes approximately

$$\epsilon = \frac{2(M_1^2-1)^{3/2}}{(\gamma+1)M_1^2}(k_u+k_d-1)^{1/2}(k_u-k_d). \tag{6}$$

From Equation (3) it follows that the inclination of the flow to the wall just downstream of the shock is given by

$$\alpha_d = \frac{2(M_1^2-1)^{3/2}}{(\gamma+1)M_1^2}\{\tfrac{1}{3}[1-(2k_u-1)^{3/2}]+(k_u+k_d-1)^{1/2}(k_u-k_d)\}. \tag{7}$$

If k_u is close to 1 the approximation (6) for ϵ is fairly good even if M_1 is not very close to 1. The errors arise mainly from those terms in the bracketed expression on the left-hand side of (4) which are omitted in deriving (6). The omitted terms are equal to

$$\frac{\gamma+1}{2(\gamma-1)} - \frac{(p_d-p_u)}{(\gamma-1)p_uM_u^2} - \frac{2}{(\gamma-1)M_u^2},$$

and partially cancel one another. If, on the other hand, k_u is near to $\frac{1}{2}$, Equation (5) becomes rather inaccurate, but any errors thereby introduced into (6) will not have an important effect on α_d as given by (7), since ϵ will then be small.

In Equation (7), k_u can vary between 1 and $\frac{1}{2}$ and k_d between 0 and k_u. For ϵ to be real, $k_u + k_d - 1$ must be positive. Under these conditions

$$\tfrac{1}{3}[1-(2k_u-1)^{3/2}]+(k_u+k_d-1)^{1/2}(k_u-k_d) \doteq k_d^{1/2}(1-k_d). \tag{8}$$

Thus if $k_u = 1$, (8) is accurately true. If $k_u = 0{\cdot}5$, so that k_d must be $0{\cdot}5$ also, A, the left-hand side of (8) is equal to $0{\cdot}333$, whilst B, the right-hand side, is equal to $0{\cdot}354$. For $k_u = 0{\cdot}75$, so that $0{\cdot}25 \leqslant k_d \leqslant 0{\cdot}75$, we have:

k_d	$0{\cdot}25$	$0{\cdot}30$	$0{\cdot}50$	$0{\cdot}75$
A	$0{\cdot}216$	$0{\cdot}317$	$0{\cdot}341$	$0{\cdot}216$
B	$0{\cdot}375$	$0{\cdot}383$	$0{\cdot}354$	$0{\cdot}216$

Hence for most possible combinations of k_u and k_d, Equation (8) is not greatly in error and (7) simplifies to

$$\alpha_d = \frac{2(M_1^2-1)^{3/2}}{(\gamma+1)M_1^2}k_d^{1/2}(1-k_d). \tag{9}$$

Replacing (7) by (9) is equivalent to saying that the flow angle behind a band of compression waves terminated by a shock is approximately the same as that behind a shock on its own giving the same downstream pressure. As mentioned in the previous section, this relation for α_d is assumed to apply along the line $x = 0$, through the foot of the shock perpendicular to the wall, and this forms one boundary condition for the flow downstream of the shock.

2.2. *The Equations for the External Flow Downstream of the Shock.* Let suffix 2 denote conditions behind the normal shock in inviscid flow. Thus

$$\frac{p_2}{p_1} = 1 + \frac{2\gamma}{(\gamma+1)}(M_1^2-1)$$

and

$$M_2^2 = \left(1+\frac{\gamma-1}{2}M_1^2\right)\Big/\left(\gamma M_1^2 - \frac{\gamma-1}{2}\right),$$

from the standard normal-shock relations. From (1) it follows that

$$\frac{p}{p_2} = \left(1-\frac{2\gamma}{\gamma+1}(M_1^2-1)k\right)\Big/\left(1+\frac{2\gamma}{\gamma+1}(M_1^2-1)\right)$$

$$= 1-\frac{2\gamma}{\gamma+1}(1-M_2^2)k. \tag{10}$$

The pressure gradient normal to the streamlines must balance the centrifugal force associated with their curvature, and hence if the angle α of the streamlines to the wall is small

$$\frac{\partial p}{\partial y} = -\rho q^2 \frac{\partial \alpha}{\partial x} = -\gamma p M^2 \frac{\partial \alpha}{\partial x},$$

where the x and y directions are parallel and perpendicular to the wall. At the sonic point, where the end of the shock meets the edge of the layer, the product pM^2 is equal to $0{\cdot}528H_0$: it does not differ enormously from this far away from the wall behind the normal part of the shock where suffix 2 conditions are achieved, as can be seen from the following Table:

M_1	p_1/H_0	M_2	p_2/p_1	$p_2M_2^2/H_0$
1·1	0·468	0·912	1·245	0·485
1·2	0·412	0·842	1·513	0·442
1·3	0·361	0·786	1·805	0·404

Hence since the pressure is close to the sonic pressure only over a small region downstream of the shock, pM^2 may be replaced by $p_2M_2^2$ downstream, and from Equation (10),

$$\frac{\partial \alpha}{\partial x} = \frac{2(1-M_2^2)}{(\gamma+1)M_2^2} \frac{\partial k}{\partial y}. \tag{11}$$

A second relation between α and k can be obtained from the continuity equation, which can be written

$$\frac{\partial(\rho q)}{\partial x} + \frac{\partial(\rho q \alpha)}{\partial y} = 0$$

approximately. Since the external flow is everywhere almost isentropic, even for M_1 as large as 1·3,

$$\frac{\rho}{\rho_2} = \left(\frac{p}{p_2}\right)^{1/\gamma}$$

and

$$\frac{I}{I_2} = \left(\frac{p}{p_2}\right)^{(\gamma-1)/\gamma}$$

where I is the enthalpy. Hence from the energy equation $I + q^2/2 = I_2 + q_2^2/2$, and from Equation (10),

$$\frac{\rho q}{\rho_2 q_2} = 1 + \frac{2(1-M_2^2)^2}{(\gamma+1)M_2^2} k(1-k) + 0(1-M_2^2)^3.$$

If the third term on the right is to be neglected here, it might appear that M_2 in the denominator of the second term ought to be set equal to 1. However the approximation is much closer if it is included. Thus consider conditions at the sonic point where $k = \frac{1}{2}$ according to the approximate relation (2). With $M_2 = 0{\cdot}786$, corresponding to $M_1 = 1{\cdot}3$,

$$1 + \frac{2(1-M_2^2)^2}{(\gamma+1)M_2^2} k(1-k) = 1{\cdot}0488$$

and

$$1 + \frac{2(1-M_2^2)^2}{\gamma+1} k(1-k) = 1{\cdot}0302,$$

whereas the correct value of $\rho q/\rho_2 q_2$ is 1·0443. Substituting the approximate relation for ρq into the continuity equation we obtain

$$\frac{\partial \alpha}{\partial y} = -\frac{2(1-M_2^2)^2}{(\gamma+1)M_2^2} \frac{\partial}{\partial x}(k-k^2). \tag{12}$$

From Equation (11) it follows that

$$\frac{\partial^2 k}{\partial \bar{x}^2} + \frac{\partial^2 k}{\partial \bar{y}^2} = \frac{\partial^2 k^2}{\partial x^2} \tag{13}$$

where

$$\bar{y} = (1 - M_2^2)^{1/2} y . \tag{14}$$

In terms of this variable Equations (11) and (12) become

$$\frac{\partial \alpha}{\partial \bar{x}} = \frac{2(1 - M_2^2)^{3/2}}{(\gamma + 1) M_2^2} \frac{\partial k}{\partial \bar{y}}$$

and

$$\frac{\partial \alpha}{\partial \bar{y}} = - \frac{2(1 - M_2^2)^{3/2}}{(\gamma + 1) M_2^2} \frac{\partial}{\partial \bar{x}} (k - k^2) .$$

To facilitate matching these relations to the relations (3) and (9) for α in the simple-wave flow region and behind the shock, we note that $(1 - M_2^2)^{3/2}/M_2^2$ is not very different from $(M_1^2 - 1)^{3/2}/M_1^2$, as can be seen from the following Table:

M_1	M_2	$(M_1^2 - 1)^{3/2}/M_1^2$	$(1 - M_2^2)^{3/2}/M_2^2$
1·1	0·912	0·080	0·083
1·2	0·842	0·203	0·222
1·3	0·786	0·338	0·381

Hence, approximately

$$\frac{\partial \alpha}{\partial \bar{x}} = \frac{2(M_1^2 - 1)^{3/2}}{(\gamma + 1) M_1^2} \frac{\partial k}{\partial \bar{y}} \tag{15}$$

and

$$\frac{\partial \alpha}{\partial \bar{y}} = - \frac{2(M_1^2 - 1)^{3/2}}{(\gamma + 1) M_1^2} \frac{\partial}{\partial \bar{x}} (k - k^2) \tag{16}$$

in the external flow downstream of the shock.

2.3. *The Boundary-Layer Thickness and Skin Friction.* Suppose the boundary-layer velocity profile upstream of the region of interaction is of the form

$$\left(\frac{u}{u_e}\right)_a = \left(\frac{y}{\delta}\right)_a^{1/K}$$

where suffix 'a' denotes conditions at a station at the upstream end of the region of interaction, suffix 'e' denotes conditions at the edge of the boundary layer, u is the velocity component parallel to the wall, and δ is the total boundary-layer thickness. The exponent K is frequently in the literature given the values 5, 7, or 9, and experimentally measured velocity profiles for a constant-pressure boundary layer can often be fitted by a power-law form with $K = 7$. At some general point suppose that

$$\frac{u}{u_e} = \left(\frac{y}{\delta}\right)^n .$$

The mass flow between the wall and the edge of the boundary layer is equal to $\int_0^\delta \rho u dy$. Upstream this equals $m_a = K(f \rho_e u_e \delta)_a/(K+1)$, and at a general point it equals $m = f \rho_e u_e \delta/(n+1)$, where f is a factor which would be equal to 1 if the Mach number were low, so that the density were constant,

equal to ρ_e across the boundary layer. For $M_1 = 1{\cdot}3$ and $K = 7$, $f_a = 0{\cdot}822$, and in general f is only a little less than 1. When the pressure rise is very rapid, as it is in the upstream part of the interaction region, it may reasonably be assumed that $m \simeq m_a$. More generally it is assumed that the rate of entrainment of fluid into the boundary layer from the external flow is the same as just upstream of the region of interaction. This is probably an underestimate, since Seddon's interesting paper[4] concerning the interaction with a normal shock with $M_1 = 1{\cdot}47$ shows that in that case the rate of mass entrainment becomes much larger downstream than it is upstream. However it is difficult to formulate a more accurate relation for the entrainment, and since the effect is only important in the downstream part of the interaction region, where the solution is necessarily crude, the simple assumption of a constant rate is probably good enough. Thus

$$\frac{f}{n+1}\rho_e u_e \delta = \frac{K f_a}{K+1}(\rho_e u_e)_a \left[\delta_a + (x - x_a)\left(\frac{d\delta}{dx}\right)_a\right]. \tag{17}$$

To a good approximation the product term inside the square brackets here may be neglected upstream of the shock, and downstream it may be replaced by $x(d\delta/dx)_a$, x being measured from the foot of the shock.

The general profile will, because of the adverse pressure gradients, be less 'full' in shape than the upstream profile, *i.e.*, n will be greater than $1/K$. This is a factor tending to make f smaller than f_a because, for the general profile as compared with the upstream one, there will tend to be a bigger difference in velocity, and hence in density, between a point in the middle of the boundary layer and the edge of the layer. On the other hand, the fact that M_e is less than M_1 tends in itself to diminish the variation in density at the downstream positions, so tending to make f larger than f_a. Thus since both f and f_a are not much less than 1, f_a/f is likely to be very nearly equal to 1. Hence (17) becomes

$$\frac{1}{n+1}\frac{M_e}{M_1}\left(\frac{T_e}{T_1}\right)^{(\gamma+1)/2(\gamma-1)}\delta = \frac{K}{K+1}\left[\delta_a + (x - x_a)\left(\frac{d\delta}{dx}\right)_a\right] \tag{18}$$

where T is absolute temperature, since in isentropic flow $\rho u \propto M T^{(\gamma+1)/2(\gamma-1)}$, and conditions at the edge of the boundary layer at station 'a' are the same as suffix 1 conditions, defined in the undisturbed upstream flow.

An additional relation is needed to determine the two unknowns, n and δ, in terms of M_e. This is provided by the so-called energy-integral equation, obtained by multiplying the equation of momentum parallel to the wall,

$$\rho u \frac{\partial u}{\partial x} + \rho v \frac{\partial u}{\partial y} = \rho_e u_e \frac{du_e}{dx} + \frac{\partial \tau}{\partial y},$$

by $2u$ and integrating from $y = 0$ to $y = \delta$, making use of the continuity equation

$$\frac{\partial(\rho u)}{\partial x} + \frac{\partial(\rho v)}{\partial y} = 0.$$

The resulting equation is

$$\frac{d}{dx}\left[\rho_e u_e^3 \int_0^\delta \frac{\rho u}{\rho_e u_e}\left(1 - \frac{u^2}{u_e^2}\right) dy\right] + 2\rho_e u_e^2 \frac{du_e}{dx}\int_0^\delta \frac{u}{u_e}\left(1 - \frac{\rho}{\rho_e}\right) dy = 2\int_0^\delta \tau \frac{\partial u}{\partial y}\, dy.$$

When there is zero heat transfer

$$I + \frac{u^2}{2} = I_e + \frac{u_e^2}{2}$$

throughout the boundary layer, so that

$$\frac{\rho}{\rho_e} = \frac{I_e}{I} = 1 - \frac{u_e^2}{2I}\left(1 - \frac{u^2}{u_e^2}\right) = 1 - \frac{\gamma - 1}{2} M_e^2 \frac{\rho}{\rho_e}\left(1 - \frac{u^2}{u_e^2}\right).$$

Hence if θ^* is the energy thickness, $\int_0^\delta \frac{\rho u}{\rho_e u_e}\left(1 - \frac{u^2}{u_e^2}\right) dy$, the energy-integral equation becomes

$$\frac{d}{dx}(\rho_e u_e^3 \theta^*) + (\gamma - 1) M_e^2 \rho_e u_e^2 \frac{du_e}{dx} \theta^* = 2 \int_0^\delta \tau \frac{\partial u}{\partial y} dy,$$

or, since

$$(\gamma - 1) M_e^2 \rho_e u_e^2 \frac{du_e}{dx} = - \rho_1 u_1^3 \left(\frac{M_e}{M_1}\right)^3 \left(\frac{T_e}{T_1}\right)^{(\gamma+1)/2(\gamma-1)} \frac{d}{dx}\left(\frac{T_e}{T_1}\right),$$

and

$$\rho_e u_e^3 = \rho_1 u_1^3 \left(\frac{M_e}{M_1}\right)^3 \left(\frac{T_e}{T_1}\right)^{(3\gamma-1)/2(\gamma-1)},$$

$$\frac{d}{dx}\left[\left(\frac{M_e}{M_1}\right)^3 \left(\frac{T_e}{T_1}\right)^{(\gamma+1)/2(\gamma-1)} \theta^*\right] = 2 \left(\frac{M_e}{M_1}\right)^3 \left(\frac{T_e}{T_1}\right)^{(\gamma+1)/2(\gamma-1)} d, \tag{19}$$

where d may be termed the non-dimensional dissipation or turbulent-energy-production integral, defined as $\int_0^\delta (\tau/\rho_e u_e^2)\{\partial(u/u_e)/\partial y\} dy$.

Where the pressure gradients are very abrupt it follows that $M_e^3 T_e^{(\gamma+1)/2(\gamma-1)} \theta^*$ remains approximately constant, since d on the right-hand side of (19) will be of the same order as upstream and 'dx' will be very small. More generally, we assume that $d = d_a$; this will not be accurate but it is probably good enough since the assumption only significantly affects matters downstream of the shock. In terms of the assumed boundary-layer profile shapes,

$$\theta_a^* = \frac{2K g_a \delta_a}{(K+1)(K+3)}$$

and

$$\theta^* = \frac{2ng\delta}{(n+1)(3n+1)},$$

where the factors g_a and g would be equal to 1 if the density were equal to ρ_e across the boundary layer. In reality they are a little less than 1, but by arguments similar to those advanced above regarding f and f_a in Equation (17), it may be assumed that g_a/g is equal to 1. Hence

$$\frac{n}{(n+1)(3n+1)} \left(\frac{M_e}{M_1}\right)^3 \left(\frac{T_e}{T_1}\right)^{(\gamma+1)/2(\gamma-1)} \delta = \frac{K}{(K+1)(K+3)} \left[\delta_a + \left(\frac{d\delta}{dx}\right)_a \int_{x_a}^x \left(\frac{M_e}{M_1}\right)^3 \left(\frac{T_e}{T_1}\right)^{(\gamma+1)/2(\gamma-1)} dx\right]. \tag{20}$$

As with the corresponding term in Equations (17) and (18), the integral on the right-hand side may be neglected upstream of the shock, and downstream its lower limit of integration may be replaced by $x = 0$.

An attempt may be made to deduce the skin friction from the boundary-layer momentum-integral equation,

$$C_f = 2\frac{d\theta}{dx} + 2\theta\left\{\frac{(2+H-M_e^2)}{M_e\left(1+\frac{\gamma-1}{2}M_e^2\right)}\frac{dM_e}{dx}\right\},$$

in the usual notation. In terms of the assumed boundary-layer profile $\theta = hn\delta/(n+1)(2n+1)$, where h is a factor, a little less than 1, arising from the variation of the density across the boundary layer. Hence from Equation (18)

$$\theta = \frac{hnK}{(2n+1)(K+1)}\frac{M_1}{M_e}\left(\frac{T_1}{T_e}\right)^{(\gamma+1)/2(\gamma-1)}\left[\delta_a + (x-x_a)\left(\frac{d\delta}{dx}\right)_a\right].$$

We may take h to be approximately constant, equal to h_a, because as M_e decreases, tending in itself to make h nearer to 1, the profile becomes less 'full' in shape, tending to decrease h, and the net variation in h is likely to be small. Thus for positions up to the shock and a little way downstream,

$$\theta = \frac{h_a nK}{(2n+1)(K+1)}\frac{M_1}{M_e}\left(\frac{T_1}{T_e}\right)^{(\gamma+1)/2(\gamma-1)}\delta_a$$

and

$$\frac{d\theta}{dx} = \frac{n(2+K)}{2(2n+1)}\frac{M_1}{M_e}\left(\frac{T_1}{T_e}\right)^{(\gamma+1)/2(\gamma-1)}C_{fa} +$$

$$+\frac{h_a K\delta_a}{K+1}\left\{\frac{M_1}{M_e}\left(\frac{T_1}{T_e}\right)^{(\gamma+1)/2(\gamma-1)}\frac{d}{dx}\left(\frac{n}{2n+1}\right) + \frac{n}{2n+1}\frac{d}{dx}\left[\frac{M_1}{M_e}\left(\frac{T_1}{T_e}\right)^{(\gamma+1)/2(\gamma-1)}\right]\right\}.$$

From Equations (18) and (20)

$$\frac{n}{3n+1}\frac{M_e^2}{M_1^2} = \frac{1}{K+3}$$

in the upstream part of the interaction region, so that

$$n = \left[(K+3)\frac{M_e^2}{M_1^2} - 3\right]^{-1}. \tag{21}$$

The other term of the momentum-integral equation to be evaluated is H, the ratio of the displacement thickness δ^* to the momentum thickness θ. In terms of the assumed profile, when there is zero heat transfer

$$\frac{\theta}{\delta} = \int_0^1 \frac{(t^n - t^{2n})}{1+\frac{\gamma-1}{2}M_e^2(1-t^{2n})}\,dt$$

where $t \equiv u/u_e$, and

$$\frac{\delta^*}{\delta} = \int_0^1 \frac{\left[1+\frac{\gamma-1}{2}M_e^2(1-t^{2n}) - t^n\right]}{1+\frac{\gamma-1}{2}M_e^2(1-t^{2n})}\,dt$$

$$= [1+(\gamma-1)M_e^2]\int_0^1 \frac{(t^n-t^{2n})dt}{1+\frac{\gamma-1}{2}M_e^2(1-t^{2n})} + \left[1+\frac{\gamma-1}{2}M_e^2\right]\int_0^1 \frac{(1-2t^n+t^{2n})dt}{1+\frac{\gamma-1}{2}M_e^2(1-t^{2n})}$$

$$= [1+(\gamma-1)M_e^2]\frac{\theta}{\delta} + \left(1+\frac{\gamma-1}{2}M_e^2\right)n\left[\frac{2\theta}{\delta} - (\gamma-1)M_e^2\int_0^1 \frac{(t^n-t^{2n})^2dt}{\left[1+\frac{\gamma-1}{2}M_e^2(1-t^{2n})\right]^2}\right]$$

integrating by parts. Now the average value of $(t^n - t^{2n})\Big/\left[1 + \frac{\gamma-1}{2} M_e^2(1-t^{2n})\right]$ over the range $0 < t < 1$ is θ/δ, so it can be assumed that the average value of $(t^n - t^{2n})^2\Big/\left[1 + \frac{\gamma-1}{2} M_e^2(1-t^{2n})\right]^2$ is roughly θ^2/δ^2, and hence

$$H = \frac{\delta^*}{\theta} = 1 + (\gamma-1)M_e^2 + 2(1-N)\left(1 + \frac{\gamma-1}{2} M_e^2\right) n, \tag{22}$$

where

$$N = \frac{\gamma-1}{2} M_e^2 \frac{\theta}{\delta}. \tag{23}$$

An average value of 0·03 may be taken for N upstream of the shock because, N being small, fractional errors made in it are not important. The momentum-integral equation becomes

$$C_f = \frac{M_1}{M_e}\left(\frac{T_1}{T_e}\right)^{(\gamma+1)/2(\gamma-1)} \left\{ \begin{array}{l} \dfrac{n(2+K)}{2n+1} C_{fa} + \dfrac{2h_a nK}{(2n+1)(K+1)} \delta_a \dfrac{dM_e}{dx}\left[\dfrac{M_e^2-1}{M_e\left(1+\dfrac{\gamma-1}{2}M_e^2\right)} - \right. \\ \left. - \dfrac{2n(K+3)M_e}{(2n+1)M_1^2} + \dfrac{3-(2-\gamma)M_e^2 + 2(1-N)\left(1+\dfrac{\gamma-1}{2}M_e^2\right)n}{M_e\left(1+\dfrac{\gamma-1}{2}M_e^2\right)}\right] \end{array} \right\}$$

This simplifies, using Equation (21), to

$$\frac{C_f}{C_{fa}} = \frac{(2+K)\dfrac{M_1}{M_e}\left(\dfrac{T_1}{T_e}\right)^{(\gamma+1)/2(\gamma-1)}}{(K+3)\dfrac{M_e^2}{M_1^2} - 1} \left\{ 1 + \frac{2\cdot 5 l_a}{M_e}\frac{dM_e}{dx}\left[\frac{1-N}{(K+3)\dfrac{M_e^2}{M_1^2} - 3} - \frac{1}{(K+3)\dfrac{M_e^2}{M_1^2} - 1}\right]\right\} \tag{24}$$

where we assume $\theta_a = Cl_a R_a^{-1/5}$, so that $C_{fa} = (8/5)CR_a^{-1/5}$, where C is a constant, l_a is the distance of station 'a' from the leading edge, and R_a is the Reynolds number based on free-stream conditions and the length l_a.

Equations (18), (20) and (24) represent a simple solution for the turbulent boundary layer subjected to sharp adverse pressure gradients, applicable up to moderate supersonic speeds provided the pressure is constant across the boundary layer. For very low supersonic Mach numbers this condition is probably satisfied in interactions between shock waves and boundary layers, but when $M_1 = 1\cdot 3$, say, the pressure is likely to vary considerably across the boundary layer at the upstream end of the region of interaction, since in the outer part of the boundary layer the pressure tends to be constant along Mach lines rather than along lines perpendicular to the wall. However, at and downstream of the point where $M_e = 1\cdot 1$, say, the pressure is likely to be fairly constant across the boundary layer. It may be expected that relations (18) and (20) would then describe the thickness and shape of the profile at such downstream positions even though in deriving the relations the pressure has been assumed to be constant across the boundary layer at all points.

The merit of this solution for the present purposes is that it gives a simple explicit relation for the boundary-layer thickness in terms of the pressure. This can be matched to the outer flow as will be described in the following sections. We conclude this section, however, with examples of the application of the method to several general cases, to demonstrate that it gives acceptable results.

Schubauer and Klebanoff's work[5] gives the most detailed experimental results for a case in incompressible flow with a fairly abrupt adverse pressure gradient after a region of almost constant pressure. An idealised version of the experimental external-velocity distribution is

$$u_e = u_1, \ 0 < l < 18{\cdot}25,$$

$$\frac{u_e}{u_1} = 1{\cdot}792 - 0{\cdot}0434l, \ l > 18{\cdot}25,$$

where l is the distance from the leading edge in feet. This fits the experimental data quite well in the region of the pressure rise, as can be seen from Fig. 6. The effective origin of the turbulent boundary layer is a little downstream of the physical leading edge, so that for the point at the beginning of the pressure rise, 18·25 ft from the actual leading edge, the effective value of l_a is 15·05 ft. It can be seen from Fig. 7 that at the position immediately upstream of where the pressure begins to rise, the boundary-layer velocity profile is quite well represented by the relation $u/u_1 = (y/2{\cdot}11)^{1/6}$, where y is in inches. Fig. 7 also shows the profiles calculated from Equations (18) and (20) at downstream positions for the idealised linear external-velocity distribution and the one-sixth power upstream profile. The full-line curves are those calculated neglecting the right-hand terms in $(d\delta/dx)_a$ of Equations (18) and (20), and the dotted curves are the results obtained when these terms are included. It can be seen that the dotted curves agree fairly well with the experimental measurements, except at the most downstream station, which is close to separation.

Fig. 8 shows the skin-friction variation deduced from Equation (24) for the full line, and from the basic momentum equation for the dotted line, corresponding to the dotted-line results of Fig. 7. The experimental points are those deduced by Spence[6] from the shapes of the velocity profiles close to the wall. Clearly the theory does not predict the skin friction adequately, even though as it happens the first approximation gives roughly the correct position of separation. The experimentally measured values of θ and H, if fed into the momentum equation, give similarly erroneous results for the skin friction. It has been argued[6] that the momentum equation is invalid for estimating the skin friction, because it neglects a term involving the Reynolds stress and also a term involving the variation, if it is present, of pressure across the boundary layer. As regards the Reynolds stress it appears from Schubauer and Klebanoff's results that this is too small to make any appreciable difference. The variation of pressure across the boundary layer may well have been important in the experiment, and also the flow may well not have been strictly two-dimensional, and for both these reasons it is invalid to use the momentum equation for the calculation of skin friction from the experimentally measured values of θ and H. However, an ideal experiment can be imagined in which the flow would be strictly two-dimensional and in which there were no variations of pressure across the boundary layer. It seems intuitively very likely that such an ideal experiment would, for the same surface pressure distribution, yield roughly the same distributions of θ, H, and C_f as the actual, imperfect, experiment. The momentum equation ought to apply almost exactly to the ideal experiment, and this is possible because the actual distributions of θ and H need not be altered much to be in harmony with the proper skin-friction distribution. Any theory of the turbulent boundary layer aspires to predict the results of such imaginary ideal experiments, and hence the skin friction ought to be deducible from the momentum equation and the theoretical values of θ and H. However, it is very stringent to test the theory by seeing if the predicted skin-friction distributions are even only moderately accurate, since it would only pass such a test if the predicted distributions of θ and H were very accurate.

It may therefore be considered to be not worthwhile to make any attempt to deduce the skin friction from Equation (24). However, the experimental results of Section 3 suggest that in interactions with normal shocks the boundary-layer profiles keep reasonably close to the power-law form, at least over the upstream part of the interaction region. If the profiles were exactly of the power-law form the theory ought to be almost exact, provided the neglect of pressure differences across the boundary layer is permissible. Hence there is a possibility that the predicted results for skin friction may be roughly correct, though clearly not too much weight can be attached to them. The method is used in default of a better one to predict the occurrence of separation, defined as taking place when the skin friction becomes zero. The usual criteria for turbulent separation will clearly fail under the conditions of very steep adverse pressure gradients encountered under the shock. Thus if we say that separation occurs when the shape parameter H reaches a certain value, this will not predict separation soon enough. As Stratford[7] has shown, if the pressure gradient suddenly became infinite after an upstream region of zero gradient, separation would occur with a vanishingly small pressure rise, and only the shape of an infinitesimal part of the profile next to the wall would be affected. Thus H at separation would be the same as for a flat plate. The Ludwieg-Tillmann skin-friction criterion[6] would fail in these circumstances for the same reason, since in deriving it, it is assumed that the 'law of the wall' equation is valid up to a distance θ from the wall.

There remains the possibility of using Stratford's separation criterion. This was deduced for conditions of sharp adverse pressure gradients, and in this respect it should be suitable for the present problem, though effects of compressibility were not considered in deriving it. The relation is

$$(2C_p)^{(K-2)/4}\left(l\frac{dc_p}{dl}\right)^{1/2} = 1{\cdot}06\beta(10^{-6}R)^{1/10}$$

where $C_p = 1 - u_e^2/u_1^2$, l is the distance from the leading edge, R is the Reynolds number based on l, and β is an empirical constant, taken by Stratford to be $0{\cdot}66$. To extend this formula to compressible flow we note that according to Equation (24), a compressible-flow case for which M_e/M_1 is some prescribed function of l, say $F(l)$, would have separation occurring at almost the same position as an incompressible case with the velocity distribution $u_e/u_1 = F(l)$. The equivalence would be exact if N in Equation (24) were zero, and in fact N is very small. Thus we may expect Stratford's formula to be applicable to the compressible case if C_p is interpreted as $1 - M_e^2/M_1^2$. In the upstream part of the interaction region $l \simeq l_a$. Also we assume that

$$\delta_a = 0{\cdot}38 l_a R_a^{-1/5}, \tag{25}$$

a formula fairly accurate up to moderate supersonic Mach numbers. Hence from Equation (2) Stratford's criterion for separation becomes

$$\left[\frac{4(M_1^2-1)(1-k)}{M_1^2}\right]^{(K-2)/4}\left[-\frac{(M_1^2-1)}{M_1^2}\frac{dk}{dX}\right]^{1/2} = 0{\cdot}116\beta, \tag{26}$$

where $X \equiv x/\delta_a$.

Stratford shows that in incompressible flow, if the pressure is constant up to station 'a' at a distance l_a from the leading edge, and then follows the law

$$C_p = 0{\cdot}850\beta^{2/3}\left\{0{\cdot}435 R_a^{1/5}\left[\left(\frac{l}{l_a}\right)^{1/5} - 1\right]\right\}^{2/K}, \tag{27}$$

the skin friction will be zero downstream of 'a', the boundary layer being everywhere just on the point of separation. This relation is compared in Fig. 9 with that deduced from Equation (24) for

zero skin friction downstream of 'a' for the case $K = 7$, $R_a = 2 \times 10^6$. It can be seen that the present theory predicts a pressure distribution of much the same form as Stratford's, and though the present theory probably makes C_p rather too large, the fact that the results are at least of the right order gives additional grounds for not dismissing Equation (24) as completely worthless for predicting skin friction in situations, such as shock-wave boundary-layer interactions, where the adverse pressure gradients are very abrupt.

As for Equations (18) and (20), further evidence in support of their reasonable accuracy is provided by the experiments of Section 3, as will be shown in that section, and also by Seddon's experiment[4] on a normal shock with an upstream Mach number of 1·47. In this latter case there were probably appreciable variations of static pressure across the boundary layer, because of the relatively high Mach number, but nevertheless the theory works quite well, as can be seen from Fig. 10, which shows the profiles 1, 2, and 3 of Seddon's paper. The upstream profile is well represented by the power law $u/u_1 = (y/0{\cdot}14)^{1/5{\cdot}5}$. This seems to fit the experimental points slightly better than the 1/7th power form suggested by Seddon. The predicted form for profile 2 is fairly close to the experimentally-measured profile. This profile station is close to separation, and the fact that the profile is much 'fuller' in shape than separation profiles with more gradual pressure gradients* illustrates the point made above, that the shape factor H is much smaller at separation when the pressure gradients are very abrupt than when they are more gradual. Profile 3 is beyond the separation point, and is not at all well represented by the simple predicted power-law form. However if the velocity profile were assumed to be of the form

$$\frac{u}{u_e} = 0,\ 0 < y < \bar{y},$$

$$\frac{u}{u_e} = \left(\frac{y - \bar{y}}{\delta}\right)^n,\ \bar{y} < y < \delta + \bar{y},$$

the theory would predict n and δ to be the same as if it is assumed that $u/u_e = (y/\delta)^n$. This is because an inner region of zero velocity makes no difference either to the mass flux or to the energy thickness. Hence $\bar{y}$ is really arbitrary according to the theory, and by putting $\bar{y} = 0{\cdot}04$, the resulting profile, shown dotted in Fig. 10, can be made to fit the experimental profile tolerably well.

This brings to light a possible defect of the theory, that since neither the energy thickness nor the mass flux is sensitive to variations of profile shape near the low-velocity end, the shape here is not really tied down by the theory. The displacement thickness is, however, critically dependent on the shape of the inner part of the profile, so we really have no right to expect the theory to give the displacement thickness accurately. Fortunately, however, it seems to be an empirical fact that upstream of separation the profiles do often approximately fit the simple power-law form, close to the wall as well as away from it, and this is the reason for the success of the method.

The power-law family of profiles seems to fail to apply before separation is reached in the case of the results of Ackeret, Feldmann, and Rott[8] for interactions between normal shocks and turbulent boundary layers on curved surfaces, convex to the flow. The experimental profiles become considerably less 'full' in shape than the predicted profiles, as can be seen from the example shown in Fig. 11, where the downstream profile station is probably close to separation. If the predicted profile is displaced outwards by an arbitrary amount, as in the dotted curve, the fit is more

* *cf.*, Fig. 7, where the most downstream profile is measured a little upstream of separation.

reasonable. It is not clear, however, why this displacement should be necessary when Seddon's separation profile and those of the experiments of Section 3 of this Paper can be fitted quite well without any such displacement. There is presumably some effect of curvature at work, and a tentative explanation of it will be advanced in Section 4, where it will be seen that the effect may be of considerable significance in affecting the conditions for separation on curved surfaces.

Michel's results[9], also obtained on a convex surface, show what at first sight appear to be 'fuller' profiles under the shock. This, incidentally, led Michel to conclude that separation was not taking place under the shock, since he assumed in effect that for separation to occur the shape parameter H must reach a value typical for separation with fairly gentle pressure gradients. This is not true, as has been pointed out above, if by separation we mean that the skin friction becomes zero, and separation in this sense may well be taking place under the shock in some of Michel's tests. It is not possible to make a direct comparison between Michel's results and those of the present theory, or between his results and those of Ackeret as typified by Fig. 11, because Michel's work was done on a bump on a tunnel wall. This meant that the boundary layer just upstream of the region of interaction consisted of a thin inner layer inside the remnants of the thick upstream layer, and hence the upstream profile cannot be well represented by a power law.

To sum up, it seems that in the main, for flat surfaces, the theory of the present section predicts the general shape of the profiles quite well, and may give some idea of the skin friction. This is provided that the departure from the initial upstream shape of the profile is not too extreme, and provided also that the pressure distribution is of the general shape envisaged by the theory. Thus there must be an initial region of zero gradient (or of favourable gradient, which can be regarded as, in effect, a shorter length of zero gradient[6,7]), followed by fairly sharp adverse gradients. The theory would not work, therefore, in cases where there are adverse gradients right from the leading edge. This restricts the application of the theory as compared with other methods. All these other methods, however, seem to involve empirical constants, whereas the present method does not, and this may be considered a point in its favour, additional to the advantage of its simplicity.

It is of incidental interest that the method even gives results of the right order of magnitude for laminar layers, if we put $K = 1$, as will be shown in an Appendix to this Paper. It is also worth noting that the present method, in its use of the mass-flux relation (18), has affinities with the method of Crocco and Lees[10], though the present method is very much simpler.

2.4. *The Interaction Between the Boundary Layer and the Simple-Wave External Flow Upstream of the Shock.* In Equations (18) and (20) the terms on the right involving $(d\delta/dx)_a$ may be neglected upstream of the shock and the edge of the boundary layer, $y = \delta$, is therefore a streamline. The relation for δ is

$$\delta = \frac{\left[(K+3)\frac{M_e^2}{M_1^2} - 2\right]}{\left[(K+3)\frac{M_e^2}{M_1^2} - 3\right]} \frac{K}{K+1} \cdot \frac{M_1}{M_e} \left(\frac{1 + \frac{\gamma-1}{2} M_e^2}{1 + \frac{\gamma-1}{2} M_1^2} \right)^{\gamma/2(\gamma-1)} \delta_a , \tag{28}$$

from (21) and (18). If $\delta/\delta_a \equiv r$ and $X \equiv x/\delta_a$, x being the distance along the surface in the stream direction measured from the sonic point under the shock, it follows from Equation (3) that

$$\frac{dr}{dX} = \frac{2(M_1^2-1)^{3/2}}{3(\gamma+1)M_1^2} [1 - (2k-1)^{3/2}] . \tag{29}$$

Hence

$$X = \frac{3(\gamma+1)M_1^2}{2(M_1^2-1)^{3/2}} \int_{0\cdot5}^{k} \frac{(dr/dk)dk}{1-(2k-1)^{3/2}},$$

or

$$-X = \frac{3(\gamma+1)M_1^2}{2(M_1^2-1)^{3/2}} \left\{ r_{0\cdot5} - \frac{r}{1-(2k-1)^{3/2}} + \int_{0\cdot5}^{k} \frac{3(2k-1)^{1/2} r dk}{[1-(2k-1)^{3/2}]^2} \right\},$$

where $r_{0\cdot5}$ is r at $k = 0\cdot5$. This may easily be evaluated numerically to give X as a function of k upstream of the shock, since r is given as a function of k from Equations (28) and (2). Calculated results are given in the following Table:

Case	$-X$ for k equal to				
	0·5	0·6	0·7	0·8	0·9
$M_1 = 1\cdot1$, $K = 5$	0	0·45	1·18	2·04	3·89
$M_1 = 1\cdot2$, $K = 5$	0	0·78	1·49	2·11	3·10
$M_1 = 1\cdot3$, $K = 5$	0	1·20	1·92	2·52	3·18
$M_1 = 1\cdot1$, $K = 7$	0	0·23	0·68	1·13	2·62
$M_1 = 1\cdot2$, $K = 7$	0	0·36	0·76	1·15	1·65
$M_1 = 1\cdot3$, $K = 7$	0	0·45	0·90	1·24	1·53

For the case $M_1 = 1\cdot3$, $K = 7$, $-dr/dk$ is slightly negative for $k = 1$, though it becomes positive for k less than about 0·9. Thus the boundary layer is predicted to decrease in thickness initially with rising pressure, rather than to increase, and the integration of the above equation for X becomes impossible for values of k close to 1. In the terminology of Crocco and Lees[10], the boundary layer is 'supercritical'. The source of the trouble is the assumption that the pressure is constant across the boundary layer. With the higher Mach numbers and 'fuller' boundary-layer profiles a considerable part of the flow in the boundary layer is supersonic, and supersonic stream tubes tend to contract on encountering a rise in pressure. In reality however the pressure is not constant across the boundary layer, but tends to be constant along Mach lines in the outer part of the layer, and this is why the solution fails upstream. Where the local Mach number at the edge of the layer has fallen, however, the pressure is likely to vary less across the layer, and the solution for X as a function of k as given in the above Table should then be applicable.

2.5. *The Interaction Downstream.* The downstream solution has necessarily to be crude, because of the complexity of the equations and the boundary conditions. The procedure we adopt is to choose a suitable mathematical form for the distribution of k in the x, $\bar{y}$ plane downstream of the shock. This distribution has a number of disposable constants which are chosen by making the distribution fit various integral conditions derived from the equations and the boundary conditions.

From Equation (15), since $\alpha \to 0$ as $x \to \infty$,

$$\alpha_d = -\frac{2(M_1^2-1)^{3/2}}{(\gamma+1)M_1^2} \int_0^{\infty} \frac{\partial k}{\partial \bar{y}} dx,$$

where α_d is the flow angle immediately downstream of the shock, assumed to lie along the line $x = 0$. Hence from Equation (9)

$$k_d^{1/2}(1-k_d) = -\int_0^{\infty} \frac{\partial k}{\partial \bar{y}} dx.$$

If we integrate this equation from $\bar{y} = 0$ to $\bar{y} = \infty$, where $\bar{y} = 0$ is at a distance from the wall equal to the thickness of the boundary layer at $x = 0$, it follows that

$$\int_0^\infty [k^{1/2}(1-k)]_{x=0}\, d\bar{y} = \int_0^\infty (k)_{\bar{y}=0}\, dx, \tag{30}$$

since $k \to 0$ as $\bar{y} \to \infty$, where the pressure approaches the full theoretical pressure behind a normal shock in inviscid flow. The line $\bar{y} = 0$ is, strictly speaking, within the boundary layer downstream of the shock, but it approximates near enough to the edge of the boundary layer.

Similarly by doubly integrating the equation of motion (13) with respect to x and $\bar{y}$ from $x = 0$ to ∞ and from $\bar{y} = 0$ to ∞ we obtain

$$-\int_0^\infty \left(\frac{\partial k}{\partial \bar{y}}\right)_{\bar{y}=0} dx = \int_0^\infty \left[(1-2k)\frac{\partial k}{\partial x}\right]_{x=0} d\bar{y}. \tag{31}$$

The two sides of Equation (31) are equal to $[(\gamma+1)M_1^2/2(M_1^2-1)^{3/2}](\alpha)_{x=\bar{y}=0}$, and this is equal to $\frac{1}{3}$, from Equation (3). Hence

$$-\int_0^\infty \left(\frac{\partial k}{\partial \bar{y}}\right)_{\bar{y}=0} dx = \frac{1}{3}. \tag{32}$$

From Equation (29)

$$\left(\frac{\partial k}{\partial x}\right)_{x=\bar{y}=0} = \frac{2(M_1^2-1)^{3/2}}{3(\gamma+1)M_1^2\delta_a(dr/dk)_{k=0.5}} \equiv -\frac{V}{\delta_a}. \tag{33}$$

Finally from Equation (15)

$$-\int_0^\infty \int_x^\infty \left(\frac{\partial k}{\partial \bar{y}}\right)_{\bar{y}=0} dx\, dx = \frac{(\gamma+1)M_1^2\Delta}{2(M_1^2-1)^{3/2}} \equiv W\delta_a, \tag{34}$$

where Δ is the effective displacement of the external flow away from the wall due to the boundary-layer growth between the shock and downstream. We may take this to be roughly given by

$$\Delta = \frac{n_m}{n_m+1}\,\delta_m - \frac{K}{K+1}\left[\delta_a + (x_m - x_a)\left(\frac{d\delta}{dx}\right)_a\right], \tag{35}$$

where suffix m denotes some downstream station where the pressure has almost reached its maximum value, which is the full downstream pressure. The term $n_m\delta_m/(n_m+1)$ here is approximately the displacement thickness at station m, and the term which is subtracted from it on the right-hand side is approximately what the displacement thickness would be at this position if there were no shock. Far downstream the displacement thickness behind the shock should grow at much the same rate as if there were no shock, so Δ should tend to a roughly constant value. Strictly (35) represents the effective displacement over the whole region of interaction, and not just between the shock and downstream, but the increase of displacement thickness up to the shock is usually fairly small compared with Δ as given by (35).

The distribution we assumed for k is

$$k = \frac{(e^{-x/A} + ze^{-x/B})}{2(1+z)}\left\{\left(1+\frac{\bar{y}}{C}\right)\left(1-\frac{x}{D}\,e^{-x/E}\right)e^{-\bar{y}/C} + \frac{x}{D}\,e^{-x/E}e^{-\bar{y}/F}\right\} \tag{36}$$

where z, A, B . . . F are constants. This makes $k = \frac{1}{2}$ at $x = y = 0$, satisfying the condition that the pressure is sonic at the foot of the shock, $k \to 0$ as x, $\bar{y} \to \infty$, satisfying the boundary conditions at infinity, and $\partial k/\partial \bar{y} = 0$ at $x = \bar{y} = 0$. This latter condition follows from (15) and (29) if we make $\partial\alpha/\partial x$ at the edge of the boundary layer continuous at $x = 0$. The assumed distribution (36) also takes

relatively simple and convenient forms along the lines $x = 0$ and $\bar{y} = 0$, *i.e.*, along the lines which roughly coincide with the shock and the edge of the boundary layer. We arbitrarily assume $z = \frac{1}{4}$ and $E = A/4$. Then at $x = 0$

$$k = \frac{1}{2}\left(1 + \frac{\bar{y}}{C}\right) e^{-\bar{y}/C}$$

and

$$\frac{\partial k}{\partial x} = -\frac{e^{-\psi/F}}{2D} - \left(\frac{1}{2D} + \frac{4}{10A} + \frac{1}{10B}\right)\left(1 + \frac{\bar{y}}{C}\right) e^{-\bar{y}/C},$$

whilst at $\bar{y} = 0$

$$k = \frac{1}{10}(4e^{-x'/A} + e^{-x/B})$$

and

$$\frac{\partial k}{\partial \bar{y}} = -\frac{(4e^{-x'/A} + e^{-x/B})xe^{-4c/A}}{10DF}.$$

If $B < 0{\cdot}1A$, say, an assumption justified *à posteriori*, Equation (30) approximates to

$$C = 0{\cdot}222A.$$

Equation (32) approximates to

$$\frac{4A^2}{250DF} = \frac{1}{3},$$

and Equation (34) becomes

$$\frac{8A^3}{1250DF} = W\delta_a.$$

Hence

$$A = 7{\cdot}5W\delta_a, \quad C = 1{\cdot}67W\delta_a, \quad \text{and} \quad \frac{1}{D} = \frac{F}{2{\cdot}7W^2\delta_a{}^2}.$$

From (33)

$$\frac{1}{10B} = \frac{V}{\delta_a} - \frac{4}{10A}.$$

Also from (31) and (32)

$$\frac{F^3}{2D(F+C)^2} - \frac{3C}{4}\left(\frac{1}{2D} + \frac{1}{10A} + \frac{1}{10B}\right) = \frac{1}{3}.$$

Hence, if $F = \bar{F}\delta_a$,

$$\frac{\bar{F}^4}{5{\cdot}4W^2[\bar{F} + 1{\cdot}67W]^2} - 0{\cdot}232\frac{\bar{F}}{W} - 1{\cdot}25WV = 0{\cdot}333.$$

Thus all the coefficients may be found if V and W are known. Equation (28) gives V, and W may be found roughly from Equations (18) and (20). In Equation (20) we crudely approximate the integral term on the right-hand side at the downstream station m by

$$\tfrac{1}{2}(x_m - x_a)\left\{\left(\frac{1}{M_1}\right)^3\left(\frac{1 + \frac{\gamma-1}{2}M_1{}^2}{1 + \frac{\gamma-1}{2}}\right)^{(\gamma+1)/2(\gamma-1)} + \left(\frac{M_2}{M_1}\right)^3\left(\frac{1 + \frac{\gamma-1}{2}M_1{}^2}{1 + \frac{\gamma-1}{2}M_2{}^2}\right)^{(\gamma+1)/2(\gamma-1)}\right\}\left(\frac{d\delta}{dx}\right)_a,$$

where M_2 is the Mach number downstream of a normal shock in inviscid flow with upstream Mach number M_1. The justification for this approximation is that M_e varies between 1 and M_2 downstream

of the shock. We assume various trial values for $\{(x_m - x_a)/\delta_a\}(d\delta/dx)_a$. Then (18) and (20) give n_m and δ_m/δ_a, and (35) gives Δ and hence W. From Equation (25)

$$\left(\frac{d\delta}{dx}\right)_a \simeq 0{\cdot}30 R_a^{-1/5},$$

and for a typical value $R_a = 2 \times 10^6$, $(d\delta/dx)_a \simeq 0{\cdot}017$. We assume $x_m - x_a \simeq 2A = 15W\delta_a$, because at $\bar{y} = 0$, $k = 0{\cdot}4e^{-x/A} + 0{\cdot}1e^{-x/B} \simeq 0{\cdot}4e^{-x/A}$ far away from the shock, since $B \ll A$, and when $x = 2A$ conditions will approach fairly closely their ultimate downstream values. Hence

$$\frac{x_m - x_a}{\delta_a}\left(\frac{d\delta}{dx}\right)_a \simeq 0{\cdot}26W.$$

If this does not agree with the original trial value, another value is chosen, and so on until the correct value is found. The coefficients in the distribution (36) for k can then be found, and the following Table gives some calculated results:

M_1	1·1	1·2	1·3	1·1	1·2	1·3
K	5	5	5	7	7	7
A/δ_a	19·5	23·8	36·7	11·7	13·1	17·2
B/δ_a	0·71	1·07	1·79	0·40	0·53	0·53
C/δ_a	4·34	5·31	8·17	2·60	2·92	3·82
D/δ_a	1·60	1·96	3·12	0·95	1·08	1·37
F/δ_a	11·4	14·0	20·7	6·9	7·6	10·3
B/A	0·036	0·045	0·049	0·034	0·040	0·031

It can be seen that in all cases $B < 0{\cdot}1A$, as assumed in the analysis above.

2.6. *General Remarks on the Solution and the Prediction of Separation.* Corresponding to the tabulated results of Sections 2.4 and 2.5, Figs. 12 to 17 show some calculated distributions of $1 - k$ (proportional to the pressure rise) as a function of $X = x/\delta_a$. It can be seen that the pressure distribution at the wall has the general form sketched in Fig. 2. The reasons for the pressure gradients becoming infinitely steep upstream with $K = 7$, $M_1 = 1{\cdot}3$, have already been pointed out, in Section 2.4. Although the gradients do not of course become infinite in reality, it is not unreasonable that the theory should predict that the position of maximum pressure gradient occurs upstream of the sonic point at the higher Mach numbers, whereas at $M_1 = 1{\cdot}1$ it occurs at the sonic point. Extrapolating this predicted trend in the pressure gradients to still higher Mach numbers, we see that we can expect the 'kink' pressure p_b, at the point of maximum curvature on the pressure distribution, to decrease as M_1 is increased. This indeed appears to be the case for the $K = 5$ results of Figs. 12, 13, and 14, though the predicted shape of the pressure distribution just downstream of the sonic point is sensitive to the arbitrary assumption made concerning z in Equation (36), and hence not much importance can be attached to p_b as deduced from Figs. 12 to 17. The falling off in p_b becomes marked when extensive separation occurs, though then the flow pattern resembles Fig. 3 rather than Fig. 2, and the theory breaks down, partly because the shock is assumed to lie close to the line $x = 0$, passing through the point of sonic pressure at the edge of the boundary layer. Seddon's results[4] show that in fact at high Mach numbers M_1 there is a 'supersonic tongue' just outside the boundary layer extending well downstream of the shock. Also, as we have seen in Section 2.3, when there is considerable separation, the boundary-layer profiles are not well represented by the simple power-law family assumed in the theory.

The way in which the boundary layer is predicted to thicken through the region of interaction is shown in the following Table:

M_1	1·1	1·2	1·3	1·1	1·2	1·3
K	5	5	5	7	7	7
δ_s/δ_a	1·056	1·126	1·232	1·033	1·064	1·102
δ_m/δ_a	1·83	2·33	3·55	1·50	1·74	2·28

Here δ_s is the boundary-layer thickness at the point of sonic pressure, under the lower end of the shock, and δ_m is the thickness at the downstream station near the pressure maximum, as discussed in Section 2.5 above. It should be borne in mind that the boundary-layer thickness downstream continues to increase with increasing distance from the shock, due to the normal 'flat plate' boundary-layer growth, so δ_m has no precise significance. For a given Mach number M_1 the length of the interaction region as a multiple of the boundary-layer thickness δ_a is roughly proportional to $\delta_s/\delta_a - 1$ or to $\delta_m/\delta_a - 1$, which increase as K is decreased. However, although $\delta_s/\delta_a - 1$ and $\delta_m/\delta_a - 1$ are much bigger for $M_1 = 1{\cdot}3$ than for $M_1 = 1{\cdot}1$, the length of the interaction region does not vary as much with Mach number. This is because the maximum flow angles α at the edge of the boundary layer are smaller at the lower Mach numbers, the maximum value of α varying as $(M_1^2 - 1)^{3/2}$. Hence at the lower Mach numbers it still takes quite a long interaction region to accommodate a relatively small increase in boundary-layer thickness.

Just behind the shock the pressure at a sufficient distance from the wall in Figs. 12 to 17 becomes close to the full downstream pressure behind a normal shock, but the gradient of pressure is initially falling. This is because the stream tubes must contract to be consistent with the streamlines being roughly parallel to the wall a long way from it, and inclined with a positive slope at the edge of the boundary layer. This tendency for there to exist regions where the pressure falls in the streamwise direction only operates downstream of the shock. Upstream, the contraction of the stream tubes outside the boundary layer due to the latter's thickening is consistent with positive pressure gradients everywhere, because in supersonic flow stream tubes contract on encountering a rise of pressure. Thus it seems intuitively reasonable that the average pressure gradients downstream of the shock should be less than those upstream. This is reinforced by the fact that the boundary layer thickens much more downstream of the point of sonic pressure than upstream of it, since its thickness is a non-linear function of pressure.

Figs. 12 to 17 also show the skin-friction distributions calculated from Equation (24) for $R_a = 1 \times 10^6$ and 5×10^6. The large negative values at $M_1 = 1{\cdot}3$ are probably unrealistic, but the general shape of the distributions is reasonably consistent with the experiments of Section 3. Separation is indicated at a Mach number M_1 of about 1·2 for the 1/7th power profiles, and rather less for the 1/5th power profiles. These figures are of the right order. Stratford's criterion (26) would seem to indicate rather lower values for M_1 giving separation, as can be seen from the following Table:

M_1	1·1	1·1	1·1	1·1	1·2	1·2	1·2	1·2	1·3	1·3	1·3	1·3
k	0·8	0·6	0·5	0·4	0·8	0·6	0·5	0·4	0·8	0·6	0·5	0·4
L.H.S. of (26), $K = 7$	0·014	0·050	0·059	0·042	0·045	0·118	0·140	0·106	0·088	0·175	0·228	0·164
L.H.S. of (26), $K = 5$	0·029	0·075	0·076	0·065	0·072	0·121	0·127	0·132	0·107	0·147	0·143	0·109

The right-hand side of (26) is equal to 0·116 if $\beta = 1$ and 0·077 if $\beta = 0{\cdot}66$, the value deduced from experiment by Stratford. This latter value of β would lead to the conclusion that separation occurs with M_1 not much above 1·1, which is too low. It may be, of course, that the pressure gradients predicted by the present theory are too steep. However, they enter Equation (26) only in a square-root form, and the gradients would have to be reduced to about $\frac{1}{4}$ of their theoretical values to make separation occur at $M_1 = 1{\cdot}2$ according to Equation (26) with $K = 7$ and $\beta = 0{\cdot}66$. The experiments of Section 3 do not suggest that the theoretical gradients are in error by as much as this. It may be that, despite the indications of Equation (24) that incompressible separation formulae can be used in cases with compressibility if C_p is interpreted as $1 - M_e^2/M_1^2$, there is in fact some compressibility effect present, and this takes the form of increasing the effective value of β in Stratford's formula. More will be said about this, however, in Section 4.

3. *The Experiments on Normal Shocks in a Pipe.* 3.1. *Description of the Apparatus.* A small blow-down tunnel was specially constructed for investigating normal shocks. The working section was a perspex pipe 25 in. long, tapering linearly between internal diameters of 5 and 5·3 in. at the upstream and downstream ends respectively. In its original form the arrangement was as shown in Fig. 18. Downstream of the main tunnel contraction there was a perforated section. By adjusting the tunnel stagnation pressure so that the pressure within this section was greater than atmospheric, air was made to blow out of the perforations into the room, so that the boundary layer formed in the main contraction was removed and the boundary layer at the entrance to the pipe was very thin. The entrance to the pipe formed a 'throat', and supersonic flow was developed in the pipe. At about half way along, where there were pressure tappings, the Mach number was about 1·25. To obtain lower Mach numbers at this position a wooden fillet could be fitted into the pipe as in Fig. 18. A normal shock could be made to occur at any desired position in the pipe by suitably positioning a cone which choked the exit to the working section.

This axially-symmetrical arrangement was chosen in preference to forming a normal shock on a flat plate in a conventional wind tunnel partly because a suitable tunnel was not conveniently available, and partly because it was felt that the interaction on a flat plate would suffer from undesirable interference effects arising in the side-wall boundary layers. However, the present arrangement was also found to have serious disadvantages, as discussed later.

In the original version of the tunnel, shown in Fig. 18, pitot- and static-pressure measurements in the stream were made with tubes which could be traversed across the pipe, but not axially. To make axial traverses through the shock, the latter was moved along the pipe relative to the pressure probe.

The perforated section was subsequently modified to the form shown in Fig. 19, with the minimum-area section at the perforations. The throat was thus formed here. By raising the stagnation pressure so that more air was blown out of the perforations the effective throat area could be reduced, so raising the Mach number of the flow entering the pipe. Thus the arrangement formed a primitive variable Mach number tunnel. To mitigate the abrupt changes of flow angle at the upstream and downstream ends of the perforated part, the ends were made in a saw-tooth form, as shown in Fig. 19. With this arrangement the Mach number at the middle part of the pipe could be varied between about 1·26 at 20 p.s.i. gauge stagnation pressure and 1·34 at 40 p.s.i. stagnation pressure. A further group of pressure tappings was inserted nearer to the upstream end of the pipe: at these tappings the corresponding Mach numbers were about 1·15 at 20 p.s.i. and 1·27 at 40 p.s.i. However, Mach numbers in between 1·15 and 1·27 could not conveniently be obtained because

weak oblique shock waves caused by the crudity of the effective tunnel 'nozzle' impinged on the upstream measurement station at stagnation pressures intermediate between 20 and 40 p.s.i.

The arrangements for making boundary-layer traverses were also improved for the later experiments. A brass tongue was made to fit into the Perspex pipe as in Fig. 20, and traverses could be made through this tongue at a number of positions along it. The traverse position could readily be altered by removing the tongue from the tunnel, pulling out the pitot tube, and moving the actuating micrometer. Thus the tube could be removed without taking the whole working section to pieces, as was necessary with the earlier arrangement of Fig. 18, and the shock did not need to be moved axially in order to make pitot traverses upstream and downstream of it. There were a number of static-pressure holes in the brass tongue. For determining skin friction two of these holes, one in the upstream measurement region and the other in the downstream, were covered by small pieces of razor blade, as in Fig. 21. These formed Stanton tubes, of the simple and convenient type first used by Hool[11], and they measured the pitot pressure much closer to the wall than was possible with a conventional pitot tube. By comparing the Stanton-tube readings with those of the same pressure holes with the shock in the same position when the razor blades were removed, the skin friction could be estimated.

For the measurement of static pressure in the stream, static tubes of the conventional type were unsuitable, since they would give false readings close behind a shock when the tip of the tube protruded through the shock whilst the holes were behind it. Hence a tube of the wedge-shaped type shown in Fig. 22 was used. This was proposed by Girerd and Guienne[12] for use in low-speed flow. Its advantage is that it is very insensitive to yaw in the plane of the front edge of the wedge and the tube axis. Fig. 22 shows that it is also suitable for use at transonic speeds where it is still insensitive to yaw and also fairly insensitive to incidence up to $\pm$ 3 deg in the plane at right angles to the apex of the wedge. The tube does not measure the true static pressure at all Mach numbers, of course, but the calibration curve is smooth and nowhere has it any very steep gradients, as do the calibration curves of most other kinds of tube at Mach numbers close to 1.

3.2. *Results obtained.* Figs. 23 and 24 show results obtained with the earlier arrangement of the tunnel, when detailed static-pressure surveys were made in the stream. The values of k shown in these figures have been computed from Equation (1), so that $k = 0{\cdot}5$ does not exactly correspond to the sonic pressure. The results of Fig. 23 were obtained with a wooden fillet in the tube, as in Fig. 18, to reduce the Mach number. It can be seen that well away from the wall the pressure rises much more steeply than at the wall. Probably in fact the pressure rise well away from the wall through the shock is virtually discontinuous, but the non-zero size of the static probe and the slight unsteadiness in shock position somewhat 'smear out' this abrupt rise. But for these factors it seems likely that the pressure behind the shock at 2 in. from the wall would be equal to the full theoretical pressure behind a normal shock, as indicated by the dotted lines in Figs. 23 and 24. This high pressure is followed by a fairly sharp fall in pressure. In this the experimental findings resemble those of the theory, as can be seen from Figs. 12 to 17. However, in the experiment the pressures become virtually uniform across the pipe at about 10 boundary-layer thicknesses downstream of the shock, and this uniform pressure is considerably below the theoretical pressure behind a normal shock. This is because the boundary layer thickens on passing under the shock, so reducing the effective area of the pipe downstream, and hence reducing the downstream pressure. Once the pressure has become uniform across the pipe, it gradually rises with distance along the pipe, due

to the slight taper of the pipe. In a case with an infinite uniform stream the pressure could not become uniform along lines perpendicular to the wall until the full normal-shock downstream pressure had been reached. Hence the external flow downstream is essentially different in the pipe experiments from what it would be in the infinite-stream case. The fact that in Figs. 23 and 24 the full normal-shock downstream pressure is achieved closer to the wall just behind the shock than in Figs. 12 to 17 is accordingly no proof that the theory is wrong in this respect.

Despite the differences in the external flow it may be that the constraint effect of the finite diameter of the pipe does not completely alter the pressure distribution at the wall. Figs. 12 to 17 compare reasonably well in this respect with Figs. 23 and 24, and also with Figs. 25 to 28. These latter figures show distributions obtained with the later arrangement of the tunnel, when the primary object was to measure skin friction, as will be discussed below. Meanwhile, reverting to the pressure distributions at the wall, we should expect these to be broadly comparable with those predicted by the theory at least up to the sonic point. However, the flow in the pipe may be said to have a 'coaxial character', in the sense that the surfaces of constant pressure, velocity, etc., in the fluid are all coaxial with the pipe axis, and thus have transverse curvature. This somewhat affects the simple-wave character of the external flow upstream of the shock, a point which is discussed further in Section 3.3. The following table compares the pressure gradients predicted by the theory with those found experimentally at the point where $k = 0{\cdot}75$, *i.e.*, where the pressure is half way between its value just upstream of the region of interaction and the sonic pressure.

Theory:	M_1	1·1	1·2	1·3	1·1	1·2	1·3
	K	5	5	5	7	7	7
	$-dk/dX$	0·18	0·15	0·14	0·27	0·26	0·30
Experiment:	Fig. No.	23	24	25	26	27	28
	M_1	1·12	1·25	1·15	1·27	1·26	1·34
	δ in.	0·138	0·165	0·12	0·10	0·19	0·17
	K	7	6	7	8	8	8
	$-dk/dX$	0·14	0·17	0·16	0·13	0·17	0·16

The theoretical value for $-dk/dX$ with $M_1 = 1{\cdot}3$, $K = 7$, is too high, due to the neglect of pressure variations across the boundary layer, leading to infinite gradients being predicted upstream for this case. For the same reason, all the other predicted pressure gradients are probably somewhat too high. The experimental values for $-dk/dX$ are probably too small, because the unsteadiness of the shock would tend to reduce the pressure gradients measured at the wall where the gradients are steep. Moreover, the coaxial character of the flow would be expected to reduce the pressure gradients slightly, as is discussed below. Hence, though the measured pressure gradients are in most cases roughly a half what would be expected from the theory, the discrepancy is probably considerably less in reality.

The values of δ and K in the table above giving the experimental pressure gradients were obtained by fitting curves of the form $u/u_e = (y/\delta)^{1/K}$ to the boundary-layer profiles measured ahead of the region of interaction. The pitot traverses determine the Mach number distributions through the boundary layer as shown in Figs. 23 and 24, and from these the velocity distributions can be deduced by assuming the total temperature to be constant across the boundary layer. From the power-law profile fitted to the measurements just upstream of the region of interaction the skin friction can be

calculated. Thus we assume that a flat plate with turbulent flow from the leading edge $\delta = 0{\cdot}38lR_e^{-1/5}$ at a distance l from the leading edge. This is a reasonably accurate formula up to moderate supersonic Mach numbers. Hence from the momentum equation

$$C_f = 0{\cdot}477\frac{\theta}{\delta}R_\delta^{-1/4}. \tag{37}$$

Here R_δ is the Reynolds number based on free-stream conditions and the length δ, and θ/δ, the ratio of the momentum thickness to the total thickness of the boundary layer, is a function of the power-law index K and of M_1, the free-stream Mach number. The numerical values of θ/δ are given in Ref. 13. The skin friction may also be deduced from the Stanton-tube readings. Since the Mach number is not much above 1, the calibration of the Stanton tube is not greatly affected by compressibility, and under these circumstances it is shown in Ref. 14 that the skin friction is given by

$$C_f = \frac{1{\cdot}77.10^{-2}}{M_e^2}\left(\frac{30}{p}\right)^{2/3}\left(\frac{\Delta p}{pd}\right)^{2/3}, \tag{38}$$

where p is the static pressure in inches of mercury absolute, Δp, in inches of mercury, is the excess pressure over the static pressure, recorded by the Stanton tube, and d is the Stanton-tube height in thousandths of an inch. It is assumed that the wall temperature is atmospheric, as was the case in the present experiments. For the razor-blade type of tube used, d is the height of the sharp edge above the surface as in Fig. 21, and it was 3·2 thousandths of an inch for the forward tube and 2·8 for the rear one. The two estimations of skin friction just ahead of the region of interaction agree quite well, as can be seen from the table:

Fig. No.	25	26	27	28
M_1	1·15	1·27	1·26	1·34
C_f, Equation (37)	0·0023	0·0020	0·0019	0·0017
C_f, Equation (38)	0·0021	0·0017	0·0021	0·0016

Thus we can place considerable confidence in the Stanton-tube measurements of skin friction upstream of the region of interaction.

The variation in skin friction under the shock wave is shown in Figs. 25 to 28. It can be seen from a comparison with Figs. 12, 13, 15 and 16 that for the lower Mach numbers the theory predicts a variation broadly similar to that found experimentally, though for $M_1 = 1{\cdot}3$, in Figs. 14 and 17, the skin friction is predicted to become much too markedly negative. This is probably because the theory does not predict the shape of the boundary-layer profiles accurately within a region of separation. In such a region, therefore, there are likely to be serious errors in the estimated skin friction, which is very sensitive to small errors in the predicted distributions of the boundary-layer momentum thickness θ and the shape parameter H, though the thickening of the boundary layer may be predicted well enough for the estimation of the pressure distributions. The theory has been worked out for Reynolds numbers R_a, based on the distance from the leading edge to station 'a', of 10^6 and 5×10^6, but the results are not very sensitive to variations in R_a. For the experimental cases effective Reynolds numbers R_a may be defined as equal to $3{\cdot}35R_{\delta a}^{5/4}$, which follows from Equation (25), and the values for Figs. 25 to 28 respectively are 7·0, 10·0, 12·7 and 19·3 times 10^6.

In Figs. 27 and 28, separation is almost certainly taking place, though the skin friction as deduced from Equation (38) does not fall quite to zero, but only becomes very small. As is discussed below, however, any reversed-flow region that there may be must certainly be extremely thin, so that the

reverse-flow velocities must be very low. Hence any 'base pressure' effect, tending to make the forward-facing Stanton tube read lower than the static pressure, will be very small, and will probably be outweighed by a small rise of pressure associated with the displacement away from the wall of the outer, downstream-moving streamlines, as sketched in Fig. 21. Even in the light of this process it does not at first sight appear that separation is occuring in Fig. 26, at the upstream set of pressure tappings, yet this case should be closely equivalent to Fig. 27, at the downstream set of tappings, because M_1 was about the same for the two cases and the upstream profiles were both roughly of the 1/8th power form. However, the results of Fig. 26 are probably somewhat anomalous because with this case there were appreciable spanwise variations of pressure, indicating that the plane of the shock was not quite normal to the tunnel axis. This presumably was due to the crudity of the nozzle. The results of Fig. 25 should be more reliable because the spanwise variations of pressure were much less. This case appears to be not too far from separation. If we accept the theoretical results of Figs. 15 and 16 as being a valid guide to the rate at which the minimum value of C_f/C_{fa} decreases with increasing M_1 until separation occurs, we can tentatively infer from Fig. 25 that separation first occurs when M_1 reaches a value of about $1 \cdot 21$.

Oil-flow measurements suggested that the cases of Figs. 26, 27 and 28 were separated but that the case of Fig. 25 was not. For these observations a thin layer of pigment-containing oil was smeared onto the surface. Where the skin friction was large the oil was teased out into filaments moving in the downstream direction, but immediately under and just behind the shock it remained unmoved at the larger values of M_1. A thick application of oil showed some movement under the shock even at the highest Mach numbers. Wavelets appeared in the oil with their fronts at right-angles to the flow direction, and these wavelets moved slowly downstream. This might happen even though the air in contact with the oil exerts a zero frictional force on it, or even a small frictional force in the upstream direction. If any irregularity in thickness of the oil layer arises, the consequent distortion of the streamlines in the downstream-moving part of the boundary layer, as sketched in Fig. 29, probably gives rise to pressure forces sufficient to move the wavelet downstream. A thinly-applied layer of oil cannot hump up into wavelets, and so remains unmoved in regions of separation. However, it is very difficult to determine exactly when, with increasing Mach number M_1, some of the oil is first brought to rest. It is thus difficult to determine exactly, either by the oil technique or by Stanton-tube measurements, what is the minimum Mach number M_1 for separation to occur. The value suggested above, $M_1 = 1 \cdot 21$ for the pipe experiments, is far from precise.

Of course, when separation is only incipient and therefore difficult to detect, as discussed above, it does not have any important practical effects. Nevertheless, it is of considerable interest to determine the conditions for incipient separation, because they represent a lower bound to the conditions which give rise to the important effects of well-developed separation.

As mentioned above and discussed in more detail in Section 3.3 the coaxial character of the flow probably reduces the instantaneous pressure gradients. The average gradients as measured are also reduced by the shock oscillation. Presumably the separation point oscillates with the shock: this, incidentally, would be a further reason for the Stanton tube to read too high a pressure at separation when the extent of the separated region is very small. However, the oscillation is probably not rapid enough to make the conditions for separation differ significantly from what they would be with a steady pressure gradients equal to the instantaneous values. Separation probably first occurs somewhere near the point of sonic pressure, and here the analysis of Section 3.3 suggests that the coaxial character of the flow decreases the instantaneous pressure gradients by about 19 per cent, as

compared with a flat-plate case with the same upstream Mach number M_1. Hence Stratford's separation criterion (26) suggests that $M_1^2 - 1$ for the first occurrence of separation is probably increased in the pipe by roughly 10 per cent, so that separation at $M_1 = 1{\cdot}21$ in the pipe would correspond to separation at about $M_1 = 1{\cdot}19$ on a flat plate. Equation (24) would similarly suggest $M_1 \doteq 1{\cdot}19$ for the equivalent flat-plate separation. This sort of figure for the minimum M_1 for separation is consistent with Figs. 12 to 17, which suggest that separation first occurs at $M_1 \doteq 1{\cdot}20$ for $K = 7$ in the upstream power-law profile, and at $M_1 \doteq 1{\cdot}16$ for $K = 5$. For Fig. 25, from which the figure of $M_1 = 1{\cdot}19$ has been inferred, the approximate value of K is 7.

The experimental results of Fig. 25 suggest that under conditions of incipient separation, the separation point will be somewhere near the position of sonic pressure, and that the skin friction will become positive again downstream. This is in line with Equation (24), because the multiplier of dM_e/dx on the right-hand side increases steadily as M_e decreases, *i.e.*, it is bigger for positions of higher pressure, but $-dM_e/dx$ itself becomes small in the downstream part of the interaction region. Hence the product is a maximum somewhere near the sonic point, and this is therefore where separation would first be expected to occur. This reasoning also suggests that the Mach number M_1 for which separation first occurs will not be much affected if the shape of the pressure distribution well downstream of the sonic point is distorted in any way. Such distortions may occur, for example, with a shock wave situated on an aerofoil, where the change of flow angle in the vicinity of the trailing edge will affect the flow well downstream of the shock, but it may not necessarily affect separation. If the surface has convex curvature in the stream direction, however, as is often the case on aerofoils, this does seem to have an important influence on the conditions for incipient separation, as is discussed in Section 4.

Figs. 30 and 31 show velocity profiles deduced from the Mach number profiles of Figs. 23 and 24. The upstream profiles have been fitted by power-law relations, and the downstream profiles then predicted by Equations (18) and (20). It can be seen that the predicted shapes downstream agree quite well with the experimental measurements, and this provides a further check on the validity of the theory. There is probably separated flow at the downstream profile position in the case of Fig. 31, but no sign of this appears in the profile. The experimental point nearest the wall was obtained with the pitot tube touching the wall, and the effective centre of the tube may well have been displaced here, so that the shape of the inner part of the measured profile may not be quite correct. However, it is clear that if there is a dead-air or reversed-flow region, it must be extremely thin. This is the reason for the small positive Stanton-tube readings and the behaviour of oil wavelets in separated regions, as discussed above. It is not possible to deduce the skin friction by trying to fit the measured velocity profile near the wall by a 'law of the wall' form. At the wall the rate of change of friction stress normal to the wall, $\partial\tau/\partial y$, is equal to the pressure gradient, dp/dx, and when the latter is very large, τ varies too violently with y for the 'law of the wall' to be applicable. Downstream of the very sharp pressure gradients, the profile probably remains distorted from the 'law of the wall' form for a considerable distance.

The region of compression-wave flow indicated in Fig. 2 is detected in the static-pressure traverses of Figs. 23 and 24, where at 0·5 in. from the wall the pressure rises much less abruptly under the shock than it does through the shock further from the wall. This effect is also shown in Figs. 32 and 33, which present the results of pitot traverses made upstream and downstream of the shock. The plotted quantity is $1 - p_T/H_0$, where p_T is the pitot pressure and H_0 the tunnel stagnation pressure. In a supersonic flow p_T is less than H_0 because of the total-head loss through the bow shock

of the pitot tube. For the fairly low supersonic Mach number of the present experiments, $1 - p_T/H_0$ is very small, but nevertheless it is clear that it is greatly reduced behind the inner part of the shock. This is to be expected because at the edge of the boundary layer the compression should, according to Fig. 2, be isentropic, with $p_T = H_0$ downstream of it, where the flow is subsonic. A little further from the wall the compression is achieved partly isentropically and partly through a weakened shock, so that the loss is still reduced. Well away from the wall the loss should be the same whether the pitot tube is behind the main shock or ahead of it, when it generates its own bow shock. The small differences between the upstream and downstream curves well away from the wall in Figs. 32 and 33 are due to the taper of the pipe and the method of measurement, moving the shock relative to the probe. When the shock was moved downstream, to obtain the distribution upstream of the shock, the Mach number immediately ahead of the pitot-tube bow shock was a little higher than that just ahead of the main shock when the latter was moved upstream. This was because the upstream position of the main shock was appreciably ahead of the pitot tube, at a position where the pipe diameter was smaller, by a small but significant amount, than the diameter at the plane of the pitot-tube mouth. The variations in pitot loss outside the boundary layer with distance from the wall upstream of the shock are due in the main to small variations of the stream Mach number across the pipe. However, the small dip in the upstream curves just at the edge of the boundary layer is probably due to the bow shock of the pitot tube interacting with the boundary layer, causing it to generate a small compression-wave region, as in Fig. 34, so reducing the pitot loss. When the pitot tube is moved right into the boundary layer, of course, the pitot loss becomes relatively very large, because of the frictional loss of total head.

The distances over which the isentropic effects of the compression-wave region associated with the main shock should be felt in Figs. 32 and 33 can be estimated from Figs. 23 and 24. Thus in Fig. 23 the upstream end of the interaction region is about 0·6 in. ahead of the sonic point. Hence the Mach wave from the upstream point, where $M_1 = 1{\cdot}12$, intersects the plane of the shock, (*i.e.*, according to Fig. 2 the vertical through the sonic point) at a distance of 0·6 cot [$\sec^{-1} 1{\cdot}12$] or 1·2 in. from the edge of the layer. The corresponding distance for the case of Figs. 24 and 33 is 0·7 cot [$\sec^{-1} 1{\cdot}25$] or 0·9 in. These distances agree very roughly with the distances over which the upstream and downstream curves of Figs. 32 and 33 differ significantly from each other, though the estimated distances may be slightly too large because the oscillation of the shock probably means that the measured upstream-influence distances are a little too large.

3.3. *Estimation of the Effects of the Coaxial Character of the Flow.* The fact that the compression-wave region extends over about an inch in the experiments, where the pipe radius is only about $2\frac{1}{2}$ in., raises the question as to how far the compression differs from the two-dimensional simple-wave type assumed in the theory of Section 2. This problem can be treated as follows.

Take co-ordinate axes x and r for the pipe as shown in Fig. 35. For the pressure gradient in the radial direction to balance the centrifugal force associated with the streamline curvature we require

$$\frac{\partial p}{\partial r} \simeq \rho_1 u_1^2 \frac{\partial \alpha}{\partial x},$$

whilst the continuity equation becomes

$$\frac{\partial(\rho u)}{\partial x} - \frac{\partial(\rho u \alpha)}{\partial r} - \frac{\rho u \alpha}{r} = 0.$$

As before we put $p/p_1 = 1 + 2\gamma(M_1^2-1)(1-k)/(\gamma+1)$, and the governing equations then become

$$\frac{\partial\alpha}{\partial x} = -\frac{2(M_1^2-1)}{(\gamma+1)M_1^2}\frac{\partial k}{\partial r} \tag{39}$$

and

$$\frac{\partial\alpha}{\partial r} + \frac{\alpha}{r} = -\frac{2(M_1^2-1)^2}{(\gamma+1)M_1^2}(2k-1)\frac{\partial k}{\partial x}. \tag{40}$$

The continuity equation here involves similar approximations to those made in the corresponding equation of Section 2.2. The term α/r in (40) vanishes when $r \to \infty$, and it represents the coaxial effect on the flow.

Assume that the pressure is constant along lines satisfying the relation $dx/dr = -C$, where

$$C = [1 + a(k)](M_1^2-1)^{1/2}(2k-1)^{1/2}.$$

If $a = 0$, these isobars have the slope $-dr/dx = (M_1^2-1)^{-1/2}(2k-1)^{-1/2}$ appropriate to two-dimensional simple-wave flow, so that $(1+a)^{-1}$ is the factor by which the slopes of the 'two-dimensional' isobars are multiplied. The assumption that 'a' is a function of k only means that along an isobar the slope is constant, *i.e.*, the isobars are straight. This will not be accurately true, but it may not be too much in error because the most upstream Mach wave of the compression-wave region will be straight with the 'two-dimensional' slope, so that $a(1) = 0$. By definition $\partial k/\partial r = C\partial k/\partial x$, so that (39) becomes

$$\frac{\partial\alpha}{\partial x} = -\frac{2(M_1^2-1)^{3/2}}{(\gamma+1)M_1^2}[1 + a][2k - 1]^{1/2}\frac{\partial k}{\partial x}.$$

Hence

$$\alpha = \frac{2(M_1^2-1)^{3/2}}{(\gamma+1)M_1^2}\int_k^1 (1+a)(2k-1)^{1/2}dk,$$

since $\alpha \to 0$ upstream, where $k \to 1$. It follows that

$$\frac{\partial\alpha}{\partial r} = -\frac{2(M_1^2-1)^{3/2}}{(\gamma+1)M_1^2}(1+a)(2k-1)^{1/2}\frac{\partial k}{\partial r}$$

$$= -\frac{2(M_1^2-1)^2}{(\gamma+1)M_1^2}(1+a)^2(2k-1)\frac{\partial k}{\partial x}.$$

Hence the continuity Equation (40) becomes

$$\frac{2(M_1^2-1)^{3/2}}{(\gamma+1)M_1^2 r}\int_k^1 (1+a)(2k-1)^{1/2}dk = \frac{(2a+a^2)2(M_1^2-1)^2}{(\gamma+1)M_1^2}(2k-1)\frac{\partial k}{\partial x}.$$

We crudely satisfy an averaged, integrated form of this equation along the edge of the boundary layer where $r \doteq$ constant $= r_b$, making the further simplifying assumption that $a(k) = A(1-k)$, where A is a constant. At B in Fig. 35 $k = \frac{1}{2}$, whilst at C and A it is 1. Hence an average value of $\partial k/\partial x$ along the edge of the boundary layer is

$$-\frac{1}{2\mathrm{AB}} = -\frac{1}{2(M_1^2-1)^{1/2}h},$$

where h is the height BC of the compression-wave region at the plane of the shock. The equation integrated from $k = \frac{1}{2}$ to $k = 1$ becomes

$$\frac{2h}{r_b}\int_{1/2}^{1}\int_{k}^{1}[1 + A(1-k)](2k-1)^{1/2}dk\,dk$$

$$= -\int_{1/2}^{1}[2A(1-k) + A^2(1-k)^2](2k-1)dk.$$

Hence

$$\frac{h}{r_b}\left[\frac{1}{5} + \frac{A}{35}\right] = -\frac{A}{12} - \frac{A^2}{96},$$

and for $h/r_b \simeq 0{\cdot}4$, as in the present experiments, $A \simeq -0{\cdot}94$. Accordingly the flow direction is given by

$$\alpha = \frac{2(M_1^2-1)^{3/2}}{(\gamma+1)M_1^2}\{0{\cdot}177[1-(2k-1)^{3/2}] + 0{\cdot}094[1-(2k-1)^{5/2}]\}.$$

When $k \to 1$, $\alpha \to \alpha_2$, where α_2 is the 'two-dimensional' value of α as given by Equation (3). At the sonic point, where $k = \frac{1}{2}$, $\alpha/\alpha_2 = 0{\cdot}81$, and when $k = 3/4$, $\alpha/\alpha_2 = 0{\cdot}89$. The fact that A is negative means that the isobars are steepened. This can be thought of as due to compression waves of the second family generated at the smaller radii, as in Fig. 35.

In support of the above crude analysis it may be worth noting that it gives answers of the same order as those given by Ward[15] for linearized flow, where k is close to 1, for the case of flow through a hollow quasi-cylinder. For such flow, if

$$\alpha = \frac{2(M_1^2-1)^{3/2}}{(\gamma+1)M_1^2}\int_{k}^{1}[1 + A(1-k)](2k-1)^{1/2}dk,$$

$$\frac{p-p_1}{\gamma p_1 M_1^2} = \frac{2(M_1^2-1)(1-k)}{(\gamma+1)M_1^2} \simeq \frac{1}{(M_1^2-1)^{1/2}}\left[\alpha + \frac{(1-A)(\gamma+1)M_1^2\alpha^2}{4(M_1^2-1)^{3/2}}\right].$$

But the continuity Equation (40) then requires

$$A \simeq \frac{1}{2(M_1^2-1)^{1/2}r(\partial k/\partial x)_{av}},$$

where $(\partial k/\partial x)_{av}$ is an average value of $\partial k/\partial x$ over the region where $\partial k/\partial x$ is significant, the average being necessary because A is taken to be constant. Also

$$\left(\frac{\partial k}{\partial x}\right)_{av} \simeq -\frac{(\gamma+1)M_1^2}{2(M_1^2-1)^{3/2}}\left(\frac{\partial \alpha}{\partial x}\right)_{ar} = -\frac{(\gamma+1)M_1^2\alpha}{2(M_1^2-1)^{3/2}(l-l_a)},$$

where l and l_a are the distances from the leading edge, l_a being the point where α first becomes non-zero. Hence, approximately

$$\frac{p-p_1}{\gamma p_1 M_1^2} = \frac{1}{(M_1^2-1)^{1/2}}\left[\alpha + \frac{\alpha(l-l_a)}{4(M_1^2-1)^{1/2}r}\right].$$

Ward's result for flow inside a hollow cylinder reduces to

$$\frac{p-p_1}{\gamma p_1 M_1^2} = \frac{1}{(M_1^2-1)^{1/2}}\left[\alpha + \frac{0{\cdot}5}{(M_1^2-1)^{1/2}r}\int_0^l \alpha dl\right]$$

in a case where the compression is abrupt, so that $l - l_a \ll (M_1^2-1)^{1/2}r$. Thus if, say,

$$\alpha = \bar{\alpha}(l-l_a)^2,\ l_a \geqslant l;\ \alpha = 0,\ l < l_a,$$

$$\frac{p-p_1}{\gamma p_1 M_1^2} = \frac{1}{(M_1^2-1)^{1/2}}\left[\bar{\alpha}(l-l_a)^2 + \frac{\bar{\alpha}(l-l_a)^3}{4(M_1^2-1)^{1/2}r}\right]$$

according to the present crude theory, whereas the correct answer is

$$\frac{p-p_1}{\gamma p_1 M_1^2} = \frac{1}{(M_1^2-1)^{1/2}}\left[\bar{\alpha}(l-l_a)^2 + \frac{\bar{\alpha}(l-l_a)^3}{6(M_1^2-1)^{1/2}r}\right].$$

If $\alpha = \bar{\alpha}(l-l_a)$, $l_a \geqslant l$; $\alpha = 0$, $l < l_a$, so that the streamline has a circular-arc segment, the present crude theory gives the correct answer. The averaging processes adopted above for $(\partial k/\partial x)_{av}$ and $(\partial\alpha/\partial x)_{av}$ are then exact, and the assumptions of the present theory are presumably correct.

Returning to the non-linear problem of the interaction with a normal shock in a pipe, we note that the boundary-layer analysis of Section 2.3 is not appreciably affected by the transverse curvature of the wall. Hence the boundary-layer thickness as a function of pressure should be unaffected, but the pressure gradients should be reduced in the same ratio as α/α_2. The measured pressure gradients were compared above with those of the flat-plate theory at the point where $k = 0{\cdot}75$, and here the small coaxial effect, combined with what are probably the bigger effects of the shock oscillation, may make the measured gradients significantly smaller than they would be on a flat plate with a steady shock. Also the reduction of the instantaneous pressure gradients in the vicinity of the sonic point should have some, fairly small, effect on separation, as discussed above.

4. *Shock-induced Separation on Two-dimensional Aerofoils.* We have seen that when turbulent separation is induced on a flat surface by a normal shock, the distance of the separation point from the upstream end of the interaction region is only a few boundary-layer thicknesses. Distortions of the shape of the pressure distribution downstream of separation are unlikely to have any effect on the conditions at the point of separation, though they may of course very much affect the extent of the separated region. As was pointed out in the introductory Section 1, surface curvature, such as is encountered on an aerofoil, would be expected to affect the downstream part of the pressure distribution, but at first sight there seems no reason to expect the upstream part of the pressure distribution to be much affected for weakly-curved surfaces up to the point of sonic pressure, where $p = 0{\cdot}528H_0$. Hence if we define the upstream Mach number M_1 as that corresponding in isentropic flow to the pressure ratio p_1/H_0, where p_1 is the pressure at the surface just upstream of the interaction, we might expect that the minimum M_1 for separation to occur on a weakly-curved surface would be very nearly the same as on a flat plate. This is assuming provisionally that the initial separation point occurs at or before the point of sonic pressure. In fact, as will be seen below, M_1 for incipient separation increases quite sharply with curvature, and we now consider why this is so.

First suppose that for a given surface pressure distribution the boundary-layer profiles are unaffected by curvature. Thus we might suppose that Equations (18) or (20) are valid irrespective of curvature. Then for weak curvature the interaction with the external flow ought to be virtually the same as on a flat plate up to the sonic point, and hence if separation first occurs at this point, the separation pressure ought to be virtually unaffected. For more strongly curved surfaces, the pressure

distribution at the surface could not remain exactly the same as on a flat plate, because the inclination of the flow at the edge of the boundary layer to its direction at the upstream end of the interaction region would be a little reduced, as in Fig. 36. The pressure gradients would need to become a little steeper to permit the flow at the edge of the boundary layer to have its proper inclination as a function of pressure relative to the upstream direction. Thus, again assuming separation occurs at or before the sonic point, we should, in virtue of Stratford's separation criterion (26), or the momentum-equation form (24), expect separation to occur at a slightly lower value of M_1, contrary to what we find experimentally.

However, as was pointed out in Section 2.3 in connection with the experiments of Ackeret, Feldmann, and Rott[8], there is some direct evidence that curvature affects the way in which the boundary-layer velocity profiles respond to the rise of pressure. For a given rise of pressure, the boundary-layer thickening seems to be increased by convex surface curvature. If this increase is sufficient, it may mean that for the correct flow angles to be achieved in the external flow the adverse pressure gradients must be reduced, despite the small direct effect of curvature, discussed in the previous paragraph, tending to work in the opposite direction. Thus separation might be delayed by this mechanism to a higher value of M_1.

A tentative physical explanation of this apparent effect on the behaviour of the boundary-layer profiles can be advanced in terms of the directions of streamlines within the boundary layer, as follows. At the sonic point the inclination of the flow at the edge of the boundary layer relative to its direction just upstream of the interaction is a function of M_1 only, independent of curvature. Hence at the point of sonic pressure the inclination between the streamline at the edge of the boundary layer and the wall is increased a little by convex surface curvature. Streamlines within the boundary layer must therefore on the average be diverging more rapidly than on a flat surface. However, the outer part of the boundary layer behaves in a quasi-inviscid manner, as shown by Stratford[7]. Thus the streamline divergence here would not be expected to be much affected by curvature, and the increase must therefore fall mainly on the inner part of the layer. It seems quite likely, therefore, that for corresponding pressures, the profiles with curved surfaces will have lower velocities near the wall, so that the boundary layer may thicken more under the action of the adverse pressure gradients.

An alternative or possibly additional reason why M_1 increases with curvature may be that the flow is modified just behind the shock, where the external flow is subsonic. As mentioned in the Introduction, Section 1, a shock on a convex surface in inviscid flow would be followed by a rapidly falling pressure. This presumably means that when a boundary layer is present the flow becomes modified downstream of the sonic point, with smaller gradients than on a flat plate, though, as we have seen above, up to the sonic point the flow would only be expected to differ greatly from that on a flat plate if curvature affects the variation in boundary-layer thickness. If for incipient separation the separation point is a little downstream of the sonic point, the reduced downstream gradients will increase M_1. The theory of Section 2 suggested that the incipient separation position was close to the sonic point, and the experiments of Section 3 confirmed that it was indeed probably in the general vicinity of this point, but it is by no means impossible that it is in reality a little downstream.

Whatever may be the true explanation, there seems little doubt that increasing convex curvature does increase M_1 for incipient separation. Evidence for this is shown in Fig. 37. Here values of M_1 for cases for which it is inferred that separation is just on the point of occurring are plotted against a

parameter t, proportional to the ratio of the boundary-layer thickness just upstream of the interaction to the local radius of curvature of the surface. In fact t is defined as

$$\frac{\pi}{180}\left[\frac{d\alpha}{d(l/c)}\right]_a\left(\frac{l_a}{c}\right)^{4/5}\frac{1}{l_a R_c^{1/5}}\int_0^{l_a}\left(\frac{M}{M_1}\right)^4 dl,$$

where α is the surface slope of the aerofoil in degrees, l is the distance from the leading edge, suffix 'a' denotes the point just upstream of the region of interaction, c is the aerofoil chord, R_c is the Reynolds number based on the Mach number, M_1, the tunnel stagnation pressure, and the chord, and M is the local Mach number corresponding in isentropic flow to the ratio of the surface pressure to the stagnation pressure. The product $(\pi/180)\,[d\alpha/d(l/c)]_a$ is equal to the ratio of the chord to the radius of curvature of the surface. In the tests a thin layer of roughness was applied to the aerofoils near the leading edge, so the boundary layer could be assumed to be turbulent from the leading edge. Hence the ratio of the boundary-layer thickness to the chord would be approximately proportional to $(l_a/c)^{4/5}R_c^{-1/5}$ if the surface pressures were uniform up to the position l_a. The term $(1/l_a)\int_0^{l_a}(M/M_1)^4 dl$ represents roughly the factor by which the 'flat plate' boundary-layer thickness is multiplied due to the upstream pressure gradients. (*cf.* Ref. 6.)

In virtue of Equation (25), t is approximately 2·6 times the ratio of the boundary-layer total thickness to the radius of curvature. The distance between the most upstream point of the interaction region and the sonic point is probably of the order of three boundary-layer thicknesses. Hence when $t = 0{\cdot}015$, the change of surface slope over this length is about 0·017 radians, or 1 deg. This is an appreciable fraction of the change of external-flow angle that occurs over the same length, this change of angle being about $3\frac{1}{2}$ deg at $M_1 = 1{\cdot}20$ and 6 deg at $M_1 = 1{\cdot}30$. Thus it is not surprising that surface curvatures sharp enough to give values of $t = 0{\cdot}015$ should significantly affect M_1 for separation.

The principle criterion used for determining when separation was on the point of taking place is represented by the open points in Fig. 37. It was based on the behaviour of the pressure p_b just behind the shock. Fig. 38 shows a family of pressure distributions, obtained at a fixed incidence for various free-stream Mach numbers M_0, for one of the aerofoils tested. Pressure has been plotted increasing downwards, as is usual with aerofoil results. The pressure at the point of maximum curvature on the pressure distribution just behind the shock can be taken as p_b. In most of the tests increasing M_0 decreases the pressure p_1 just upstream of the region of interaction, so increasing the local upstream Mach number M_1, and increasing the likelihood of separation. In these circumstances it is usually found that p_b abruptly decreases at a certain value of M_0, and correspondingly of M_1. Thus in Fig. 38, p_b is appreciably less for $M_0 = 0{\cdot}890$ than it is for $M_0 = 0{\cdot}885$. The condition immediately before this decrease occurs, *i.e.*, in Fig. 38, $M_0 = 0{\cdot}885$, $M_1 = 1{\cdot}231$, is taken to be the condition for incipient separation. This criterion was suggested by Pearcey[16]. The underlying idea is that once separation has occurred, the boundary layer can no longer withstand such a sharp adverse gradient, and hence the pressure gradients fall off downstream of separation. This reduction of the downstream gradients implies a reduction of p_b. Figs. 27 and 28 provide examples of the way in which increasing M_1 beyond the value for separation decreases p_b. Corresponding to the reduction of p_b, the flow pattern tends to change from the type shown in Fig. 2 to that of Fig. 3.

For the filled symbols of Fig. 37, the first occurrence of separation was inferred from Stanton-tube pressures. A piece of razor blade was fixed over one of the static-pressure holes on the aerofoil surface, as in Fig. 21. The static hole had to be selected by inspection of the pressure-distribution

family. This would sometimes suggest that the shock which seemed likely to be provoking incipient separation was situated in a fortunate position with respect to a pressure hole, so that the p_b-pressure position, somewhere near which separation was most likely to occur, was just over the hole. In these circumstances the pressure recorded by the hole should in theory be unaffected by fixing a Stanton tube over it. In practice the Stanton tube might slightly increase the recorded pressure, due to the streamline displacement affect of Fig. 21, discussed in Section 3 above. At lower free-stream Mach numbers the shock would be too weak to provoke separation, and the Stanton pressure would be more definitely higher than the static pressure, whilst at higher Mach numbers, the shock would move behind the hole, and the Stanton pressure would again exceed the static pressure. The technique was therefore to plot the static pressure of the selected hole as a function of M_0, and then to plot the pressure measured with the Stanton tube, as in Figs. 39 and 40. If the two curves met at any point, this definitely indicated separation, and even a close approach might well mean separation. Failure of the two curves to approach closely would not necessarily mean that separation did not occur, but merely that it did not occur at the chosen hole position. Likewise incipient separation might in fact occur at a rather lower Mach number M_1 than that for which the Stanton pressure became equal to the static pressure. The method did, however, possess the advantage over the p_b-divergence method that it was direct, and not based on inference. Likewise it was not easy to find p_b precisely, since the static holes on the aerofoils were not very closely spaced, and it was possible to draw the pressure-distribution family in a variety of slightly different ways, still making the curves pass through all the experimental points.

Fig. 37 shows that the two criteria for separation give results which are reasonably consistent, if some elasticity is permitted in the interpretation of the Stanton-tube results. Thus the Stanton-tube results of Fig. 40, corresponding to the pressure distributions of Fig. 38, were taken as confirming that separation occurs for $M_0 = 0{\cdot}885$, $M_1 = 1{\cdot}231$, the conditions for p_b-divergence, even though the Stanton tube reads a slightly higher pressure than the static pressure here. In the case of Fig. 39, however, for a more curved surface, separation was taken to occur when the Stanton and static-pressure curves actually meet, at $M_0 = 0{\cdot}765$, $M_1 = 1{\cdot}282$. It might very well be objected that this means adopting a more stringent criterion for separation in the curved surface cases, and that accordingly the trend in Fig. 37 is exaggerated. If we were to assume that separation occurs whenever the difference between the p/H_0 values of the Stanton and static-pressure readings does not exceed $0{\cdot}012$, the minimum difference in Fig. 40, then separation would be taken as occurring in the case of Fig. 39 at a value of M_0 of about $0{\cdot}757$. The corresponding value of M_1 would have been $1{\cdot}260$, as compared with the value $1{\cdot}282$ where the curves meet. Likewise the Stanton-tube point giving the highest value of M_1 in Fig. 37 would have had its M_1 reduced from $1{\cdot}310$ to about $1{\cdot}290$. Thus the trend of increase of M_1 with curvature would have been somewhat reduced. However, in the author's opinion the procedure actually adopted for defining separation in the Stanton-tube points of Fig. 37 is defensible, as follows. Where the surface is locally flat the dead-air region, when it first occurs, is very thin, and the Stanton tube then probably indicates wrongly a small positive skin friction, as discussed in Section 3. Where the surface is curved, however, it may curve away from underneath the separated layer, giving a thicker dead-air region in which the Stanton tube correctly indicates zero skin friction. This is closely connected with the way the profiles at separation seem to become less 'full' in shape on convex surfaces, as discussed above. These arguments are reinforced by the fact that the oil technique, subject to the usual difficulties of precise interpretation, appears to confirm that incipient separation occurs according to the criteria adopted in Fig. 37.

The tentative value $M_1 = 1{\cdot}19$ deduced for incipient separation on a flat plate from the pipe experiments of Section 3, is not too far off the straight line drawn through the results in Fig. 37, with $M_1 = 1{\cdot}215$ at zero curvature. The considerable scatter of the experimental points about the line may be partly due to the difficulties in finding M_1 accurately by either technique used. It is also almost certainly partly due to the influence of other factors. Thus compression or expansion waves, incident upon the interaction region from upstream, would modify the interaction and hence affect M_1 for separation. Likewise the pressure distribution upstream of the region of interaction must affect the shape, as well as the thickness, of the boundary-layer profile just upstream, though the factor t only includes the effect on the thickness. However, provided the gradients immediately upstream are only moderate, the upstream profile will probably not differ a lot from a 1/7th power form. The theory of Section 2 suggests that small differences in the shape do not make an enormous difference to M_1 for separation, which is predicted to be about $1{\cdot}20$ for $K = 7$ and about $1{\cdot}16$ for $K = 5$. The factor multiplying dm_e/dx in the skin-friction Equation (24) increases rather sharply as K is decreased for a given ratio M_e/M_1, but dM_e/dx is predicted to be decreased, *i.e.*, the pressure gradients are less severe for the less full upstream profiles, so the net effect on separation is not too large. Nevertheless, all in all it is clear that there are other factors, besides the curvature parameter, t, affecting M_1 for incipient separation, but since the results of Fig. 37 cover a fairly wide range of aerofoil shapes and incidences, it seems that the surface-curvature factor is probably the principal one.

Fig. 41 shows the results, corresponding to those of Fig. 37, for the downstream pressure p_b as a function of the curvature parameter t. The large scatter is indicative of the difficulty in defining p_b accurately, but there is clearly a trend for p_b to be less on curved surfaces than on flat ones. This is in line with what was said earlier in this section concerning the inviscid-flow effect of curvature, namely the falling pressure behind the shock, tending, when a boundary layer is present, to make the pressure gradients fall off more rapidly downstream of the sonic point. It also agrees with the finding of Holder and Cash[17] that relatively high values of p_b are encountered for a shock on a flat surface in the absence of separation, or when separation is only incipient. The filled Stanton-tube points of Fig. 41 tend to be lower than the rest, because the Stanton-tube method often tends to indicate separation a little later than the p_b-divergence method. Hence for such Stanton-tube points, p_b will have decreased relative to the value taken on the divergence basis. The duct experiments of Section 3 give values of p_b rather lower than the results of Fig. 41 extrapolated to zero curvature. This is probably because the transverse curvature of the flow pattern in the pipe, discussed in Section 3, reduces the pressure gradients near the point of sonic pressure, and correspondingly the constraint effect of the finite-diameter pipe reduces the downstream pressures.

Fig. 1 shows the appearance of the shock in a schlieren photograph when separation is judged to be on the point of occurring from a locally flat surface. In fact the case is that with $M_0 = 0{\cdot}885$ in Figs. 38 and 40. The interaction region has a broadly similar appearance in all the other cases judged as being on the point of separation, though there is a tendency for the compression waves to form a more definite front limb to the shock at higher surface curvatures. Fig. 42 gives an extreme example of this, corresponding to the point $t = 0{\cdot}0123$, $M_1 = 1{\cdot}288$ in Fig. 37. The apparent kink in the surface of the aerofoil in Fig. 1 and in Fig. 42 is a 'direct shadow' effect due to the fact that the schlieren pictures are focussed on the central plane of the tunnel, and not on the edge of the model nearest to the light source. Upstream of the shock the light rays close to the surface of the model become bent away from it due to the rapid density changes associated with the way in

which the velocity changes abruptly from zero at the wall to quite a high value close to it. Behind the shock the velocities close to the wall are greatly reduced, except with very weak shocks (*cf.* Figs. 23 and 24), so the deflection of the light rays is correspondingly reduced. Thus the surface of the model appears distorted outwards upstream of the shock, but more nearly in its true position downstream.

The foregoing has been concerned with incipient separation. It must be emphasized that the occurrence of such separation does not immediately lead to any marked change in the overall character of the flow over the aerofoil. Such pronounced changes only occur if the thickness of the boundary layer at the trailing edge increases markedly, so as to affect the circulation. The rate of change of the pressure at the trailing edge with free-stream Mach number M_0 is a sensitive indicator of such effects of shock-induced separation[16, 18]. It is not unreasonable to suppose that the boundary layer at the trailing edge is always close to separation when trailing-edge-pressure divergence occurs, and in many cases the boundary layer will be close to the condition of separation all the way between the shock and the trailing edge. Very crudely the pressure distribution on the aerofoil between the shock and the trailing edge will resemble that of Fig. 9, which plots Equation (27) predicted by Stratford[7] to give zero skin friction downstream of the point at a distance l_a from the leading edge, the pressure upstream of the station 'a' being assumed uniform. Equation (27) can be written

$$1 - \frac{u^2}{u_1^2} = 0{\cdot}850\beta^{2/3}\left\{0{\cdot}435R_c^{1/5}\left(\frac{l_a}{c}\right)^{1/5}\left[\left(\frac{l}{l_a}\right)^{1/5} - 1\right]\right\}^{2/K}.$$

Hence at the trailing edge where $l = c$ and the external-flow Mach number is M_T,

$$1 - \frac{M_T^2}{M_1^2} = 1{\cdot}60\beta^{2/3}\left[1 - \left(\frac{l_a}{c}\right)^{1/5}\right]^{2/7}, \tag{41}$$

where, in line with what was said in Section 2.3, we interpret velocity ratios in Stratford's formulae as Mach number ratios, and we take $R_c = 4 \times 10^6$ and $K = 7$. Most 'flat plate' turbulent velocity profiles can be fitted approximately with a power law of index $K = 7$, the value $R_c = 4 \times 10^6$ is not untypical of aerofoil tests, and the results are very insensitive to the value of R_c chosen. Fig. 43 shows results obtained on aerofoils for conditions where trailing-edge-pressure divergence is just occurring. The results are mainly from unpublished experiments performed by various workers at the N.P.L. under the guidance of Mr. H. H. Pearcey. The ratio M_T/M_1, where the trailing-edge Mach number M_T is deduced from the local pressure and the tunnel stagnation pressure, is plotted as a function of the shock position l_a/c. Equation (41) with $\beta = 0{\cdot}66$, as used by Stratford, is also plotted. The dotted part of the line indicates where the theory underlying (41) becomes invalid. The chain-dotted curve represents the result deduced from the theory of Section 3, Equation (24). Equation (41) would agree quite closely with this if the empirical factor β were taken to be 1, not $0{\cdot}66$. It was suggested in Section 2.6 that the value $\beta = 1$ might give better results for separation behind shocks than $\beta = 0{\cdot}66$. The experimental results of Fig. 43 appear to contradict this, since they fit the theoretical curve with $\beta = 0{\cdot}66$ reasonably well, better than the curve derived from Equation (24). However it must be borne in mind that drastic simplifications have been made in saying that the experimental situation of shock-induced trailing-edge-pressure divergence resembles that envisaged in Stratford's theory. Thus the agreement may be partly fortuitous. Nevertheless Fig. 43 suggests that although trailing-edge-pressure divergence, like any other boundary-layer effect, must depend on the shape of the pressure distribution over the whole surface of the aerofoil, the fine details of this distribution are relatively unimportant compared with a few dominant, coarse characteristics, such as the shock position, M_1, and M_T. By contrast, the conditions for incipient

separation at the shock probably do depend on either the small-scale details of the shape of the pressure distribution under the shock, as they are affected by curvature, or on the minutiae of the effects of curvature on the response of a boundary layer to abrupt adverse pressure gradients.

5. *Separation Induced by Swept Shocks.* On swept-back wings shocks which are nearly normal to the surface close to it, but which are swept with respect to the stream often occur. It is therefore of interest to consider under what conditions such shocks give rise to separation.

We might suppose that for incipient separation, the component Mach number M_{1N} normal to the shock would vary with the ratio of the boundary-layer thickness to the surface curvature in a plane perpendicular to the shock in much the same way as M_1 varies with t in Fig. 37. In particular for a locally flat surface M_{1N} would not be far off 1·215, the figure suggested by the results of Fig. 37, or 1·19, the result inferred from the experiments of Section 3. It would be reasonable to expect this if the flow behaved in a quasi-two-dimensional manner, such that the flow patterns in the boundary layer at different stations along the shock were similar. For then referred to axes x, y, and z, with x parallel to the wall normal to the shock, y normal to the wall, and z parallel to both the wall and the shock, derivatives with respect to z would vanish, and the equations of motion, subject to the usual boundary-layer approximations, would be

$$\rho u \frac{\partial u}{\partial x} + \rho v \frac{\partial u}{\partial y} = -\frac{dp}{dx} + \frac{\partial \tau_x}{\partial y},$$

$$\rho u \frac{\partial w}{\partial x} + \rho v \frac{\partial w}{\partial y} = \frac{\partial \tau_z}{\partial y},$$

and

$$\frac{\partial (\rho u)}{\partial x} + \frac{\partial (\rho v)}{\partial y} = 0,$$

where u, v and w are the velocity components in the x, y and z directions, and τ_x and τ_z are the frictional stresses on planes parallel to the wall in the x and z directions. In laminar flow τ_x and τ_z would be $\mu(\partial u/\partial y)$ and $\mu(\partial w/\partial y)$ respectively, and so would mainly depend on the shapes of the u and w profiles respectively. If we suppose that similarly in turbulent flow there is no direct coupling between τ_x and the z-direction flow, the equations for the x-direction flow would be independent of those for the z-direction. They would be identical with the equations for the corresponding two-dimensional case with the normal component flow, except that the density and viscosity would vary more widely across the boundary layer in the three-dimensional case, on account of the total Mach number at the edge of the layer being higher. However, provided the total external-flow Mach number did not exceed 2, say, it might be thought that this would lead only to a small difference from the two-dimensional case. Such difference that it did make would be expected to be in the direction of reducing M_{1N} for incipient separation, since the relatively higher wall temperatures and consequent lower densities near the wall in the three-dimensional case would be expected to facilitate separation slightly.

Quite a different conclusion is however reached by Rogers and Hall[19] on the basis of oil-flow measurements on swept wings. They find that the component Mach number M_{1N} for incipient separation increases with shock sweep, up to about 1·4 when the effective shock sweep is in the region of 45 deg. The effective sweep is defined as $\phi - \theta$, where ϕ is the sweep of the shock relative to the free stream, as in Fig. 44, and θ is the angle of the streamlines at the edge of the boundary

layer just ahead of the shock. The criterion adopted for judging separation is as follows. When a thin layer of pigment-containing oil is smeared on to the surface, it becomes teased out into filaments by the action of the airflow. The shock wave abruptly turns the oil filaments on the surface, and for a strong enough shock the filaments run tangentially together near the shock to form a well-defined line, the separation line, as in Fig. 45. When there is extensive separation many of the filaments behind this separation line lie parallel to it, or run towards it, but separation is judged to be incipient when only the oil filament immediately behind the separation line lies parallel to it, those further behind being more sharply swept. Fig. 45 shows what is judged to be an incipient shock-induced separation, according to this criterion. It may be, however, that this is not the appropriate criterion to take if comparison is being made with two-dimensional tests. Rogers and Hall assumed that the separation line coincided with the shock position, and measurements were later made with static probes to see if this was true. Inaccuracies in the traverse gear made it difficult to position the probes precisely, but insofar as the measurements could be trusted they suggested that for a shock near the leading edge the shock does indeed virtually coincide with the separation line, but further back on the wing, the shock is more highly swept than the separation line, the difference in angle of sweep being of the order of 3 deg. In these latter circumstances we should judge M_{1N} for incipient separation to be lower if we were to take as our criterion of separation that the oil filaments should be turned parallel to the true position of the shock, rather than that they should just form a separation line. This is because we should choose a case where the oil filaments are turned through a smaller angle, and also because the angle of $\phi - \theta$, used in finding the normal component, would be taken to be greater. It is not contended that this criterion is superior to that used by Rogers and Hall. On the contrary, their definition is probably more logical as a definition of separation in three dimensions. However, by relating directions to the shock itself we might get better agreement with the two-dimensional results. This is because when the streamlines near the wall have been turned parallel to the shock, the velocity components perpendicular to the shock that they originally possessed will have been destroyed, and this is analogous to the bringing to rest of the fluid near the wall in a two-dimensional separation. Of course the fact that the shock is not parallel to the separation line, or with weaker shocks to the locus of points where the oil filaments abruptly turn, means that the flow under the shock is not quasi-two-dimensional. The upstream influence of the shock on the boundary layer is bigger for the more downstream positions along the shock. This makes it impossible in practice on a swept wing to decide what the precise position of the shock is, unless traverses are made in the stream above the wing. It also means that there is no real reason to suppose that the component Mach number M_{1N} for incipient separation, defined in either way, should be close to what it would be in two-dimensional flow, since the relationship between the thickening of the boundary layer and the pressure gradients normal to the shock or to the separation line may be quite different from what it is in two-dimensional flow.

In fact, however, Stanbrook's experiments[20], where separation is related to the shock direction as discussed above, do give reasonable agreement with two-dimensional results. In these experiments a shock was generated by a plate sticking out perpendicularly from the flat wall of a supersonic tunnel at an incidence to the stream, as shown in Fig. 46. The interaction between the shock generated at the leading edge of the plate and the turbulent boundary layer on the wall was studied. Separation was judged to occur when a filament of oil ran from the junction of the leading edge of the plate and the wall along the shock direction, which in this experiment was known from the

incidence of the plate. For free-stream Mach numbers between 1·6 and 2·0, the pressure ratio p_2/p_1 across the shock that was judged in this way to produce incipient separation was almost constant, at about 1·48. It follows from equation (1) that the corresponding component Mach number is given by

$$1{\cdot}48 = 1 + \frac{2\gamma}{\gamma + 1}(M_{1N}^2 - 1),$$

or $M_{1N} = 1{\cdot}19$. The shock-sweep angle for incipient separation varied between about 43 deg at a free-stream Mach number of 1·6 to 53 deg at a free-stream Mach number of 2·0. Thus according to Stanbrook's experiments and his criterion for incipient separation, increasing sweep does not increase M_{1N}, the value obtained being roughly the same as the two-dimensional result for flat surfaces.

In Stanbrook's experiments the boundary layer was quite thick. When he judged incipient separation to be occurring, the oil filaments did not run together near the shock to form a separation line. Instead the filaments turned parallel to the shock, but were not fused together, those originating from points further from the leading edge of the shock-generating plate running progressively further upstream of the shock as indicated in Fig. 46. Thus the locus of points where the oil filaments were abruptly turned from their original free-stream direction was less swept back than the shock. The filaments only fused along a line starting from the plate leading edge and running increasingly ahead of the shock at higher incidences than those judged by Stanbrook to represent incipient separation.

The question, therefore, seems largely to revolve around the definition of separation. It is not certain that defining it in Stanbrook's way would always give approximate agreement with the two-dimensional results. Some of the data used by Rogers and Hall in their analysis were from cases with shocks close to leading edges. Here the boundary layer is very thin, and though the upstream effect of the shock as a multiple of the boundary-layer thickness may still increase with distance along the shock, the boundary-layer thickness is so small that the angle between the shock and the oil separation line must be small. It is difficult to see, therefore, how the values for M_{1N} deduced according to the separation-line criterion from such cases could be significantly reduced by defining separation with reference to the shock direction instead. It may be that some of these cases were with curved surfaces, so that M_{1N} ought to be rather greater than on a flat surface, according to Fig. 37. Perhaps, however, the proper conclusion is that interactions with swept shocks are essentially three-dimensional phenomena, and it is therefore unreasonable to look for close quantitative relations with the corresponding two-dimensional interactions.

6. *Concluding Remarks.* A theory has been presented for the interaction between a normal shock in an infinite stream and a turbulent boundary layer on a flat surface. This involves a new and simple method for calculating the effects of sharp adverse pressure gradients on the velocity profiles of a turbulent boundary layer. The theory as a whole gives reasonable results, predicting that the pressure distribution at the wall has an initial region of sharp adverse gradients followed by a long 'tail' of greatly reduced gradients. Separation is predicted to occur when the upstream Mach number exceeds about 1·2. For much higher Mach numbers, when extensive separation occurs, the assumptions underlying the theory would become unrealistic. For small regions of separation, the boundary-layer profiles in the separated region appear quite 'full' in shape, and would not at first sight suggest the presence of separation.

Experiments on normal shocks in a pipe have broadly confirmed the approximate validity of the theory. The interaction in a pipe differs, however, from that on a flat plate in an infinite stream partly because of the 'coaxial' or transverse-curvature effects on the supersonic part of the flow, and partly because of the constraint effect of the finite pipe diameter on the downstream flow. The boundary layer thickens on passing through the shock, so reducing the effective downstream area of the pipe and hence reducing the downstream pressures. Because of these effects, it might have been preferable from the point of view of providing comparisons with the theory to have performed the experiment on a flat plate, on the lines of Seddon's experiments[4], but at lower Mach numbers. However, with this arrangement there may be serious interference effects due to the interactions on the side and top walls of the tunnel, and in any case a suitable tunnel was not conveniently available for such experiments.

Results obtained on aerofoils in a slotted-wall tunnel do however provide interesting information concerning the minimum local upstream Mach number necessary to provoke separation. It appears that this Mach number increases as the convex curvature of the surface increases.

Finally we have considered interactions between turbulent boundary layers and shocks which, though perpendicular to the wall, are swept back relative to the stream. Such interactions occur on swept-back wings. The relation between the first occurrence of separation and the component Mach number perpendicular to the shock or to the separation line has been considered. The difficulty is how to define separation. If it is defined as occurring when the streamlines in the boundary layer closest to the wall become turned under the shock to be parallel to it, then it seems that in some cases, at least, the component Mach number for incipient separation is much as in two-dimensional flow. If, however, separation is defined as first occurring when the streamlines closest to the wall first run in together tangentially to form a line, the separation line, then the component Mach number normal to this line is often much higher than the corresponding two-dimensional value. The swept-shock interaction is, however, essentially three-dimensional, and two-dimensional criteria should not really be expected to apply to it.

Acknowledgments. The experiments on normal shocks in a pipe, described in Section 3, were performed by Mr. J. L. Attridge, and the results for incipient separation on aerofoils, discussed in Section 4, were obtained by Miss R. L. Warren and Miss S. E. Woolgar, under the guidance of Mr. J. Osborne. Useful discussions were held with Mr. H. H. Pearcey and Mr. E. W. E. Rogers.

LIST OF SYMBOLS

C_f Skin friction coefficient, $2\tau_w/\rho_e u^2_e$

C_p Pressure coefficient, $1 - u^2_e/u^2_1$ or $1 - M^2_e/M^2_1$

d Dissipation integral, $\int_0^\delta \frac{\tau}{\rho_e u^2_e} \frac{\partial}{\partial y}\left(\frac{u}{u_e}\right) dy$

$f = \frac{(n+1)}{\rho_e u_e \delta} \int_0^\delta \rho u \, dy$

$g = (n+1)(3n+1)\theta^*/2n\delta$

$h = (n+1)(2n+1)\theta/n\delta$

I Enthalpy

k Defined by Equation (1)

K Exponent in power-law form for upstream profile, viz.

$$\left(\frac{u}{u_e}\right)_a = \left(\frac{y}{\delta}\right)^{1/K}$$

l Distance from the leading edge

M Mach number

n Exponent in power-law form for profile at general position, viz.

$$\frac{u}{u_e} = \left(\frac{y}{\delta}\right)^n ; \qquad \to \frac{1}{K} \text{ upstream}$$

p Pressure

q Speed along a streamline

T Absolute temperature

u X-component velocity

v y-component velocity

x Distance parallel to wall measured from line normal to wall through lower end of shock

$X = x/\delta_a$

y Distance from wall along normal

$\bar{y} = (1 - M_2^2)^{1/2} y$ (strictly $(1 - M_2^2)^{1/2}(y - \delta_s)$, where δ_s is boundary-layer thickness at point of sonic pressure)

α Angle between flow and wall

β Empirical constant in Stratford's separation criterion (26)

γ Ratio of specific heats

δ Boundary-layer total thickness

δ^* Boundary-layer displacement thickness, $\int_0^\delta \left(1 - \frac{\rho u}{\rho_e u_e}\right) dy$

θ Boundary-layer momentum thickness, $\int_0^\delta \frac{\rho u}{\rho_e u_e}\left(1 - \frac{u}{u_e}\right) dy$

θ^* Boundary-layer energy thickness, $\int_0^\delta \frac{\rho u}{\rho_e u_e}\left(1 - \frac{u^2}{u_e^2}\right) dy$

μ Viscosity

ρ Density

τ Turbulent friction stress parallel to the wall

τ_w = τ at the wall

Suffices

$_1$ Denotes conditions at the edge of the boundary layer just upstream of the region of interaction (upstream free-stream conditions on a flat plate)

$_2$ Denotes conditions behind a normal shock in inviscid flow corresponding to suffix $_1$ upstream conditions

a Denotes conditions at a station 'a' at the upstream end of the region of interaction

b Denotes conditions immediately behind the shock, where the pressure distribution at the surface has its maximum curvature

d Denotes conditions outside the boundary layer immediately downstream of the shock

e Denotes conditions at the edge of the boundary layer

u Denotes conditions outside the boundary layer immediately upstream of the shock

REFERENCES

No.	*Author*	*Title, etc.*
1	C. Ferrari	Sul flusso transonico con onda d'urto attaccata ($M_\infty < 1$): caso del moto stazionario. *Atti. Accad. Naz. Lincei, Rend. Sc. fis. mat. e nat.* Vol. 26. p. 114. 1959.
2	G. E. Gadd	The possibility of normal shock waves on a body with convex surfaces in inviscid transonic flow. *Z.A.M.P.* Vol. 11. p. 51. 1960.
3	G. E. Gadd	The interaction between a weak normal shock wave and a turbulent boundary layer. A.R.C. C.P. 424. June, 1957.
4	J. Seddon	The flow produced by interaction of a turbulent boundary layer with a normal shock wave of strength sufficient to cause separation. Paper presented at the AGARD boundary-layer meeting in London in April, 1960.
5	G. B. Schubauer and P. S. Klebanoff ..	Investigation of separation of the turbulent boundary layer. N.A.C.A. Report 1030. 1951.
6	B. Thwaites (editor)	*Incompressible aerodynamics.* Chapter 2. Oxford University Press. 1960. [Chapter 2 is based on material submitted by D. A. Spence.]
7	B. S. Stratford	The prediction of separation of the turbulent boundary layer. *J. Fluid Mech.* Vol. 5. p. 1. 1959.
8	J. Ackeret, F. Feldmann and N. Rott ..	Untersuchungen an Verdichtungsstössen und Grenzschichten in schnell bewegten Gasen. Institut für Aerodynamik E.T.H. Zürich. Nr. 10. 1946.
9	R. Michel	Étude expérimentale de la couche limite turbulente et de son intéraction avec l'onde de choc sur un demi-profil en écoulement transsonique. O.N.E.R.A. Note Technique No. 47. 1958.
10	L. Crocco and L. Lees	A mixing theory for the interaction between dissipative flows and nearly isentropic streams. *J. Ae. Sci.* Vol. 19. p. 649. 1952.
11	J. N. Hool	Measurement of skin friction using surface tubes. *Aircraft Engineering.* Vol. 28. p. 52. 1956.
12	H. Girerd and P. Guienne	Nouvelles sondes de pression statique pour mesures aérodynamiques. *C.R. Acad. Sci.*, Paris. Vol. 228. p. 651. 1949.

REFERENCES—*continued*

No.	*Author*	*Title, etc.*
13	M. Tucker	Approximate turbulent boundary-layer development in plane compressible flow along thermally insulated surfaces with application to supersonic-tunnel contour correction. N.A.C.A. Tech. Note 2045. 1950.
14	G. E. Gadd, W. F. Cope and J. L. Attridge	Heat transfer and skin friction measurements at a Mach number of 2·44 for a turbulent boundary layer on a flat surface and in regions of separated flow. A.R.C. R. & M. 3148. October, 1958.
15	G. N. Ward	*Linearized theory of steady high-speed flow.* Cambridge University Press. 1955.
16	H. H. Pearcey	Some effects of shock-induced separation of turbulent boundary layers in transonic flow past aerofoils. (Paper No. 9 presented at the Symposium on Boundary-Layer Effects in Aerodynamics at the N.P.L., 31st March to 2nd April, 1955.) A.R.C. R. & M. 3108. June, 1955.
17	D. W. Holder and R. F. Cash	Experiments with a two-dimensional aerofoil designed to be free from turbulent boundary-layer separation at small angles of incidence for all Mach numbers. A.R.C. R. & M. 3100. August, 1957.
18	H. H. Pearcey	A method for the prediction of the onset of buffeting and other separation effects from wind-tunnel tests on rigid models. A.R.C. 20,631. December, 1958.
19	E. W. E. Rogers and I. M. Hall ..	An introduction to the flow about plane sweptback wings at transonic speeds. *J. R. Ae. Soc.* Vol. 64. p. 449. 1960.
20	A. Stanbrook	An experimental study of the glancing interaction between a shock wave and a turbulent boundary layer. A.R.C. C.P. 555. July, 1960.
21	N. Curle	The effects of heat transfer on laminar boundary-layer separation in supersonic flow. A.R.C. 21,986. May, 1960.
22	G. E. Gadd	Boundary-layer separation in the presence of heat transfer. N.P.L./Aero./400. February, 1960.

APPENDIX

Application of the Boundary-Layer Theory to Laminar Layers

Interactions between laminar boundary layers and shock waves can already be dealt with simply and effectively[21, 22], and the boundary-layer theory of the present paper is not seriously suggested as an alternative method for such interactions. However, it does perhaps increase one's faith in the general validity of the theory to note that it does give results of the right order of magnitude for laminar interactions.

For laminar layers we may crudely assume the upstream profile to be linear in y, i.e., $K = 1$. Then neglecting the terms in $(d\delta/dx)_a$ in equations (18) and (20) we obtain for $\gamma = 1{\cdot}4$.

$$\frac{\delta}{\delta_a} = \frac{\left(2\frac{M_e^2}{M_1^2} - 1\right)}{\left(4\frac{M_e^2}{M_1^2} - 3\right)} \frac{M_1}{M_e}\left(\frac{1 + 0{\cdot}2M_e^2}{1 + 0{\cdot}2M_1^2}\right)^3$$

$$\simeq \left(1 - \frac{(3 + 1{\cdot}8M_1^2)}{1 + 0{\cdot}2M_1^2}\, t\right) \Big/ (1 - 8t),$$

where $M_e = M_1(1 - t)$. The linearised simple-wave pressure relation gives

$$\frac{d\delta}{dx} = \frac{(M_1^2 - 1)^{1/2}}{1 + 0{\cdot}2M_1^2}\, t.$$

To give the correct skin friction at station 'a' for a case with Prandtl number equal to 1 and viscosity proportional to absolute temperature we put

$$\delta_a = l_a(1 + 0{\cdot}2M_1^2)/(0{\cdot}332\sqrt{R_a}),$$

where l_a is the distance of station 'a' from the leading edge and R_a is the Reynolds number based on l_a. Hence

$$\frac{l - l_{0{\cdot}01}}{l} = \frac{3{\cdot}01(5 - 0{\cdot}2M_1^2)(1 + 0{\cdot}2M_1^2)}{(M_1^2 - 1)^{1/2}\, R_a^{1/2}} \int_{0{\cdot}01}^{t} \frac{dt}{t(1 - 8t)^2}$$

The pressure distribution corresponding to this relation is compared in Fig. 47 with experimental results for a case with $M_1 = 2$, $R_a \simeq 2 \times 10^5$. It can be seen that the theoretical pressure curve is of the right general shape, but that the maximum pressure gradients are much too large and the rise of pressure to the 'plateau' is nearly twice as high as it should be. However, it is perhaps surprising that the predicted pressure increases, though too large, should nevertheless be of the right order of magnitude, since the power-law profiles only bear the crudest similarity to the actual ones in laminar flow. The use of a more realistic family of profiles might give better results, though not necessarily, since the outer edge of the boundary layer is not well defined in the actual profiles. The same difficulty arises in the Crocco-Lees method[10], which also uses the mass-flux condition. For turbulent boundary layers, the edge of the layer is rather better defined. In order to do justice to the inner part of the laminar layer, where viscosity is important, it might be preferable to use a two-parameter family of profiles, satisfying the condition that $\partial(\mu\, \partial u/\partial y)/\partial y = dp/dx$ at the wall, in addition to the mass-flux and energy-thickness conditions.

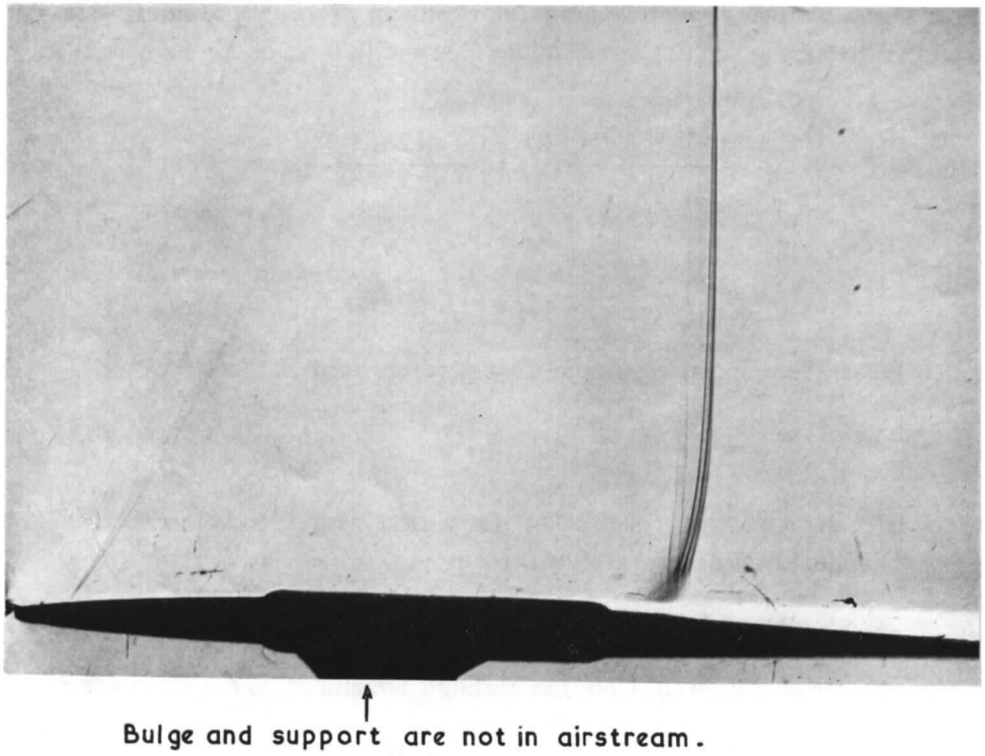

FIG. 1. Nearly-normal shock wave on an aerofoil in transonic flow.

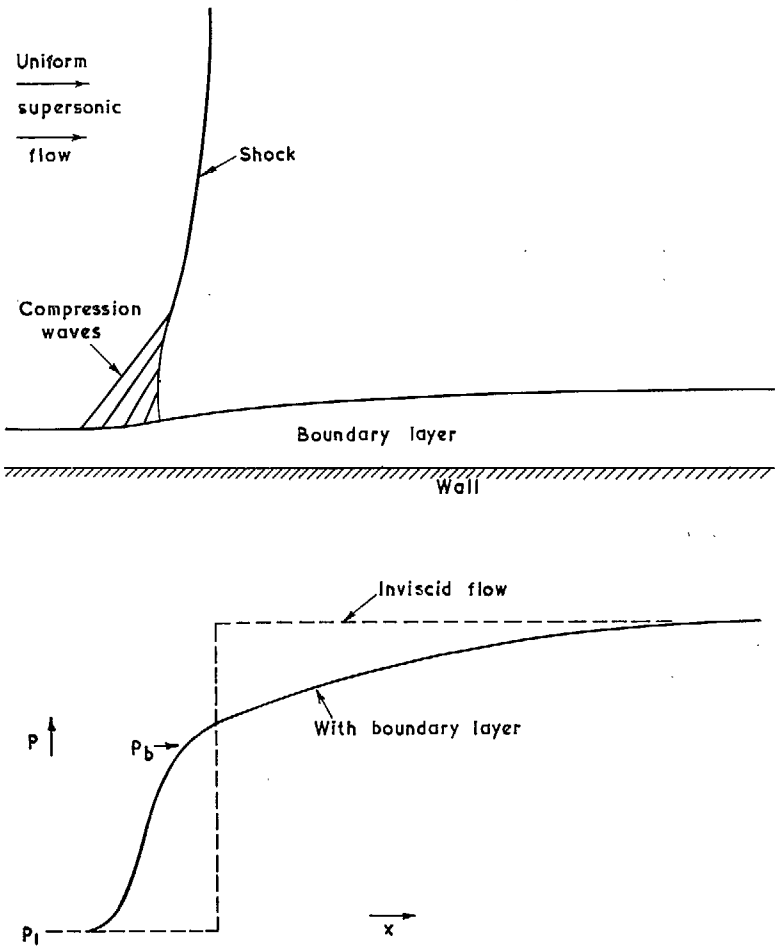

FIG. 2. Flow pattern and pressure distribution when the shock is not strong enough to cause much separation.

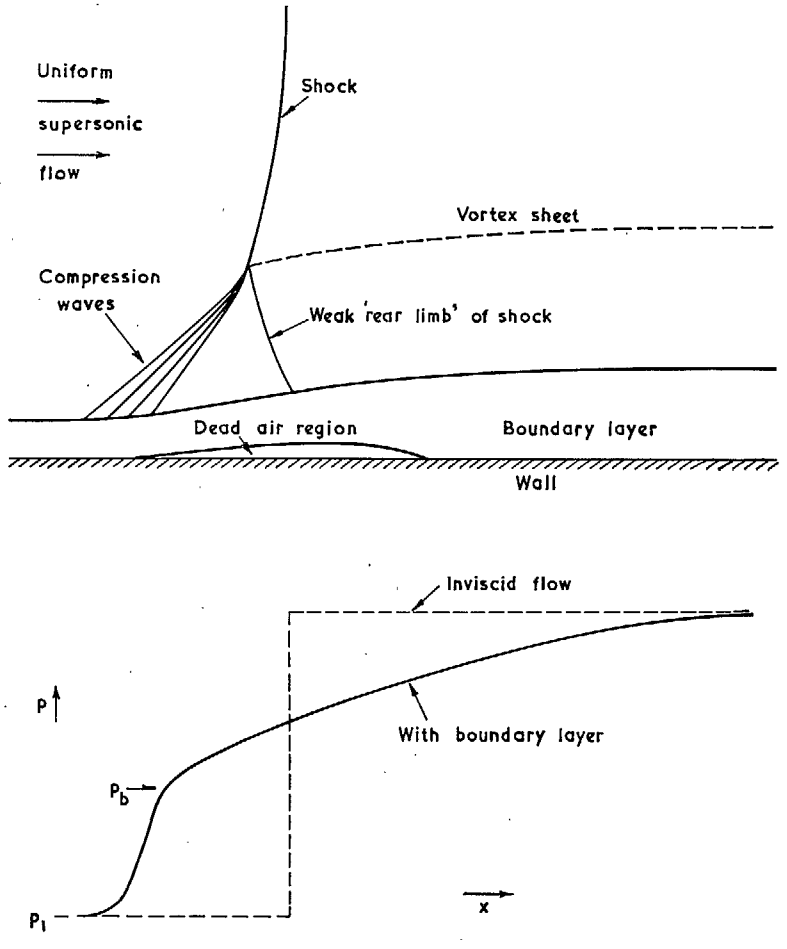

FIG. 3. Flow pattern and pressure distribution with a strong shock.

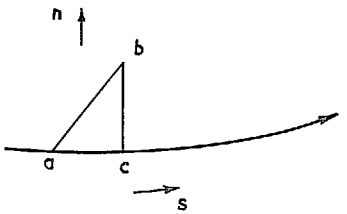

FIG. 4. Streamline in simple-wave region.

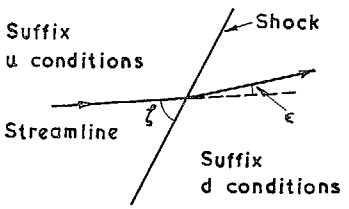

FIG. 5. Oblique shock wave.

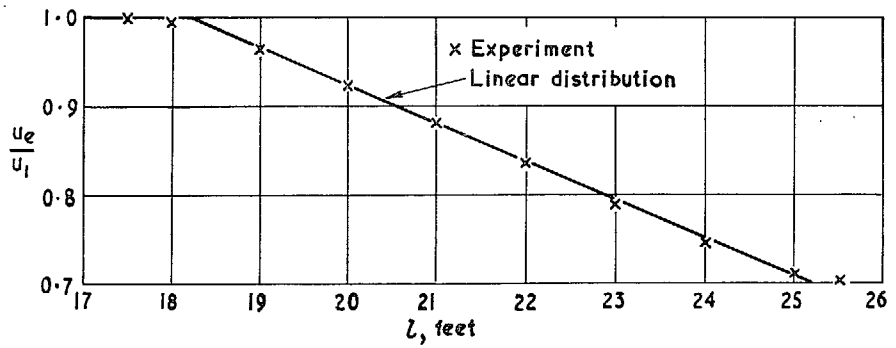

FIG. 6. Schubauer and Klebanoff's external velocity distribution.

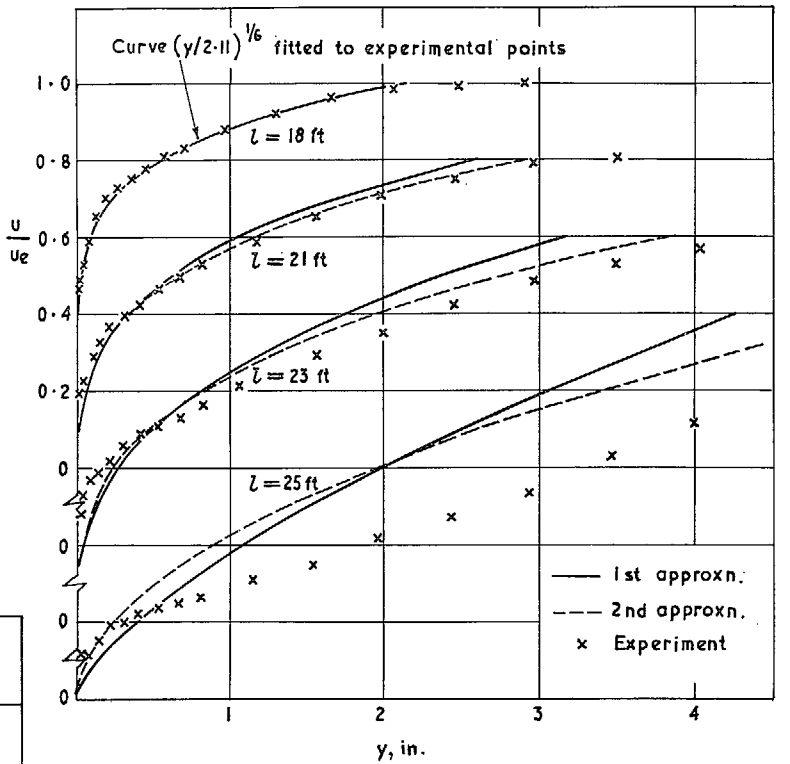

FIG. 7. Predicted and experimental profiles at different distances l from the leading edge for Schubauer and Klebanoff's experiments.

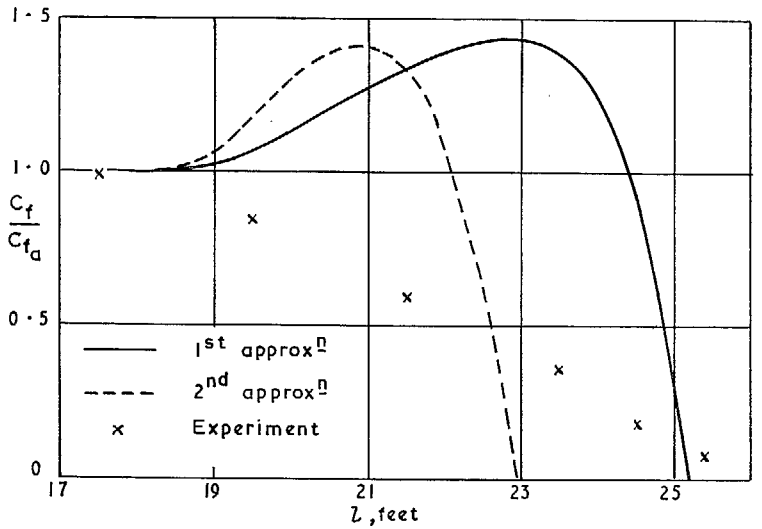

FIG. 8. Predicted and experimental skin-friction distributions for Schubauer and Klebanoff's experiments.

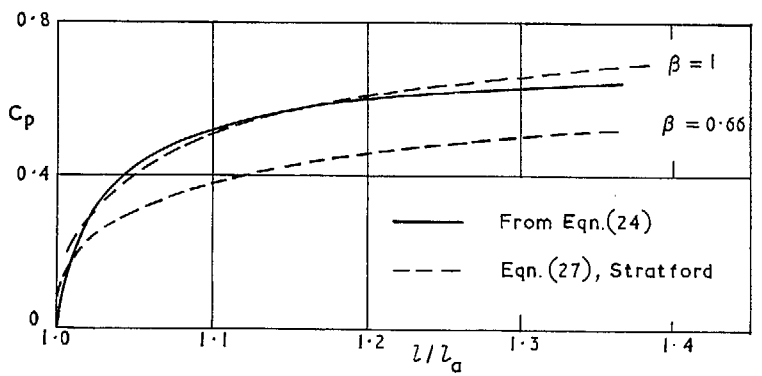

FIG. 9. Pressure distributions predicted to give zero skin friction for $l > l_a$.

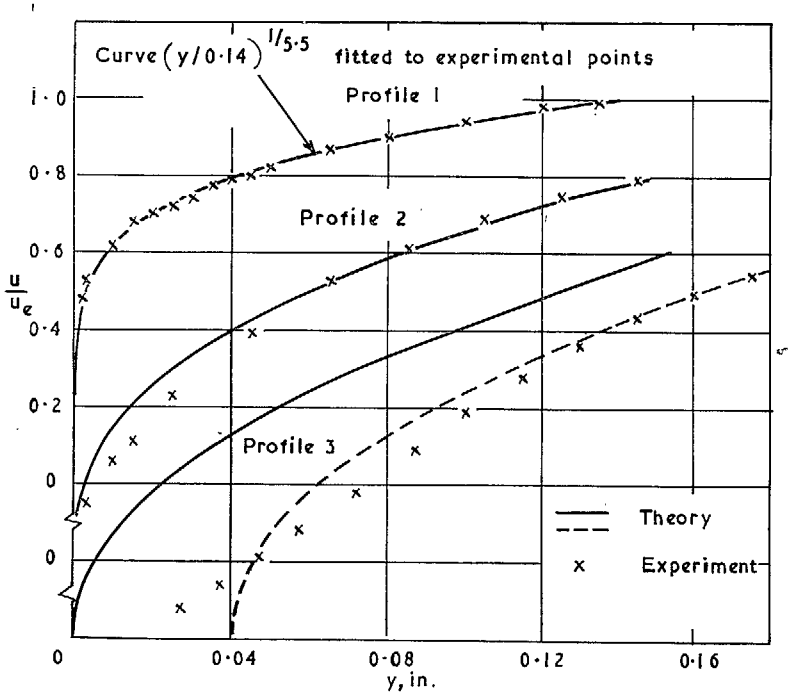

FIG. 10. Predicted and experimental profiles for Seddon's experiments.

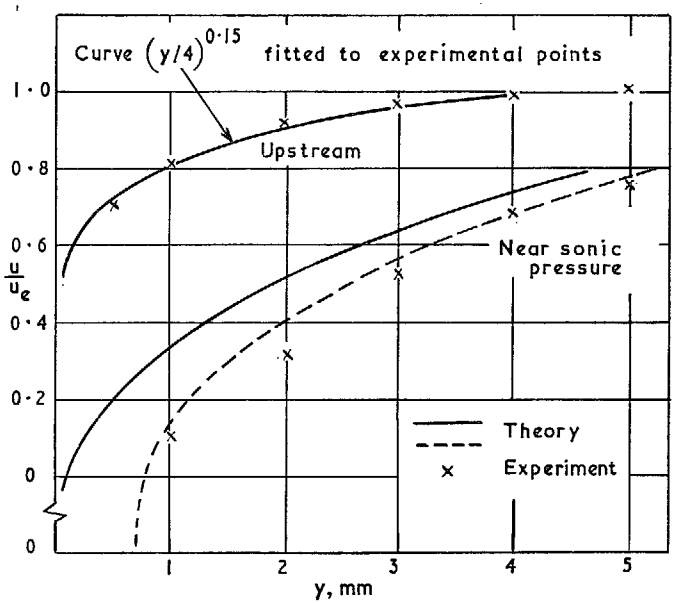

FIG. 11. Predicted and experimental profiles for experiments of Ackeret, Feldman and Rott.

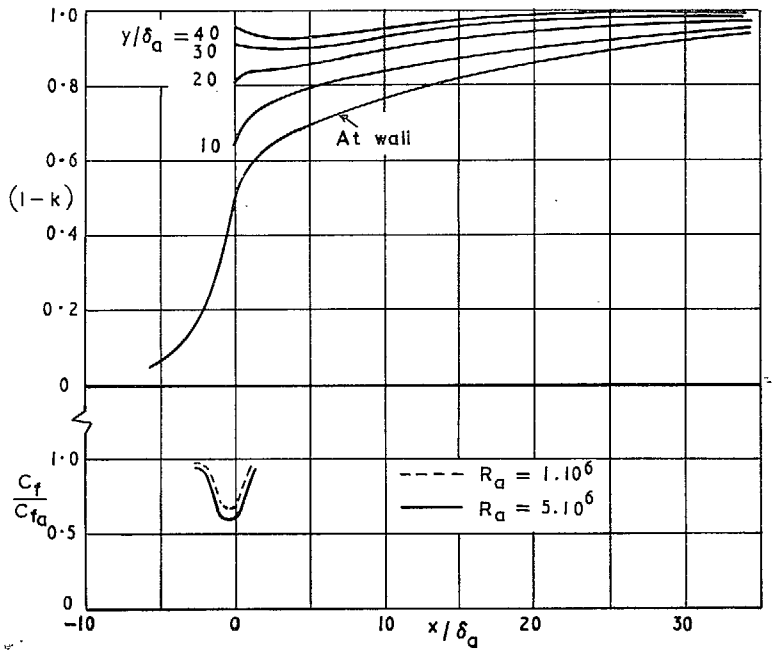

FIG. 12. Predicted pressure and skin-friction distributions for the case $M_1 = 1{\cdot}1$, $K = 5$.

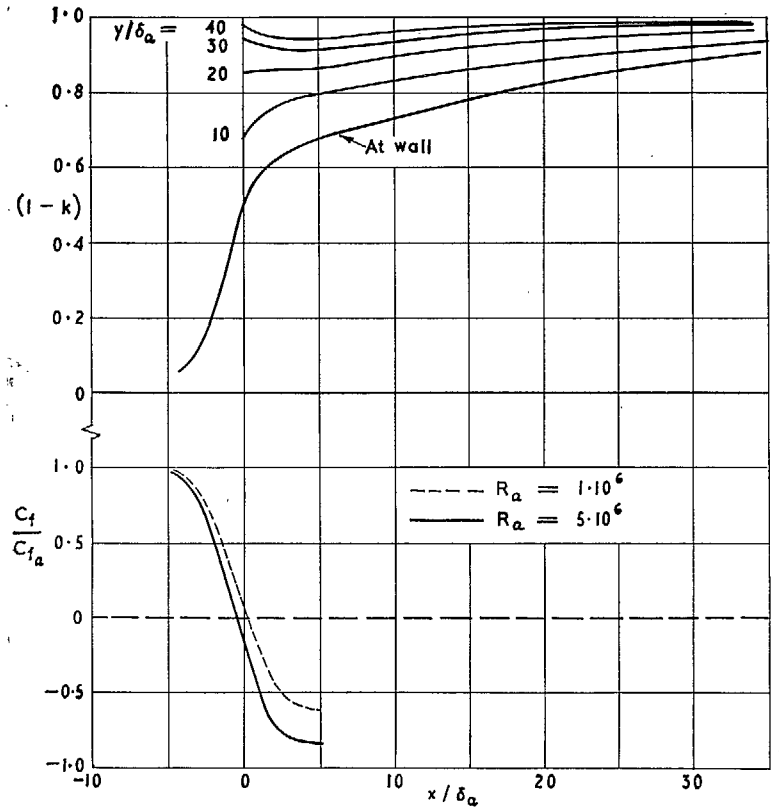

FIG. 13. Predicted pressure and skin-friction distributions for the case $M_1 = 1{\cdot}2$, $K = 5$.

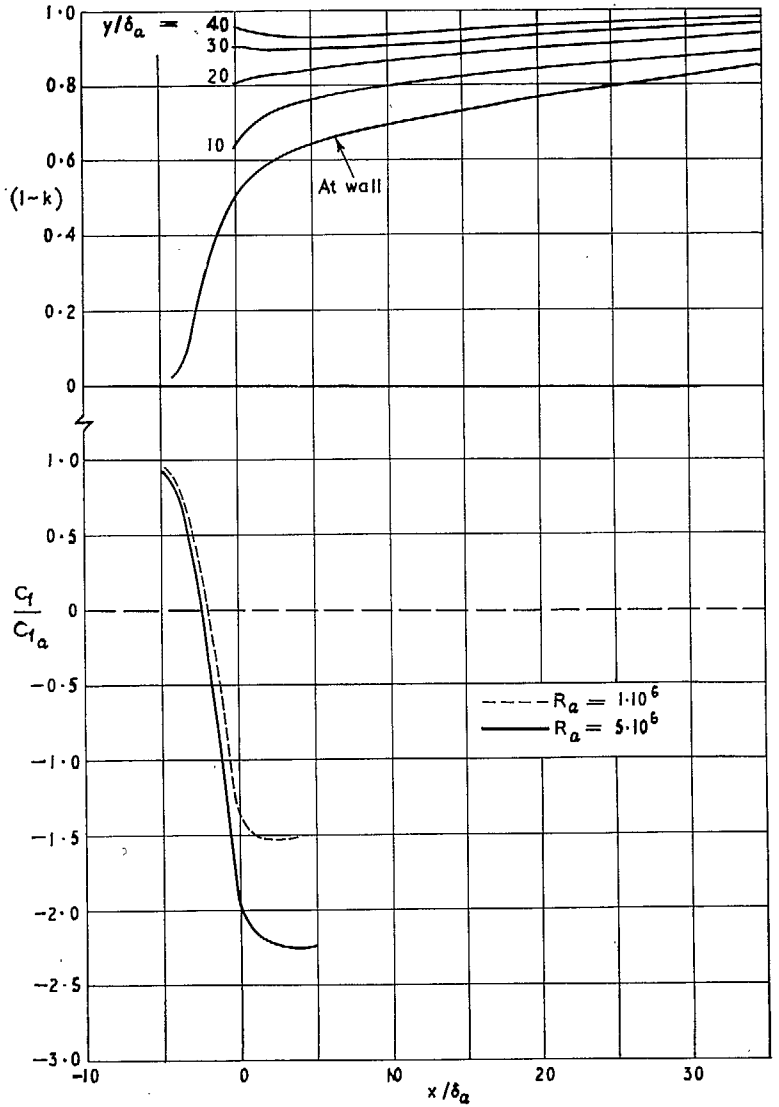

FIG. 14. Predicted pressure and skin-friction distributions for the case $M_1 = 1{\cdot}3$, $K = 5$.

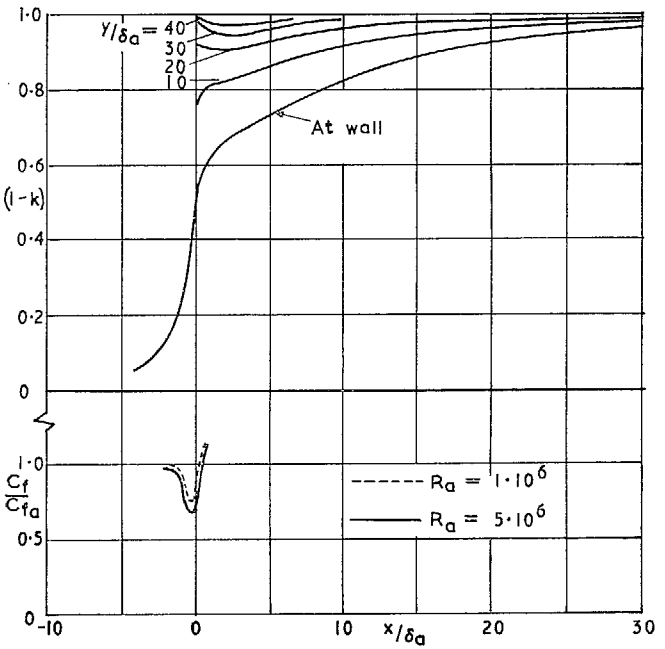

FIG. 15. Predicted pressure and skin-friction distributions for the case $M_1 = 1{\cdot}1$, $K = 7$.

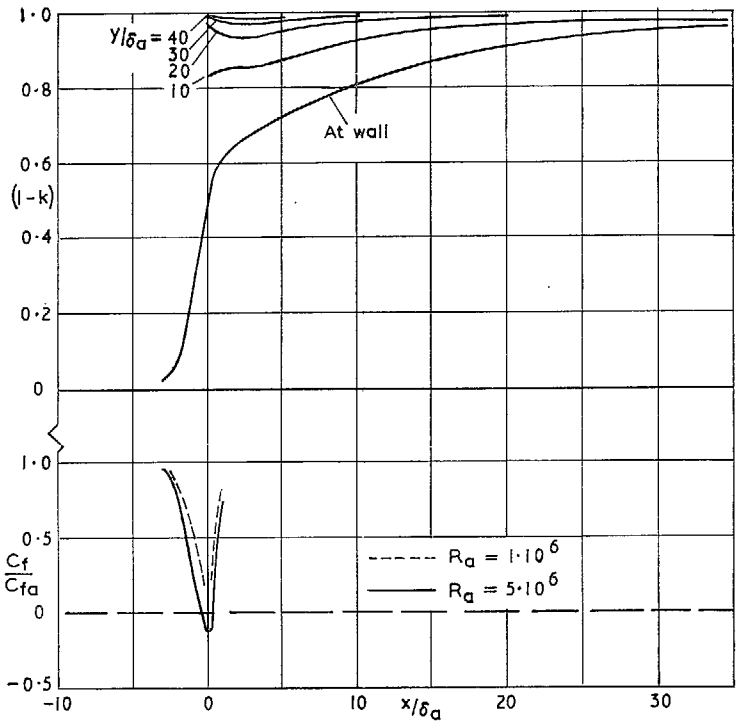

FIG. 16. Predicted pressure and skin-friction distributions for the case $M_1 = 1{\cdot}2$, $K = 7$.

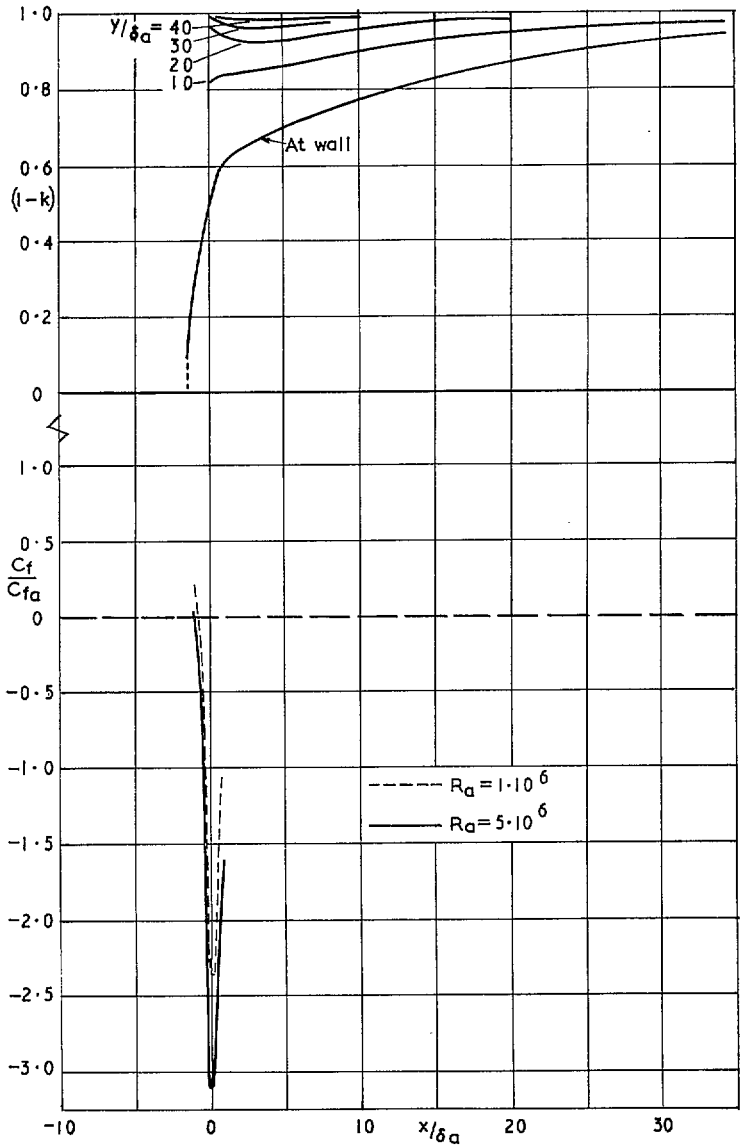

FIG. 17. Predicted pressure and skin-friction distributions for the case $M_1 = 1{\cdot}3$, $K = 7$.

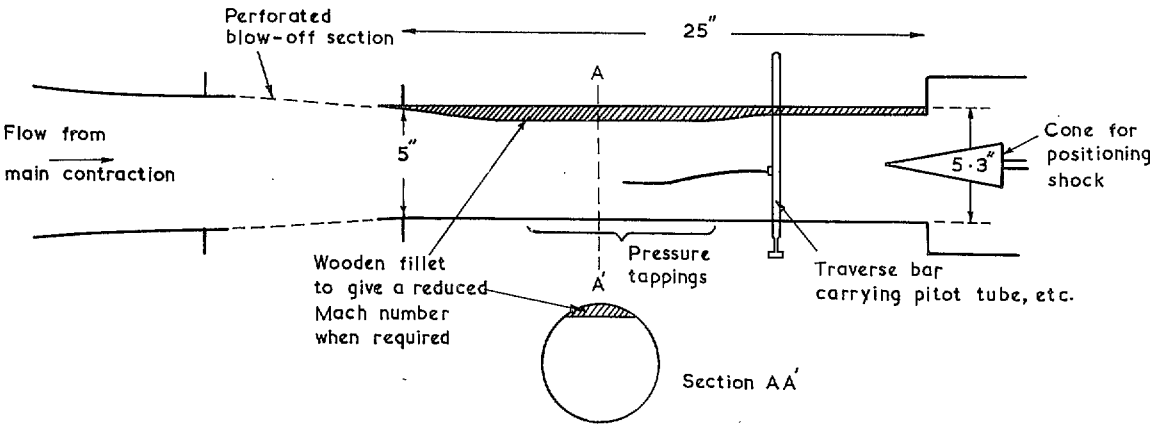

FIG. 18. Original arrangement or working section of normal-shock tunnel.

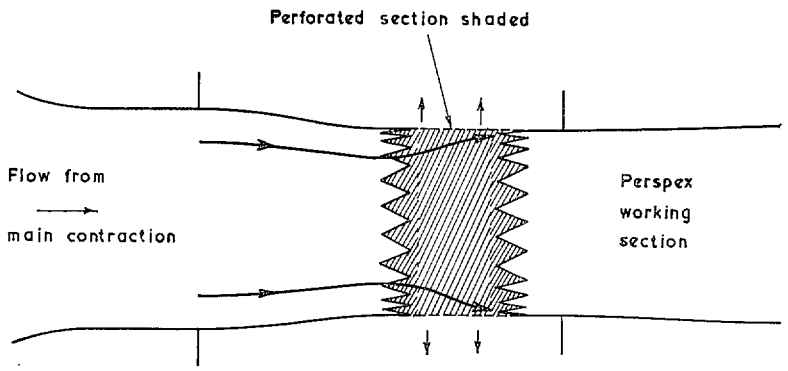

FIG. 19. Modified form of perforated section showing streamlines forming a throat.

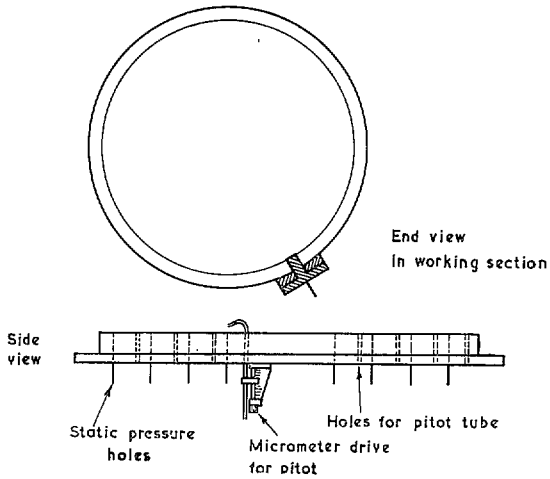

FIG. 20. Brass tongue.

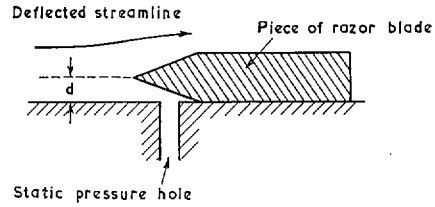

FIG. 21. Razor-blade Stanton tube.

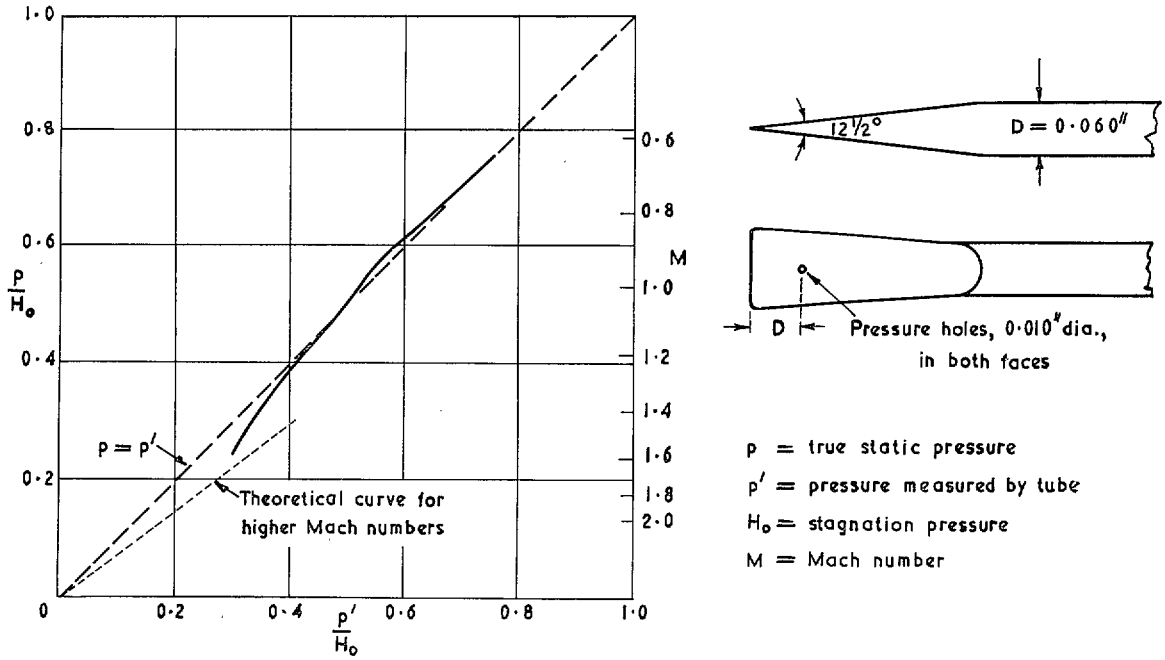

FIG. 22. The static tube of the type used by Girerd and Guienne, and its calibration in transonic flow.

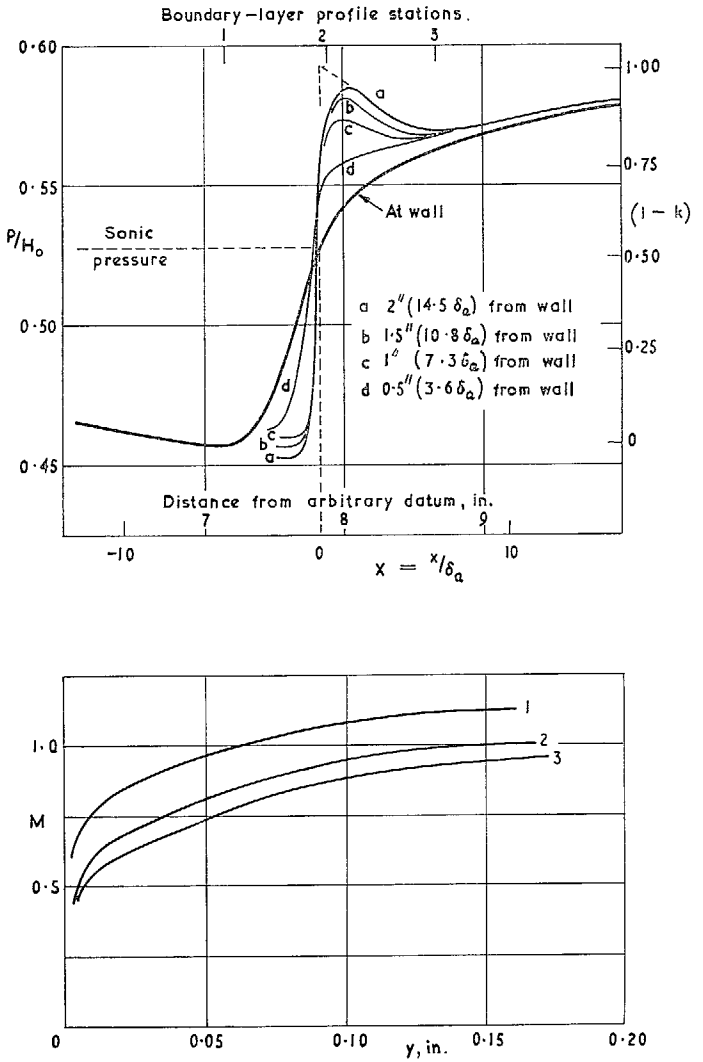

FIG. 23. Pressure distributions and boundary-layer profiles in pipe, $M = 1{\cdot}12$.

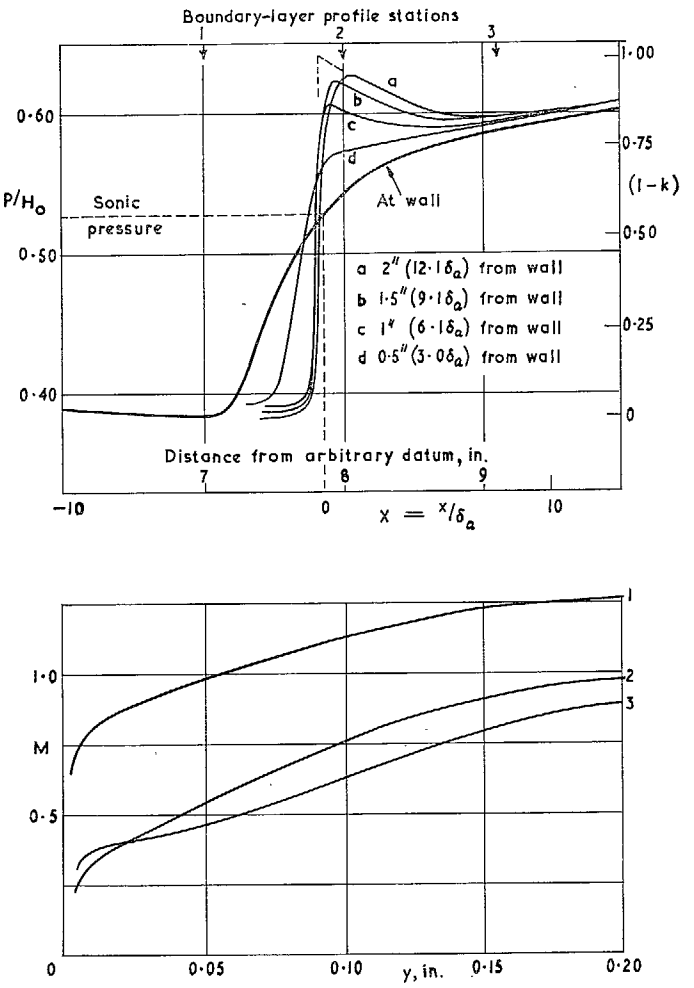

FIG. 24. Pressure distributions and boundary-layer profiles in pipe, $M_1 = 1{\cdot}25$.

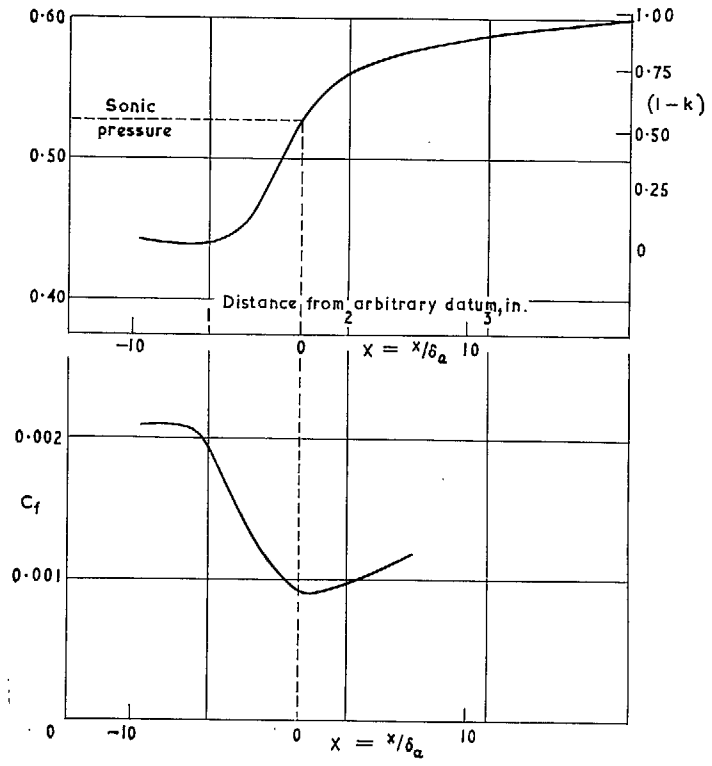

FIG. 25. Surface-pressure and skin-friction distributions in pipe, $M_1 = 1{\cdot}15$.

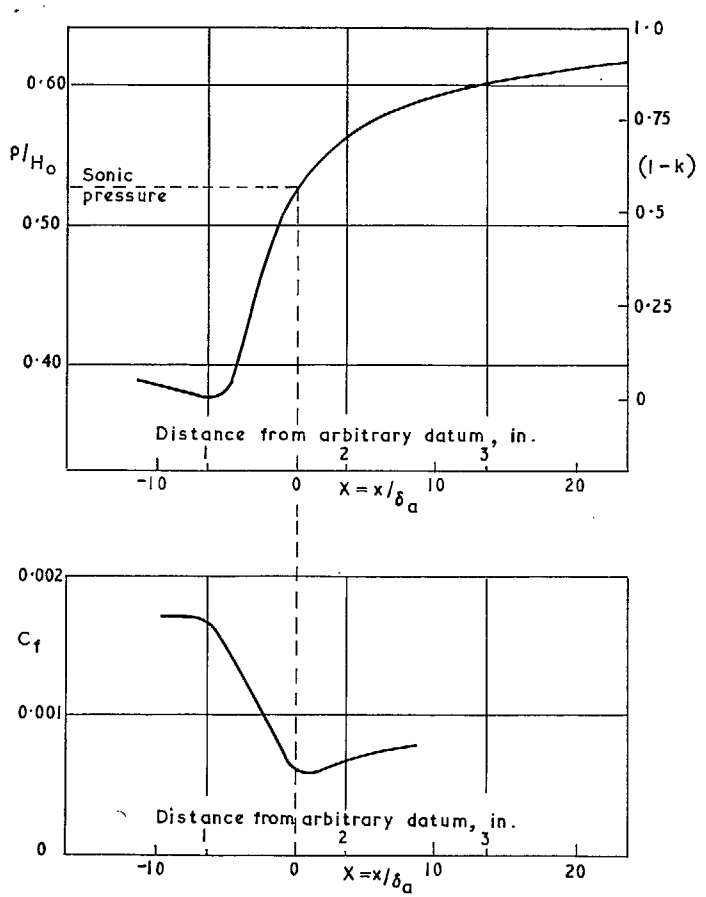

FIG. 26. Surface-pressure and skin-friction distributions in pipe, $M_1 = 1{\cdot}27$.

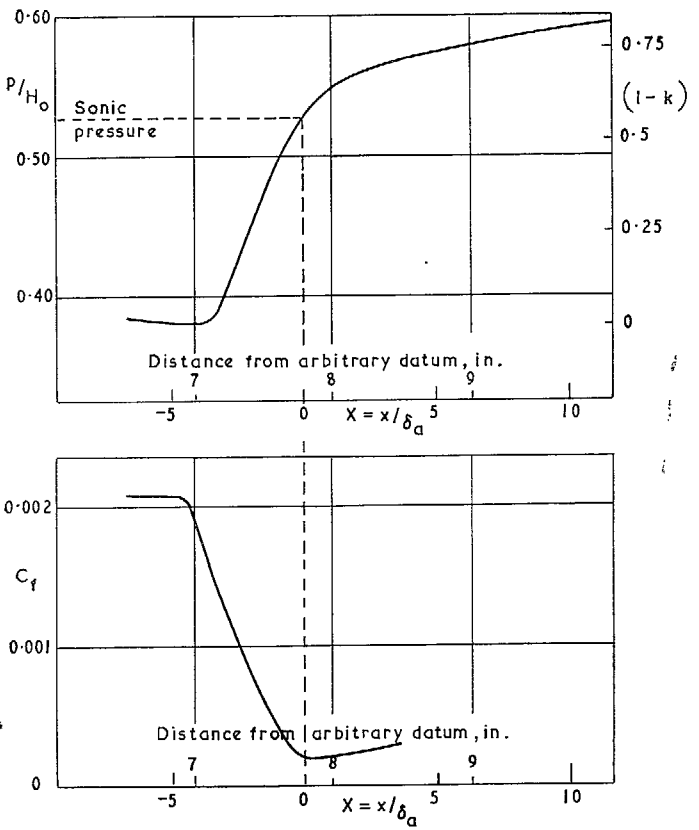

FIG. 27. Surface-pressure and skin-friction distributions in pipe, $M_1 = 1{\cdot}26$.

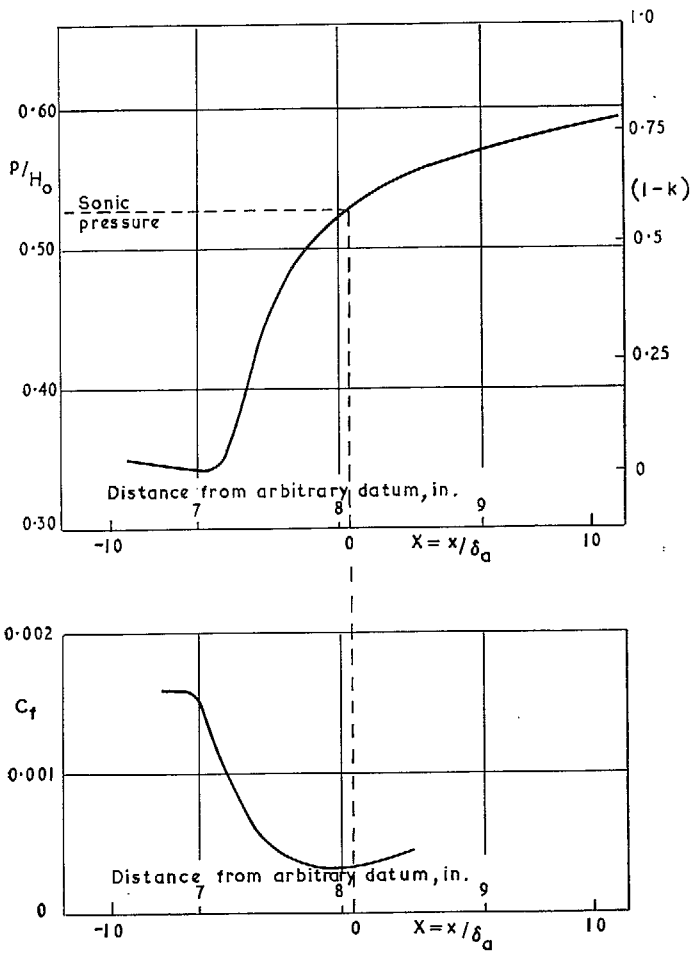

FIG. 28. Surface-pressure and skin-friction distributions in pipe, $M_1 = 1{\cdot}34$.

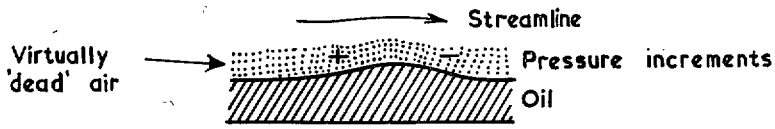

FIG. 29. Formation of oil wavelet.

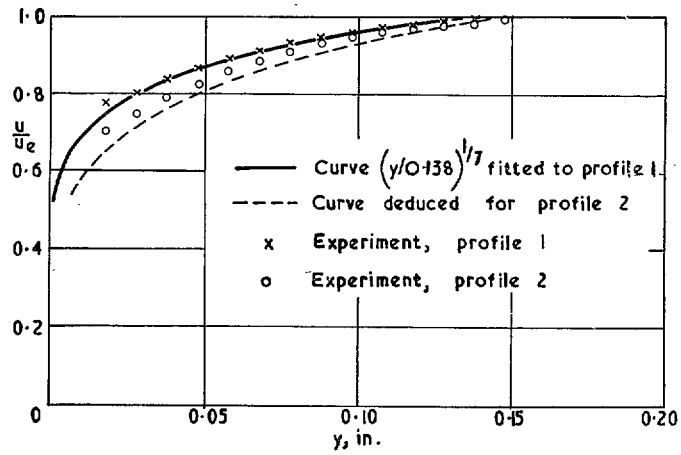

FIG. 30. Experimental and theoretical profiles, $M_1 = 1 \cdot 12$.

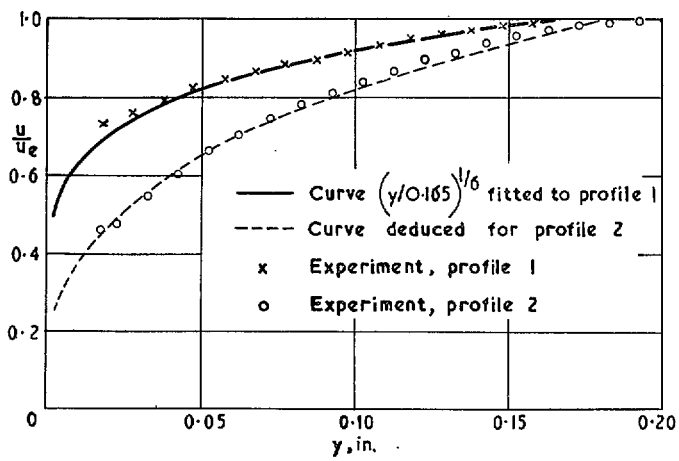

FIG. 31. Experiment and theoretical profiles, $M_1 = 1 \cdot 25$.

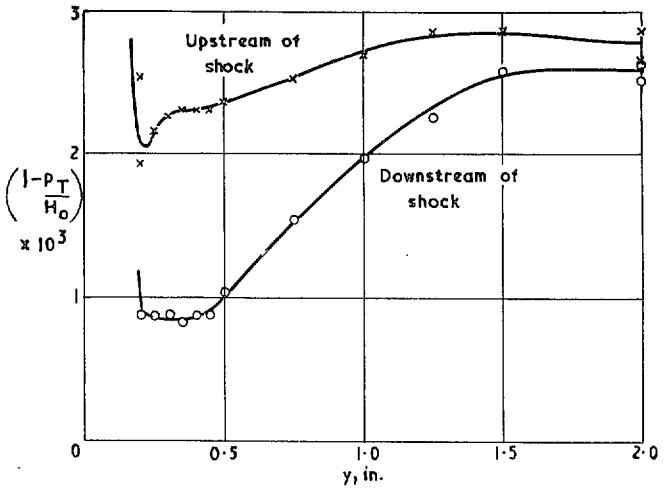

FIG. 32. Pitot-loss traverses, $M_1 = 1{\cdot}12$.

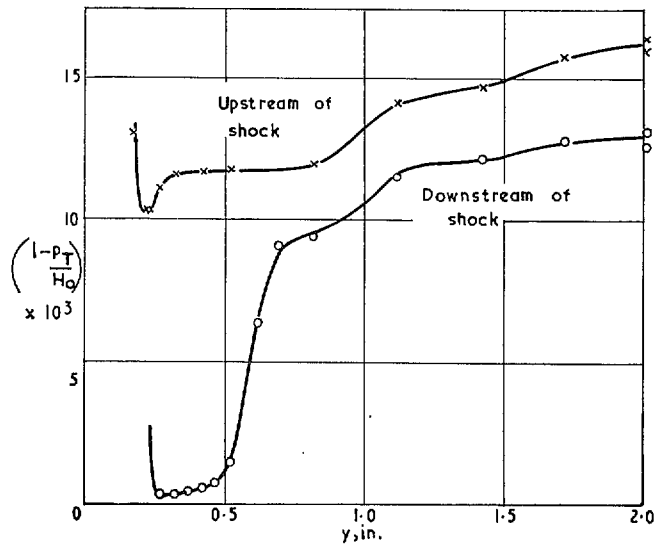

FIG. 33. Pitot-loss traverses, $M_1 = 1{\cdot}25$.

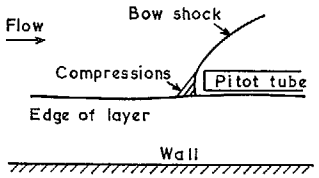

FIG. 34. Flow when pitot tube is near edge of layer.

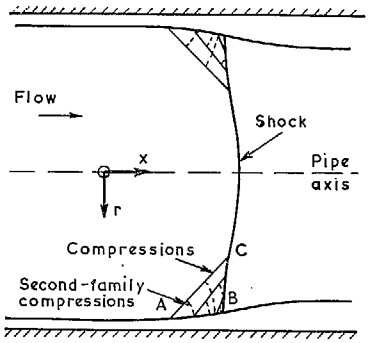

FIG. 35. Interaction in pipe.

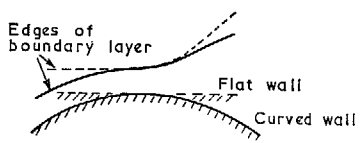

FIG. 36. Interactions on flat and curved walls, if rates of boundary-layer thickening are the same.

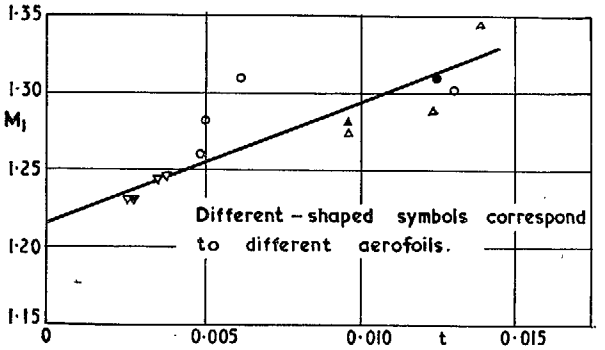

FIG. 37. Effect of curvature parameter t on Mach number M_1 for incipient separation.

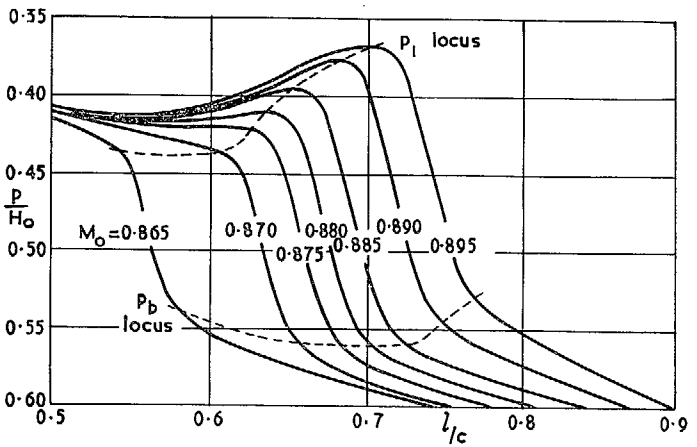

FIG. 38. Family of pressure distributions for aerofoil at fixed incidence. l = distance from leading edge, c = chord.

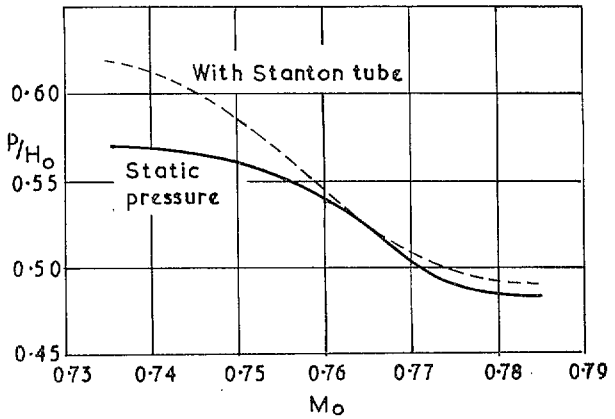

FIG. 39. Pressure variation at a single hole with and without Stanton tube.

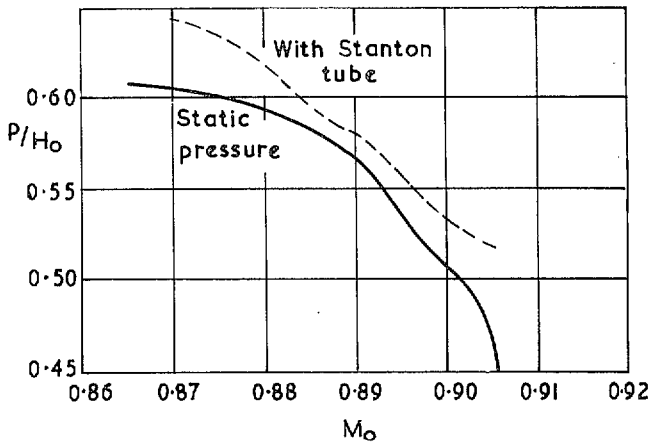

FIG. 40. Pressure variation at a single hole with and without Stanton tube.

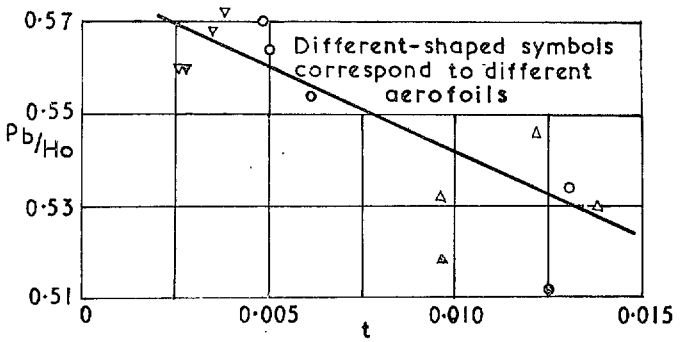

FIG. 41. Variation of p_b with curvature parameter t.

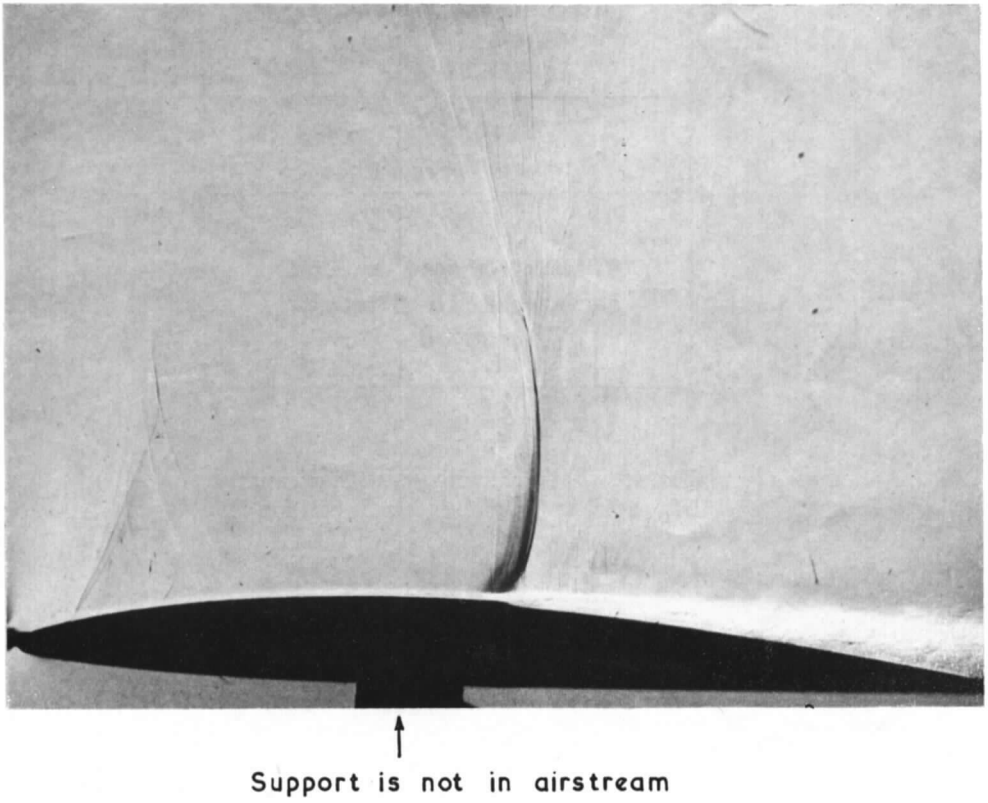

FIG. 42. Shock on an aerofoil with considerable surface curvature.

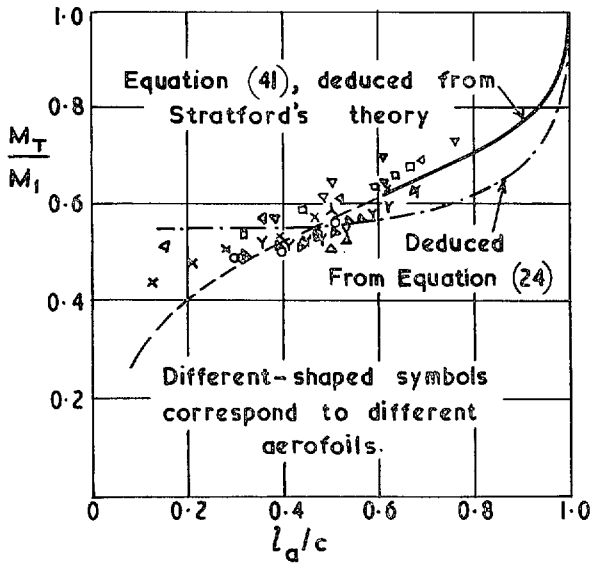

FIG. 43. Ratio of trailing-edge Mach number M_T to M_1 as function of shock position l_a/c.

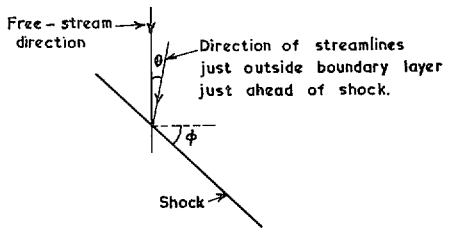

FIG. 44. Definition of shock-sweep angle ϕ and streamline angle θ.

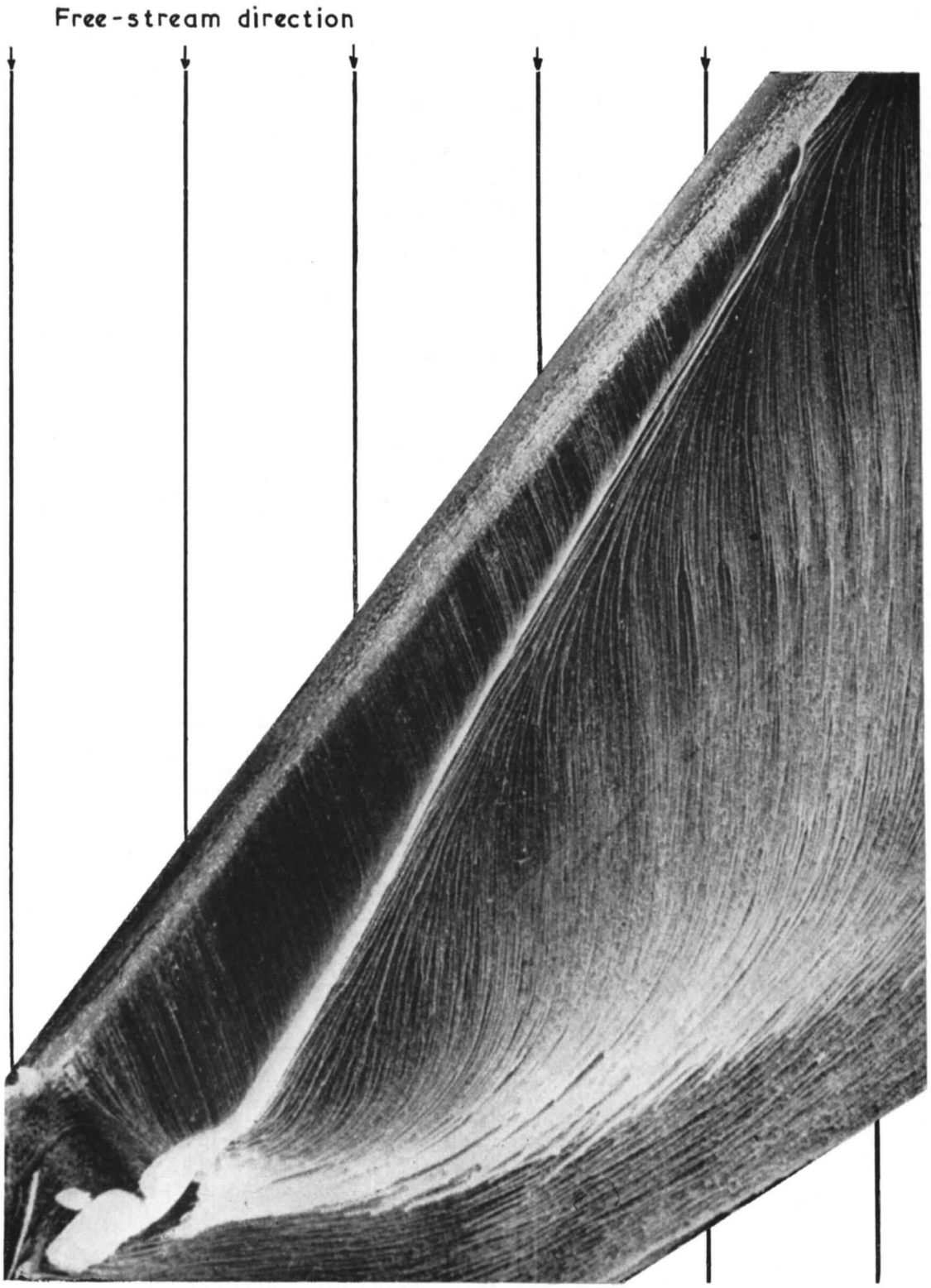

FIG. 45. Oil pattern showing incipient separation at a shock on a swept wing.

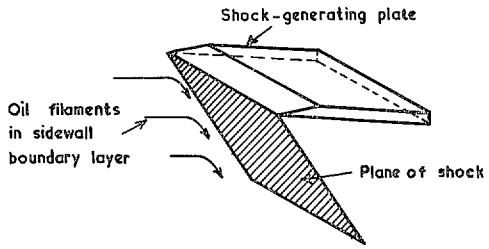

FIG. 46. Oblique view of Stanbrook's arrangement for interactions with swept shocks.

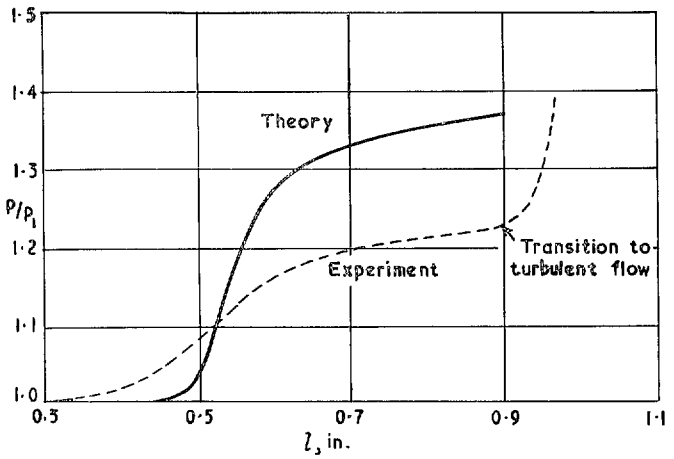

FIG. 47. Theoretical and experimental pressure distributions for laminar interaction with $M_1 = 2$, $R_a \doteq 2 \cdot 10^5$.

(83853) Wt. 67/1876 K.5 3/62 Hw.

Publications of the Aeronautical Research Council

ANNUAL TECHNICAL REPORTS OF THE AERONAUTICAL RESEARCH COUNCIL (BOUND VOLUMES)

1941 Aero and Hydrodynamics, Aerofoils, Airscrews, Engines, Flutter, Stability and Control, Structures. 63*s.* (post 2*s.* 3*d.*)

1942 Vol. I. Aero and Hydrodynamics, Aerofoils, Airscrews, Engines. 75*s.* (post 2*s.* 3*d.*)
Vol. II. Noise, Parachutes, Stability and Control, Structures, Vibration, Wind Tunnels. 47*s.* 6*d.* (post 1*s.* 9*d.*)

1943 Vol. I. Aerodynamics, Aerofoils, Airscrews. 80*s.* (post 2*s.*)
Vol. II. Engines, Flutter, Materials, Parachutes, Performance, Stability and Control, Structures. 90*s.* (post 2*s.* 3*d.*)

1944 Vol. I. Aero and Hydrodynamics, Aerofoils, Aircraft, Airscrews, Controls. 84*s.* (post 2*s.* 6*d.*)
Vol. II. Flutter and Vibration, Materials, Miscellaneous, Navigation, Parachutes, Performance, Plates and Panels, Stability, Structures, Test Equipment, Wind Tunnels. 84*s.* (post 2*s.* 6*d.*)

1945 Vol. I. Aero and Hydrodynamics, Aerofoils. 130*s.* (post 3*s.*)
Vol. II. Aircraft, Airscrews, Controls. 130*s.* (post 3*s.*)
Vol. III. Flutter and Vibration, Instruments, Miscellaneous, Parachutes, Plates and Panels, Propulsion. 130*s.* (post 2*s.* 9*d.*)
Vol. IV. Stability, Structures, Wind Tunnels, Wind Tunnel Technique. 130*s.* (post 2*s.* 9*d.*)

1946 Vol. I. Accidents, Aerodynamics, Aerofoils and Hydrofoils. 168*s.* (post 3*s.* 3*d.*)
Vol. II. Airscrews, Cabin Cooling, Chemical Hazards, Controls, Flames, Flutter, Helicopters, Instruments and Instrumentation, Interference, Jets, Miscellaneous, Parachutes. 168*s.* (post 2*s.* 9*d.*)
Vol. III. Performance, Propulsion, Seaplanes, Stability, Structures, Wind Tunnels. 168*s.* (post 3*s.*)

1947 Vol. I. Aerodynamics, Aerofoils, Aircraft. 168*s.* (post 3*s.* 3*d.*)
Vol. II. Airscrews and Rotors, Controls, Flutter, Materials, Miscellaneous, Parachutes, Propulsion, Seaplanes, Stability, Structures, Take-off and Landing. 168*s.* (post 3*s.* 3*d.*)

Special Volumes

Vol. I. Aero and Hydrodynamics, Aerofoils, Controls, Flutter, Kites, Parachutes, Performance, Propulsion, Stability. 126*s.* (post 2*s.* 6*d.*)
Vol. II. Aero and Hydrodynamics, Aerofoils, Airscrews, Controls, Flutter, Materials, Miscellaneous, Parachutes, Propulsion, Stability, Structures. 147*s.* (post 2*s.* 6*d.*)
Vol. III. Aero and Hydrodynamics, Aerofoils, Airscrews, Controls, Flutter, Kites, Miscellaneous, Parachutes, Propulsion, Seaplanes, Stability, Structures, Test Equipment. 189*s.* (post 3*s.* 3*d.*)

Reviews of the Aeronautical Research Council

1939–48 3*s.* (post 5*d.*) 1949–54 5*s.* (post 5*d.*)

Index to all Reports and Memoranda published in the Annual Technical Reports

1909–1947 R. & M. 2600 6*s.* (post 2*d.*)

Indexes to the Reports and Memoranda of the Aeronautical Research Council

Between Nos. 2351–2449	R. & M. No. 2450 2*s.* (post 2*d.*)
Between Nos. 2451–2549	R. & M. No. 2550 2*s.* 6*d.* (post 2*d.*)
Between Nos. 2551–2649	R. & M. No. 2650 2*s.* 6*d.* (post 2*d.*)
Between Nos. 2651–2749	R. & M. No. 2750 2*s.* 6*d.* (post 2*d.*)
Between Nos. 2751–2849	R. & M. No. 2850 2*s.* 6*d.* (post 2*d.*)
Between Nos. 2851–2949	R. & M. No. 2950 3*s.* (post 2*d.*)
Between Nos. 2951–3049	R. & M. No. 3050 3*s.* 6*d.* (post 2*d.*)

HER MAJESTY'S STATIONERY OFFICE

from the addresses overleaf

Printed and published by
HER MAJESTY'S STATIONERY OFFICE

To be purchased from
York House, Kingsway, London W.C.2
423 Oxford Street, London W.1
13A Castle Street, Edinburgh 2
109 St. Mary Street, Cardiff
39 King Street, Manchester 2
50 Fairfax Street, Bristol 1
35 Smallbrook, Ringway, Birmingham 5
80 Chichester Street, Belfast 1
or through any bookseller

Printed in England

S.O. Code No. 23-3262